NTNU
Norwegian University of Science and Technology

Faculty of Engineering
Department of Geoscience and Petroleum

Master`s thesis (60p)

Name	Joakim Navestad Hansen
Title	Comparison of existing performance prediction models for hard rock tunnel boring based on data collected at the Follo Line Project
Supervisor	Prof. II Eivind Grøv
External supervisor	Fredrikke Sofia Grønlund Syversen, Bane NOR
Dato	15. mai 2018

Abstract

In the Norwegian hard rock tunnelling history, drill and blast has mainly been used as the excavation method. At the Follo Line Project, which will be the longest railway tunnel in Scandinavia when it opens in 2021, tunnel boring machines have been applied. Before and during construction of a tunnel project, a correct prediction of penetration rate is important, and the choice of the most accurate prediction model is crucial. To find the most accurate model, the penetration rates will be predicted by several models and further compared with the actual penetration rate achieved at the Follo Line Project. This is the main scope of the thesis.

The prediction models used are listed below:

- NTNU model by Bruland (2000)
- CSM model by Rostami (1997)
- Gehring model by Gehring (1995)
- Q_{tbm} model by Barton (2000)
- Model by Hassanpour et al. (2011)
- NTNU model by Macias (2016)
- MCSM model by Yagiz (2002)
- Alpine model by Wilfing (2016)
- Model by Yagiz (2008)
- Model by Farrokh et al. (2012)

The performance prediction models will be fed with collected geological data from site, found both by laboratory testing and field inspections. The company has already collected most of the geological data, but the candidate will collect the remaining data. Calculation of geological parameters like $k_{s\text{-}tot}$ and Q-values will be necessary.

Due to difficulties with geological inspections on a double-shielded TBM, methods like face inspections, cross-passage inspections and OTV-analyses will be performed to gain information about the input parameters. Laboratory tests will be performed to find UCS-values, DRI-values, mineralogical compositions, brittleness values and densities. In addition to the geological parameters, machine data will be downloaded.

As a secondary scope, machine- and geological data will be compiled and presented. In addition, sensitivity analyses of the input parameters will be performed to determine the most influential parameters, both in reality and in the models. The outcome of these investigations will be analyzed to evaluate the suitability of the models at this project.

Supervisor | **Candidate**

Abstract

In the Norwegian hard rock tunnelling history, drill and blast has mainly been used as excavation method. At the Follo Line Project, which will be the longest railway tunnel in Scandinavia when it opens in 2021, tunnel boring machines have been applied. Before and during construction of a tunnel project, a correct prediction of penetration rate is important, and the choice of the most accurate prediction model is crucial. The overall purpose of this thesis is to compare existing performance prediction models with the aim of finding the most accurate model for hard rock tunnel boring based on data collected at the Follo Line Project.

To detect the most accurate model, the penetration rates have been calculated by using several models and further compared with the actual penetration rate achieved at the Follo Line Project. The prediction models used are listed below:

- NTNU model by Bruland (2000)
- CSM model by Rostami (1997)
- Gehring model by Gehring (1995)
- Q_{tbm} model by Barton (2000)
- Model by Hassanpour et al. (2011)
- NTNU model by Macias (2016)
- MCSM model by Yagiz (2002)
- Alpine model by Wilfing (2016)
- Model by Yagiz (2008)
- Model by Farrokh et al. (2012)

In general, most of the performance prediction models show promising results compared to the achieved penetration rate. The NTNU models and the Alpine model turned out to be the most accurate ones. If conservative results are sought for, the MCSM-model and the model by Yagiz show promising results.

One of the secondary scopes was to determine the most influential parameters, both related to the achieved and the predicted penetration rate. A sensitivity analysis of the various parameters has been performed for this purpose. The outcome of this analysis shows that the applied cutter thrust, rock mass fracturing and uniaxial compressive strength are the most influential parameters on the penetration rate, both in reality and in the models.

To strengthen the accuracy and reliability of the predictions, it is recommended to use more than one prediction model in the calculations. Thus, the sources of error connected to the models will be limited. The Follo Line Project is a well-suited project to compare hard rock prediction models due to the varying geology throughout the tunnel alignment.

Sammendrag

I norsk tunnelhistorie har konvensjonell drivemåte tradisjonelt vært den ledende metoden. Follobaneprosjektet, som vil bli den lengste jernbanetunnelen i Skandinavia når den åpner i 2021, er imidlertid drevet med tunnelboremaskiner. Nøyaktig estimering av inndrift er viktig både før og under bygging av et tunnelprosjekt, og i så måte er det avgjørende å velge den mest presise estimeringsmodellen. Hovedformålet med denne oppgaven er derfor å finne den mest presise estimeringsmodellen for inndrift basert på data samlet på Follobaneprosjektet. Dette har blitt gjort ved å sammenligne estimert inndrift fra flere inndriftsmodeller med den faktisk oppnådde inndriften på Follobaneprosjektet.

Inndriftsmodellene som har blitt benyttet er:

- NTNU-modellen av Bruland (2000)
- CSM-modellen av Rostami (1997)
- Gehring-modellen av Gehring (1995)
- Q_{tbm}-modellen av Barton (2000)
- Modellen av Hassanpour et al. (2011)
- NTNU-modellen av Macias (2016)
- MCSM-modellen av Yagiz (2002)
- Alpine-modellen av Wilfing (2016)
- Modellen av Yagiz (2008)
- Modellen av Farrokh et al. (2012)

Generelt viser de fleste inndriftsmodellene lovende resultater i forhold til den oppnådde inndriften på Follobanen. Begge NTNU modellene og Alpine-modellen viste seg imidlertid å være de mest nøyaktige. Hvis konservative resultater er ønskelig, viser MCSM-modellen og Yagiz sin modell lovende resultater.

Ett av sekundærformålene med oppgaven var å fastslå de mest innflytelsesrike input-parameterne, både i forhold til oppnådd og estimert inndrift. I den sammenheng har det blitt utført en følsomhetsanalyse av de forskjellige parameterne. Utfallet av denne analysen viste at benyttet matekraft, oppsprekkingsgrad og trykkfasthet var de mest innflytelsesrike parameterne som påvirket inndriften. Dette gjelder både i forhold til oppnådd og estimert inndrift.

For å styrke troverdigheten og nøyaktigheten til inndriftsestimeringen, anbefales det å benytte mer enn én inndriftsmodell i beregningene. På den måten vil feil og mangler knyttet til modellene bli begrenset. Alt i alt er Follobaneprosjektet et velegnet prosjekt for å sammenligne inndriftsmodeller for harde bergforhold.

Preface

This thesis is written as a part of my Master`s Thesis in Engineering Geology at the Department of Geoscience and Petroleum, the Norwegian University of Science and Technology (NTNU). The study has been carried out during the fall of 2017 and spring of 2018 at the Follo Line Project.

The topic of the study is prediction of penetration rates in TBM tunneling. Hard rock tunnel boring became interesting for me during the course TGB4190 – Engineering Geology of Rocks, Advance Course at NTNU. When the opportunity to work and write at the Follo Line Project arose, I couldn't miss it, especially not when the tunnels are excavated by tunnel boring machines.

The results are a product of my own work and are not affected by any of the contractor`s nor client`s perspective. In some aspects of the thesis (e.g. structure or presentation style), I have been inspired by an unpublished examination work which focus on the same topic. Due to their contractor`s wish, the origin of this examination work will stay undisclosed.

The main purpose of this thesis is to find the superior hard rock prediction model based on collected data at the Follo Line Project. The thesis is done in cooperation with Bane NOR and I have been located at the Åsland site during the whole writing period.

Oslo, 15.05.2018

Joakim Navestad Hansen

Cover page picture by Einar Aslaksen, 2017

Acknowledgements

During the last nine months, multiple people have helped and supported me. This thesis could not have been completed without their help, and I would like to show them my gratitude.

First, I would like to thank my supervisor Eivind Grøv for invaluable guidance and assistance. Your professional expertise related to engineering geology has helped me a lot. Quick and well-organized responds to e-mails and phone calls have been appreciated.

Fredrikke Syversen, my supervisor at Bane NOR. Thank you for your positive and energetic approach to everything you do. You have been supportive, enthusiastic, generous and fully understanding during these months. I look forward to further work with you.

Four big votes of thanks are owed to the geologists at the project, who possess lots of valuable knowledge. Marcus Lawton has answered questions daily, especially Excel related. Agnethe Finnøy has helped me with graphs. Bjørnar Gammelsæter has been an essential help with exploration in the archives. Guro Isachsen`s calculation skills have been invaluable. Thank you all for your immense geological knowledge and great friendship.

Arnulf Hansen, Thor Skjeggedal, Inge Rasmussen and Steinar Johannessen have answered a lot of questions, especially related to TBM performance and specifications. I am grateful for your kindness and support.

Special thanks to my good friend and former office partner, Artyom Andreev. His insight and competence on the topic have been essential. Thank you for your suggestions and input.

Furthermore, I would like to thank the rest of the Bane NOR employees at Åsland site. Your kind and welcoming approach have been important to me. It has been a pleasure sharing many cups of coffee, and I look forward to further work together.

My good friend and fellow student, Lars Peder Bakkevold, deserves special thanks. The daily phone calls and discussions have been crucial. Our cooperation and close friendship have definitely improved the outcome. Good luck with your own master`s thesis this spring!

Thank you to my family and friends for being supportive and uplifting during my education.

Rachel Dykeman, thank you for your time and efforts spent proofreading the thesis.

Finally, I extent my gratitude to my girlfriend, Ragnhild. Your comments and proofreading have been essential. Thank you for your endless patience and encouragement during these months. My gratitude is immensurable.

Table of contents

List of figures

List of tables

Abbreviations

AVS	Abrasion Value Cutter Steel
BTS	Brazilian Tensile Strength
CLI	Cutter Life Index
D&B	Drill and blast
Dip	Orientation of the planes of weakness
DRI	Drilling Rate Index
ISRM	International Society for Rock Mechanics
MWD	Measurement While Drilling
NPR	Net penetration rate (m/h)
NTNU	Norges Teknisk-Naturvitenskapelige Universitet (Norwegian University of Science and Technology)
OTV	Optical Televiewing
PR	Penetration rate (mm/rev)
ROP	Rate of penetration (m/h)
RPM	Cutterhead velocity (rev/min)
RQD	Rock Quality Designation (%)
SINTEF	Stiftelsen for industriell og teknisk forskning
SJ	Sievers' J-value
Strike	Orientation of the planes of weakness
TBM	Tunnel Boring Machine
UCS	Uniaxial Compression Strength

1 Introduction

The aim of this chapter is to contextualize the thesis. The purpose, research objectives, scope and limitations will be introduced.

1.1 General remarks

The development of underground infrastructure has increased significantly during recent decades and the great demand of infrastructure projects is expected to continue to increase in the future. The need to excavate deeper and longer, especially in urban areas, is continuously growing, and building tunnels using tunnel boring machines (TBM) is an important method employed by the tunneling industry (Macias, 2016).

Using TBMs as an excavation method leads to high investments and geological risks (Macias, 2016). Therefore, accurate performance predictions are of major importance in order to control risk and avoid delays. Several performance prediction models are made to calculate penetration rates and cutter consumptions. The various models require different input parameters, including both geological- and machine related parameters. As output, the net penetration is predicted. Some of these prediction models are based on empirical data while others are numerical or analytical models (Macias, 2016).

1.2 Purpose and objectives of the thesis

The overall purpose of this thesis is to compare existing performance prediction models with the aim of finding a superior model for hard rock tunnel boring based on data collected from a selected tunnel section at the Follo Line Project. Both geological- and machine related data will be gathered to provide a good basis for all the prediction models. By comparing the predicted penetration rates towards the actual penetration rates achieved at the project, the accuracy of each performance prediction model can be determined.

Some secondary objectives are established, listed in the following:

- To compile information about the geology in the project area. The information is compiled in templates and include information about rock mass fracturing, Q-values and laboratory test results.

- To gather machine data connected to the performance, including weighted average values of cutter thrust, cutterhead velocity (RPM) and net penetration rate (NPR).

- To determine the most influential parameters, both related to the achieved NPR and the predicted NPR. In that context, a sensitivity analysis will be performed.

1.3 Scope and limitations

The field data that has been acquired for this report is intended to support the objectives mentioned in Section 1.2. A broad variation of models has been investigated and several different input parameters have been obtained. Some of the models have been modified, and both original and updated versions were chosen. Table 1.1 present the prediction models investigated in this thesis.

Table 1.1 – *Performance prediction models investigated in this thesis.*

Performance prediction model	Reference
NTNU model	Bruland (2000)
Modified NTNU model	Macias (2016)
CSM model	Rostami (1997)
MCSM model	Yagiz (2002)
Gehring model	Gehring (1995)
Alpine model	Wilfing (2016)
Q_{tbm} model	Barton (2000)
Model by Yagiz	Yagiz (2008)
Model by Hassanpour et al.	Hassanpour et al. (2011)
Model by Farrokh et al.	Farrokh et al. (2012)

Naturally, some limitations are connected to such a big project when the available time on the project site is limited. There are in total four TBMs in operation at the Follo Line Project, which presents an immense potential in terms of data to be acquired. Due to this fact, it was necessary to establish some limitations in order to finish the research within the given timeframe. As a result, this report has been set to focus on one tunnel boring machine: Inbound north TBM number 1 (S980 – Euphemia). The tunnel section length in TBM 1 have been limited to 4.5 km of investigated tunnel.

Some of the models predict more than the NPR only, which include analyses of utilization, weekly advance rates, cutter consumptions and specific cost estimates. These subjects have not been predicted in this thesis. The prediction of NPR is the only parameter all the prediction models calculate, and is therefore the only comparable parameter.

1.4 Outline

A summary of the content in each chapter are presented in Table 1.2.

Table 1.2 – *Summary of the content in each of the eight chapters in this thesis.*

Chapter	Content
Chapter 1: Introduction	Background for the research carried out, purpose and objectives, scope and limitations
Chapter 2: Background and theoretical framework	Brief introduction to basic concepts and terminology related to hard rock tunnel boring. Information about the project
Chapter 3: Hard rock prediction models	Presentation of the different hard rock prediction models
Chapter 4: Methodology	Detailed descriptions of the methodologies used to acquire geological- and machine related data
Chapter 5: Results	Results obtained from field work, machine performance, calculated penetration rates and sensitivity analyses
Chapter 6: Comparison and discussion	Comparison of predicted penetration rates towards achieved penetration rates. Discussions regarding model behavior and influential parameters
Chapter 7: Conclusion	Conclusive remarks that address the objectives presented in Chapter 1.2

2 Background and theoretical framework

In this chapter, fundamental theory related to tunnel boring in hard rock conditions is described in order to give a general insight into the field. Such theory includes a presentation of the tunnel boring machine types and their rock breaking mechanisms that influence on the performance predictions. In addition, a comparison of excavation methods is presented in order to enlighten the reasons for method choice. Finally, information about the Follo Line Project is presented.

2.1 Hard Rock Tunnel Boring

A tunnel boring machine is a machine used for full excavation of a tunnel. The basic elements of a TBM are the cutterhead, the cutterhead carrier, the machine frame, the gripper shoes and the driving equipment. At the cutterhead, several disc cutters are installed in order to propagate cracks when the cutterhead is rotated against the tunnel face (Macias, 2016). These cutter rings are not powered, but roll in concentric rings against the face (Bruland, 2000a).

Hard rock conditions is a frequent used term that is vaguely defined. Eide's (2016) thesis presented some rough limits of the term hard rock, which was originally presented in the NTNU prediction model (Bruland, 2000a).

The definition included:

- *"The rock drillability expressed by the Drilling Rate Index (DRI) is in the range of approx. 20 to 80, roughly corresponding to a compressive strength in the range of approx. 350 MPa to 25 MPa.*
- *The rock type has medium to low porosity, less than approximately 10 % (volumetric).*
- *The rock mass degree of fracturing expressed by the average spacing between planes is larger than approx. 50 mm.*
- *The rock will break as chips (by brittle failure) between the disc cutters.*
- *The rock mass has a strength such that the excavated tunnel generally will need only light support in the form of rock bolts or shotcrete (except for weakness zones and other singular phenomena)"* **(Bruland, 2000a:7).**

2.1.1 Brief history

Excavation of tunnels with the use of TBMs is a widely used technique across the world. Boring for full-face excavation purposes began in the early 1880s and the first TBMs as we know them today originate from the 1950s. In the following decades, the TBM technology has significantly accelerated with the introduction of the rolling cutters (Macias, 2016).

In Norway, TBMs were frequently used to excavate tunnels during the seventies and eighties. During this period, 258 kilometers of tunnel were excavated and most of the projects were related to hydro power development (Hansen, 1998). Due to the end of the great hydropower era in Norway, as well as a couple of unsuccessful TBM projects, TBM was an excavation method that was not actively used for over twenty years (Holtet & Grue, 2013). During these years, all the tunnels in Norway were excavated by drill and blast (D&B); an excavation method the Norwegian tunnel industry has a good reputation for. Efficient and safe excavation by D&B, in addition to the lack of awareness regarding the possibilities for TBMs, are believed to be the primary reasons for the lack of TBM-projects in Norway during this period (Berg, 2015).

Despite this trend in the industry, three projects have since 2013 been excavated by TBMs: The Røssåga Hydropower Tunnel, the New Ulriken Railway Tunnel and the Follo Line Project. Based on this trend, it seems reasonable to expect that future projects will consider the use of TBMs as an excavation method. The three recent TBM projects may represent the start of a new tunnel boring era in Norway.

The following timeline is based on a table published by Hansen (1998), and depicts the most influential TBM projects in the history of Norwegian tunnel excavation (Fig. 2.1).

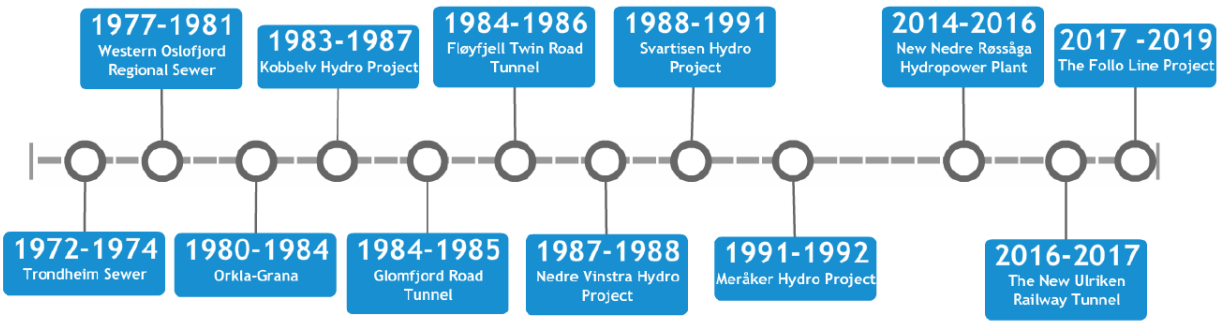

Figure 2.1 – *Timeline of selected TBM projects in Norway.*

2.1.2 Tunnel Boring Machines

Several kinds of tunnel boring machines exist. The three main types of TBMs are 1) Gripper TBM, 2) Single Shield TBM and 3) Double Shield TBM. The choice of TBM is mainly determined by the expected rock mass conditions. The principle of how the TBMs are excavating are the same for all three types. The choice of the most suitable TBM is in general controlled by the investment costs, the rock mass conditions and the water inflow regulations (Barla & Pelizza, 2000).

Barla & Pelizza (2000) presented advantages and disadvantages for each hard rock TBM type (Table 2.1).

Table 2.1 – *Advantages and disadvantages of different tunnel boring machines (Barla & Pelizza, 2000).*

Gripper TBM (open)	Single Shield TBM	Double Shield TBM
Advantages		
Easy to operate Applicable only in hard rocks Flexibility of supports Construction cost Limited investment	Application range more widespread than for open TBMs Safety Precast lining installation High performances	Larger application range Safety Support and lining flexibility High performances Drive in difficult ground conditions
Disadvantages		
Gripping in soft or unstable rock Support installation in unstable rock	Two work phases Not applicable in weak ground Need of precast lining Higher initial investment Complex to operate Squeezing ground – risk of jamming	High investment Complex to operate Higher maintenance costs Squeezing ground – risk of jamming

Information about these TBM types is briefly presented in the following subchapters.

Gripper TBM

The Gripper TBM is often described as an open TBM without any protective shield. As the name suggests, this TBM utilizes grippers in order to brace itself radially against the tunnel walls during excavation (Herrenkneckt, 2018a). As presented in Table 2.1, the Gripper TBM is often applied when drilling massive rock mass and when the water inflow regulations are flexible. The reason for this is the lack of a protective shield. The stand-up time needs to be sufficient in order to install the permanent rock support. If the TBM encounters zones with unfavorable rock mass conditions, pre-grouting and bolts can be added. In addition, post-excavation support can be installed (Eide, 2014).

The Gripper TBMs range from open with no shields, to open with partial shields in the roof or walls to protect the working crew. With their partial shields, the Gripper TBMs offer a diameter reduction compared to the closed shield types. This allows a flexible reaction to expanding rocks and prevents the machine from jamming. If necessary, the machine can be retracted completely (Herrenknecht, 2018a).

Figure 2.2 shows an example of a Gripper TBM.

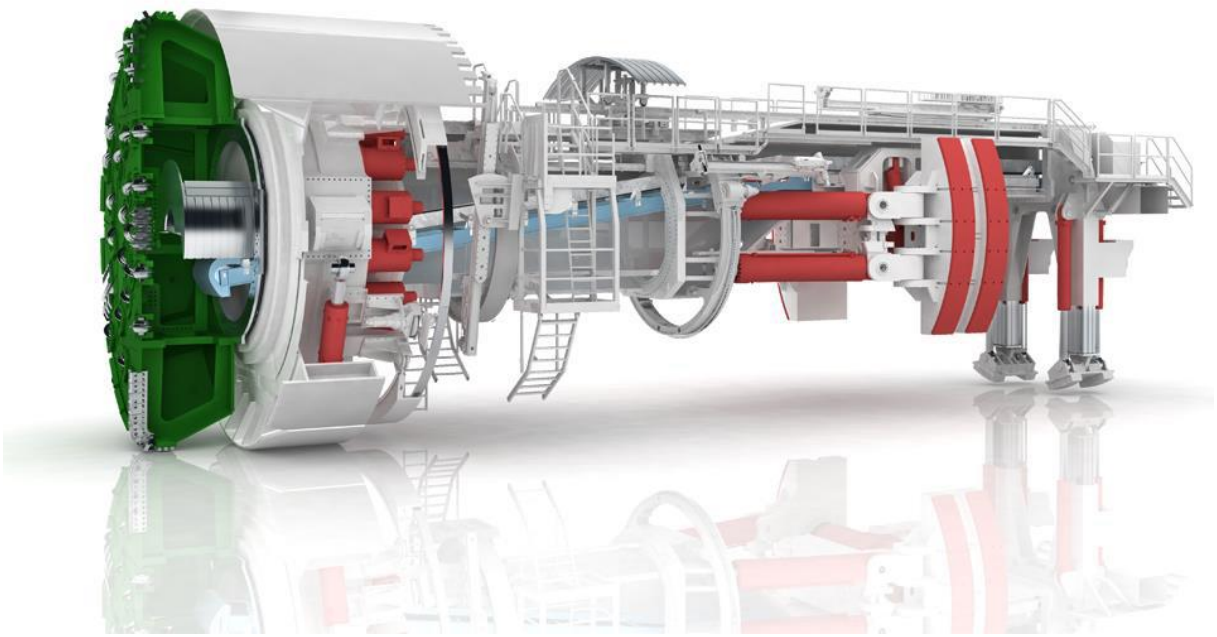

Figure 2.2 – *Example of a Gripper TBM, also called open TBM (Herrenknecht, 2018a).*

Single Shield TBM

The single shield TBM has a shield that prohibits the inside of the machine from being exposed to the surrounding ground. This shield extends from the cutterhead to the point where the tunnel lining is installed, and works as a protection for the crew. The tunnel lining consists of prefabricated concrete elements installed to form a complete ring around the tunnel perimeter. These TBMs are appropriate in cases where the majority of the rock mass is expected to be unfavorable with special regard to stability and water ingression (Maidl et al. 2008).

Unlike the Gripper TBM, the single shield TBM is not equipped with grippers. Instead, it pushes itself forward by several thrust cylinders that are braced axially against the previously built concrete lining (Herrenknecht, 2018b). These cylinders and concrete segments are visible in the illustration of a single shield TBM (Fig. 2.3).

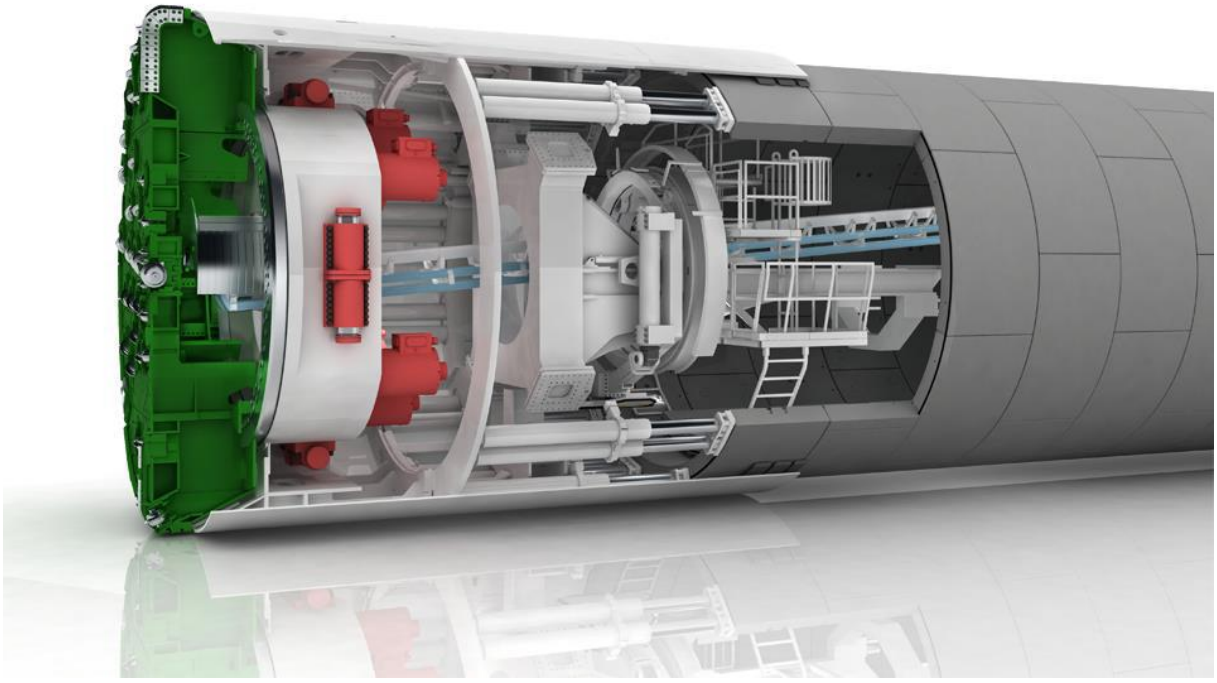

Figure 2.3 – *Example of a Single Shield TBM (Herrenknecht, 2018b).*

Double Shield TBM

The Double Shield TBM operates as a hybrid of the two previously described TBM models. It has both the gripper feature of the Gripper TBM and the protective shield feature of the Single Shield TBM. Hence, it has two types of shields, one gripper shield and one front shield (Herrenknecht, 2018c).

If the rock conditions allow it, the machine can utilize gripper shoes and propel itself forward in a similar fashion to the Gripper TBM. In this mode, concrete elements can be erected while the machine is boring. In cases when the rock conditions do not allow the grippers to brace themselves against the tunnel walls, the Double Shield TBM can switch to a single shield mode. In this mode, the thrust will be provided by the jacks braced against the previously built concrete elements. This mode does not allow to be installed during boring (Eide, 2014).

An illustration of the Double Shield TBM are presented in Figure 2.4.

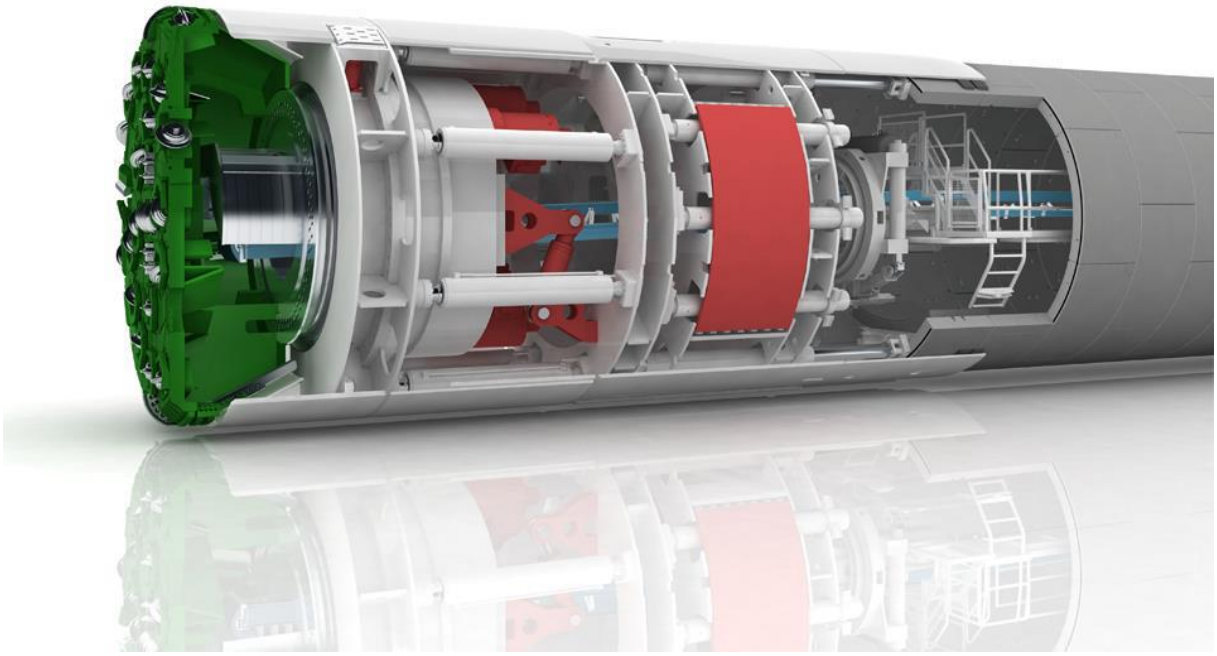

Figure 2.4 – *Example of a Double Shield TBM (Herrenknecht, 2018c).*

2.2 Influential TBM elements

In the following subchapters, the most important systems that influence the performance of the machines are presented.

2.2.1 The rock breaking process

"Hard rock tunnel boring leads the interaction between the rock mass and the machine, which is a process of great complexity. The tunneling system around the excavation process has a great relevance in the final goal of performance predictions for hard rock TBMs, which is the estimation of time and cost" **(Macias, 2016:i).**

Macias (2016) points out that the excavation process is relevant for the performance prediction results. In order to predict the performance results, the rock breaking process is vital. The fragmentation process is similar regardless to the machine type, and is initiated when the cutterhead is rotated and force is applied against the tunnel face. From Figure 2.5, one can see that radial cracks will appear when thrust force is applied. This will cause rock fragments to loosen between the adjacent kerfs, which is a process called chipping. These chips are formed between the cutter edges or against existing planes of weaknesses in the rock mass (Macias, 2016). How these chips are formed can affect the performance of the TBM.

By studying the shape of the chips, one can decide whether the chips are caused by tensile or shear failure. It seems to be a general agreement that tensile failure is the most likely type of failure, supported by Eide (2014).

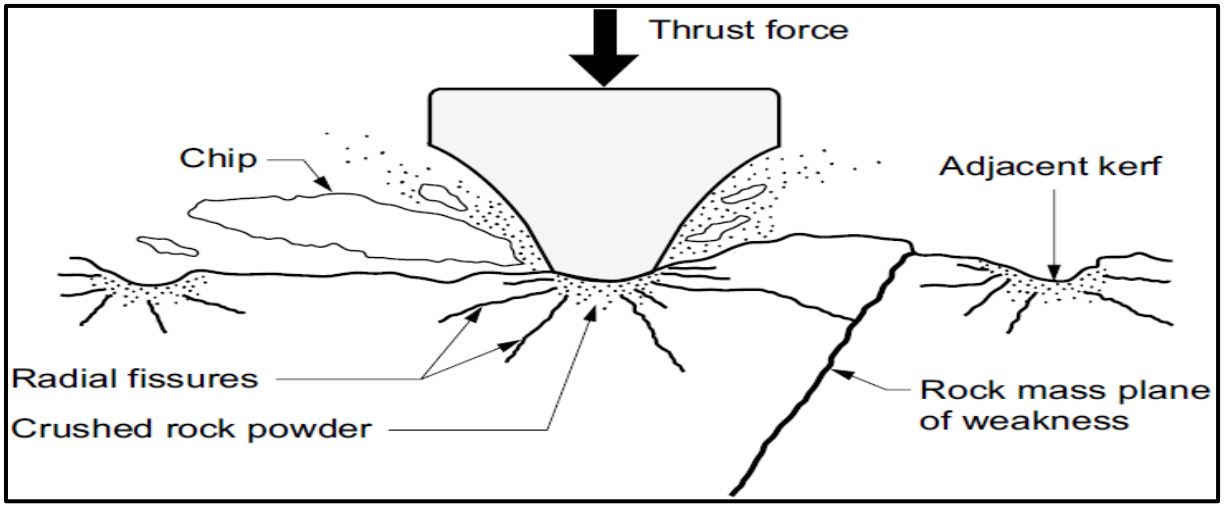

Figure 2.5 - *Illustration of the rock breaking process (Bruland, 2000d).*

2.2.2 The boring system

The boring system is a collective name for the cutterhead and its installed disc cutters. The design of this system has a significant impact on the tunneling performance. Based on Bruland (2000d) and Hansen et al. (2017), some items related to the boring system can influence directly on the net penetration rate:

- Larger cutter diameter permits the use of larger thrust forces. Smaller cutter diameter leads therefore to more efficient boring. Reduced cutter spacing the same.
- The cutters should be placed in a double spiral starting from the center of the cutterhead to improve the efficiency.
- Greater cutterhead stiffness reduces vibrations and is generally believed to give a better rate of penetration.
- Lower cutterhead velocity (RPM) has a positive influence on the penetration rate.
- The optimal cutter ring shape should be as narrow as possible. However, a cutter ring with a constant cross section thickness is preferred, which gives a more even penetration rate.

2.2.3 The thrust- and clamping system

As described in Chapter 2.1.2, different TBM types have different methods to propel the cutterhead forward. The forces are created either by the grippers against the walls or by bracing against the concrete lining. The applied thrust is of massive importance to the basic penetration rate (Bruland, 2000d). According to Bruland (2000a), a 15% increase of the thrust can lead to a 50% increased penetration rate. The applied thrust plays therefore a major role regarding the penetration rate. The exact influence of the applied thrust is presented in the results (Chapter 5).

Figure 2.6 illustrates the general importance of gross cutter thrust to the penetration rate.

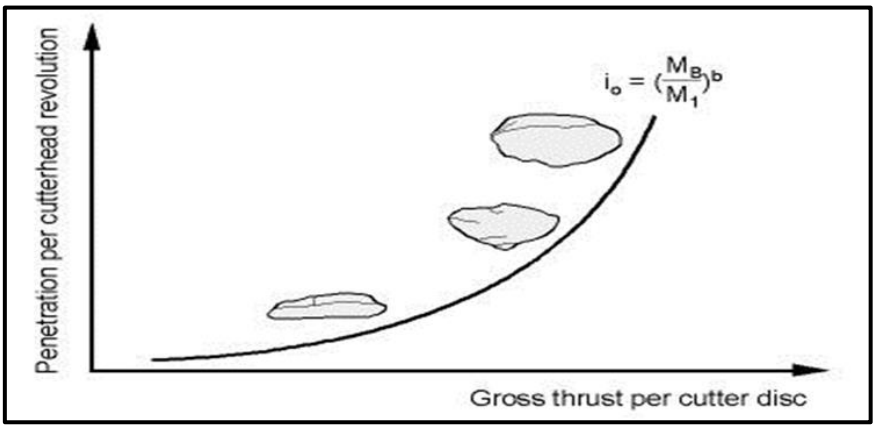

Figure 2.6 – *General progress of a penetration test curve (Bruland, 2000a)*

2.2.4 Other systems

In addition to the rock breaking process and the boring system, several other systems have an impact on the tunneling performance. Examples of these are the muck removal-, the rock support- and the backup system. According to their low significance on the basic penetration rate (more important on the advance rate), these systems are not described in detail. Works associated with these systems are typical time consuming and frequent.

2.3 Comparison of excavation methods

A large number of underground constructions excavated in hard rock conditions employ both the drill and blast (D&B) excavation and TBM methods. Both methods are widely and successfully used, although a few projects have been unsuccessful (Macias, 2016). Choosing the wrong method can potentially be catastrophic. There are several parameters which are of great importance when determining the excavation method. These are presented in Table 2.2 (Macias & Bruland, 2014)

Table 2.2 – *Important parameters regarding excavation method choice (Macias & Bruland, 2014).*

Important parameters to evaluate when deciding excavation method	
Project design considerations	*Costs*
Final purpose considerations	*Overbreak and tunnel profile quality*
Health, safety and working environment	*Environmental disturbance*
Advance rate	*Temporally access and implantation layout*
Flexibility and risk	*Contractual considerations in the choice of the excavation method*
Ground stability	

A list of advantages and disadvantages regarding excavation method is presented in Table 2.3 (Macias and Bruland, 2014). Adjectives such as *more* or *less*, *higher* or *lower*, must be understood in a comparative context between the different excavation methods.

Table 2.3 – *Advantages and disadvantages with the two different excavation methods (Macias & Bruland, 2014)*

Drill and blast (D&B)	**Tunnel boring machine (TBM)**
Advantages	
• More flexible regarding geometry, radiuses and slopes. The geometry can fit every project type. • Shorted delivery time of equipment. More flexible for geology changes. • Less extensive pre-investigations are required. • No need for big financial investments in the beginning of the project. • Do not require big amount of electricity.	• Higher stability in normal conditions because of circular profile and less damage to the surrounding rocks. • Favorable in water tunnels because of much lower frictional head loss. • All risk of handling and storing of explosives are avoided. • Rock support are installed from protected areas. • Normally higher advance rate and more favorable for longer tunnels. • Lower environmental disturbances. • Better work environments without gas emissions from blasting etc. • Several similar work operations.
Disadvantages	
• More unstable due to possible blast-induced fractures. • Higher frictional head loss. • Risk of handling and storing explosives. • Some of the rock support installed from unsupported work area. • Normally lower advance rates. • Higher environmental disturbance. • Bad work environments with gas emissions. • Harder to perform several work operations simultaneously.	• Limitations regarding geometry, radiuses and slopes. • Circular geometry is not preferable for road tunnels, rock caverns etc. • Longer delivery time of equipment. • More sensitive to geology changes. • Extensive geological pre-investigations • Requires finance in the beginning of the project, which can lead to negative cash flows. • Demands high mobilization, which requires more electricity.

2.4 The Follo Line Project

This subchapter will provide information specifically about the Follo Line Project. Descriptions about the project area, the tunnel boring machines in use and the geology along the tunnel alignment will be presented.

2.4.1 Project description

The Follo Line Project is currently the largest onshore infrastructure project in Norway and will be the longest railway tunnel in Scandinavia when it opens in 2021. The Follo Line stretches between the cities of Oslo and Ski and will reduce the travelling time from 22 to 11 minutes (Fig. 2.7). The project is owned by Bane NOR, and the contractor is a joint venture of Acciona and Ghella (AGJV).

22 km of railway tracks are being built in two separate tunnels with a length of 20 km each, making a total excavation length of more than 40 km tunnel. Close to the cities, the tunnel is mainly excavated by drill and blast (D&B). In sensitive areas, mechanical splitting (D&S) is used as an excavation method. The rest of the tunnel is excavated by four TBMs. Figure 2.7 shows where the different excavation methods are used at the Follo Line Project.

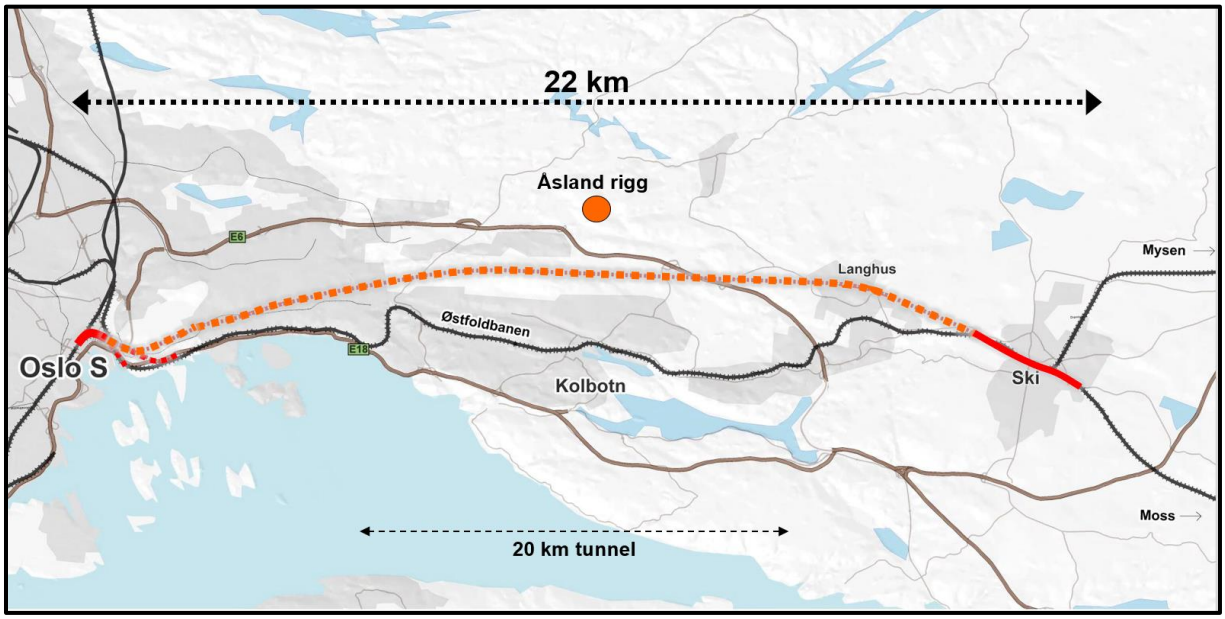

Figure 2.7 – *Excavation methods. The red and orange line displays the Follo Line. The red, solid lines illustrate the parts excavated by blasting and splitting, while the orange dotted line shows the part that will be excavated by TBMs. Notice the orange dot, illustrating where the main rig area is located (Bane NOR, 2018a).*

2.4.1.1 Tunnel boring machines

Two Double Shield TBMs originate from the rig area at Åsland and move outwards towards the north and south, respectively (Fig. 2.8). All four machines were installed and assembled in a large underground cavern at Åsland site area early 2017, and the first machine is scheduled to achieve breakthrough autumn 2018. This machine excavates the inbound north tunnel (TBM 1), which is the tunnel in scope in this thesis. Cross passages are excavated every 500 meters to make it possible for evacuation in emergency situations. The rock is supported by concrete lining consisting of several segments produced at site, made up of 1.8 m wide rings.

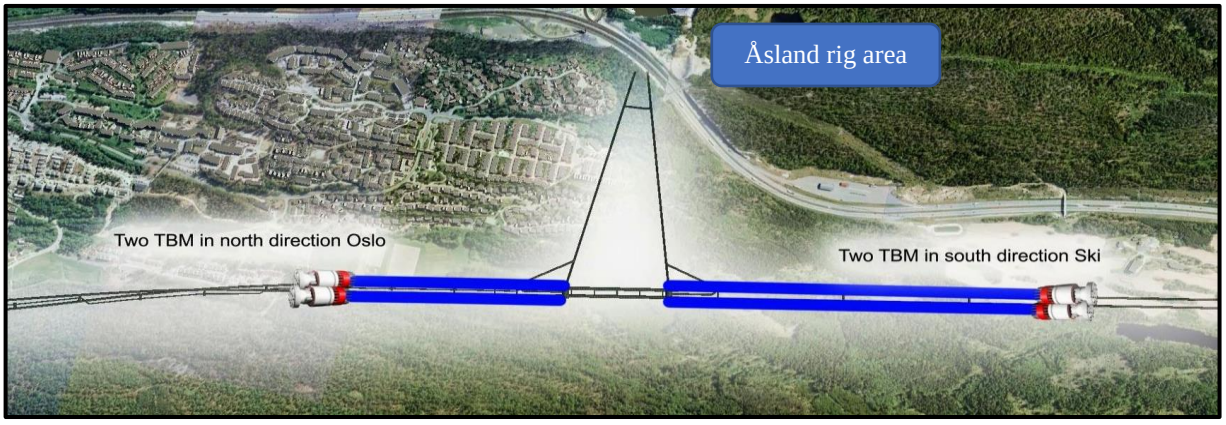

Figure 2.8 – *Two TBMs are operating in each direction from Åsland rig area (Bane NOR, 2018b).*

The technical specifications are listed in Table 2.4.

Table 2.4 – *Technical TBM specifications (Hansen et al., 2017).*

Technical TBM specifications	
Number of TBMs	*4*
Rock support	*Waterproof concrete lining*
TBM diameter	*9.96 m*
Cutter diameter	*19 inch (483 mm)*
Number of cutters	*71*
Max. recommended thrust	*315 kN/cutter*
Max. applied thrust	*(315 kN/cutter * 71) +3200 (drag) = 25 565 kN*
Cutterhead power	*13 VFD motors * 350 kW = 4 550 kW*
Cutterhead velocity	*11 115 kNm at 3.67 RPM*
Max. overload torque	*16 672 kNm at 3.67 RPM*
Total length	*150 m*
Total weight	*2 300 metric ton*

The tunnel boring machines operating at the Follo Line Project are illustrated in Figure 2.9.

Figure 2.9 – *The four tunnel boring machines operating at the Follo Line Project. Clockwise from the upper right corner: TBM 1 – Euphemia, TBM 2 – Ellisiv, TBM 4 – Anna, TBM 3 – Magda (Bane NOR, 2018a).*

2.4.2 Geology

The geology in the project area is highly decisive for the machine performance. In the following subchapters, a general regional scope of the geology will first be presented. Then, the most important information about the local geological variations obtained from the pre-investigations will be presented.

2.4.2.1 Regional geology

Based on information from the Geological Survey of Norway (Graversen, 1984), the geological conditions along the tunnel alignment are compiled in an internal geological report (Bane NOR, 2018a). According to this report, the rocks in the project area consist predominantly of Precambrian gneisses.

The Precambrian gneisses that occur in the project area are described in Table 2.5. They are divided into three main groups:

- Tonalitic to granitic gneiss,
- Quartz-feldspathic gneiss and
- Biotitic augen gneiss.

Appendix A illustrate a profile of the whole tunnel alignment, where the present rock types and weakness zones are illustrated. In addition, fracture information and joint rosettes are added to the profile.

In addition to the main groups of rocks, several generations of intrusions occur. Parts of the older intrusions still have the character of diabase while others have been transformed into amphibolite and folded into the gneisses. These amphibolite dykes make up a larger portion of the project area than the Permian intrusives. The youngest Permian intrusives are both dykes and sills which follow both weak layers in the foliation and along weakness zones. One such special intrusion is a 20-30 m thick rhomb porphyry dyke that can be followed from Ekeberg southward over a distance of about 15 km.

The geological profile is illustrated in Appendix A.

Table 2.5 – *Typical characteristics for the Precambrian gneisses present in the project area (Bane NOR, 2018a).*

Typical characteristics for the Precambrian Gneisses	
Tonalitic to granitic gneiss	Tonalitic gneiss consists of about 30% quartz, 40% feldspar, 20% biotite, and various accessorial minerals, including chlorite and muscovite. Granitic gneiss contains about 30% quarts, 65% feldspar, 5% biotite plus, accessorial minerals. Tonalitic gneiss has a dark color while granitic gneiss is lighter gray. The reason for the color differences is in the variation in content of dark micas.
Quartz-feldspathic gneiss	Quartz-feldspar rich gneiss is termed supracrustal gneiss because relict sedimentary structures are present. This lithology typically contains 40% quartz, 50% feldspars of different variations. Dark micas (biotite) are the dominating dark mineral, but a number of other minerals occur accessorial.
Biotitic augen gneiss	Biotite rich augen gneiss contains 25% quartz, 60% feldspar, 10% biotite and garnet. The lithology is described as homogeneous and grey, with 2-4 cm long eyes of feldspar and in some places with several cm large garnet minerals. The foliation is well developed.

2.4.2.2 Pre-investigations

When using TBMs as an excavation method, comprehensive geological pre-investigations are needed. As presented in Chapter 2.2, the TBMs are sensitive to changing geological conditions, which may affect the achieved penetration rates.

From autumn of 2007 until 2012, geologists from the Norwegian National Rail Administration (NNRA) and Multiconsult executed extensive pre-investigations in the project area. Seismic refraction surveys, resistivity measurements, core drillings, drilling of groundwater wells and geotechnical drillings have been executed.

Lithology

The rock types presented in the previous subchapter are confirmed by the pre-investigations. The different gneisses are hard to distinguish, and the investigations indicate the following distribution:

North Stretch:

- Gneiss: 86,13 %
- Amphibolite: 9,57 %

South Stretch:

- Gneiss: 80,46 %
- Amphibolite: 8,94 %

Fracturing

The fracture investigations show two main joint sets which run through the entire tunnel alignment.

1. One joint set typically has an E-W oriented strike with steep dip.
2. The second joint set, have N-S oriented strike with a westward dip of 35°-90°. This joint set follows the foliation.

A few joint sets have been observed that do not fit the definition of a joint set, due to uneven distribution. Hence, these are referred to as sub-horizontal joints. The average joint spacing varies along the tunnel alignment from 0.8 m – 1.0 m for the E-W joint sets. For the N-S joint sets the average joint spacing varies from 0.5 m – 1.1 m.

Intact rock properties

Laboratory investigation of rock samples have been carried out and the results from these investigations are presented in the following (Fig. 2.10 to 2.13). Table 2.6 classifies the various categories with related values.

In general, the geology in the entire project area is represented by low DRI- and CLI values, very high UCS values and relatively high quartz content. This classification is based on the ISRM standards presented in Table 2.6. The results related to the specific area in scope are presented in Chapter 5.

Figure 2.10 illustrates a histogram for DRI along the tunnel alignment.

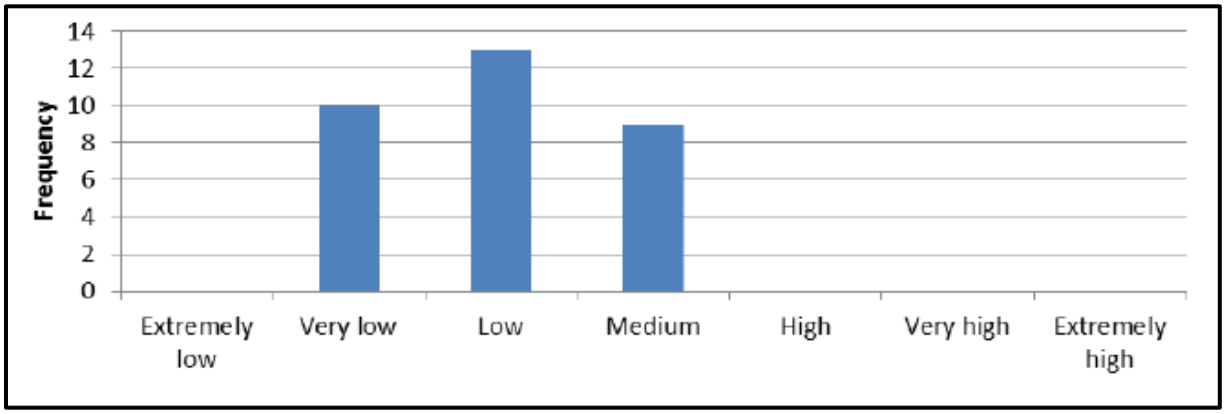

Figure 2.10 – *Histogram for DRI along the tunnel alignment (Bane NOR, 2018a).*

Figure 2.11 illustrates a histogram for CLI along the tunnel alignment.

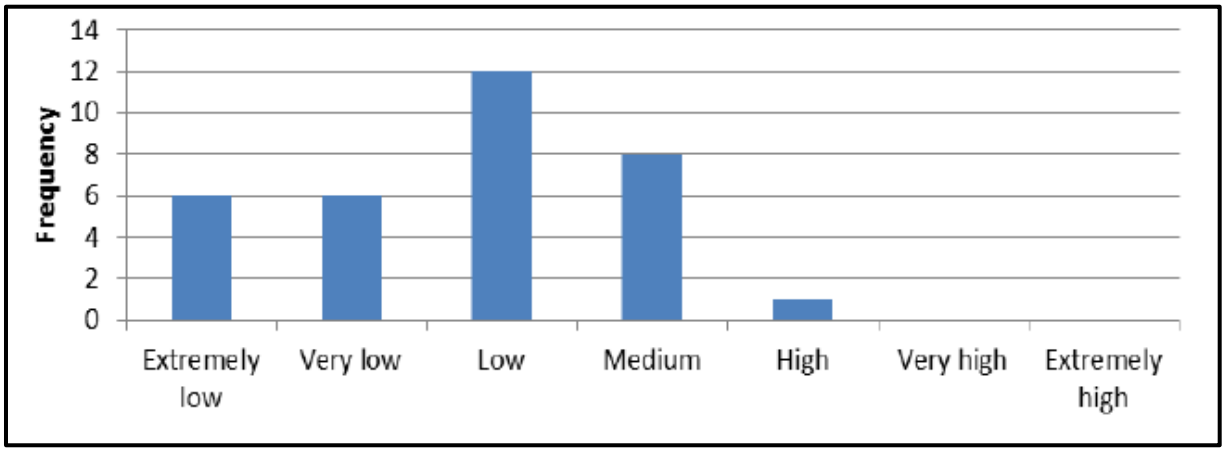

Figure 2.11 – *Histogram for CLI along the tunnel alignment (Bane NOR, 2018a).*

Figure 2.12 illustrates a histogram for UCS along the tunnel alignment.

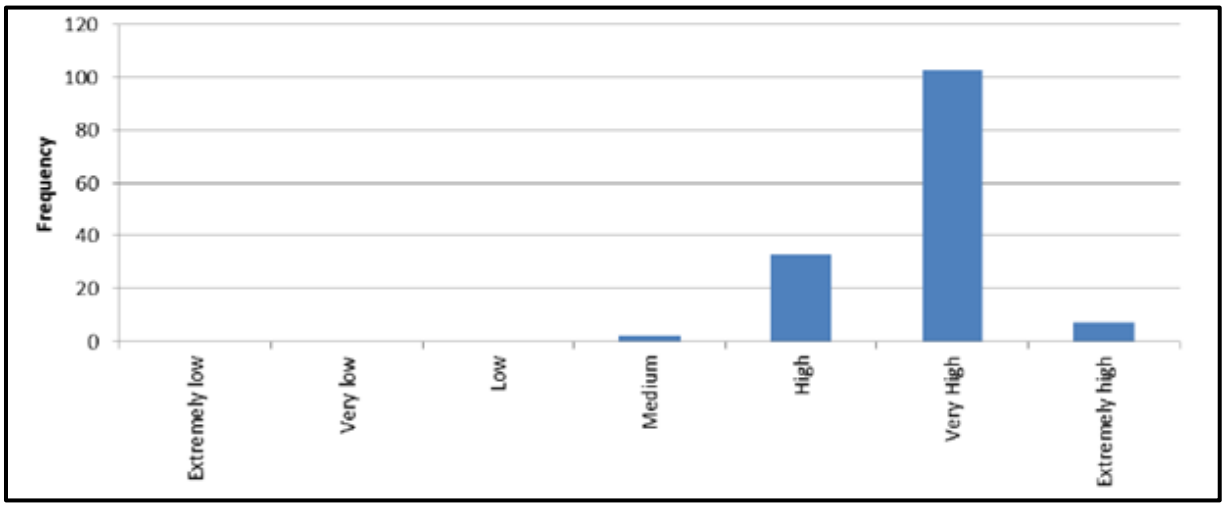

Figure 2.12 - *Histogram for UCS along the tunnel alignment (Bane NOR, 2018a).*

Figure 2.13 illustrates a histogram for quartz content along the tunnel alignment.

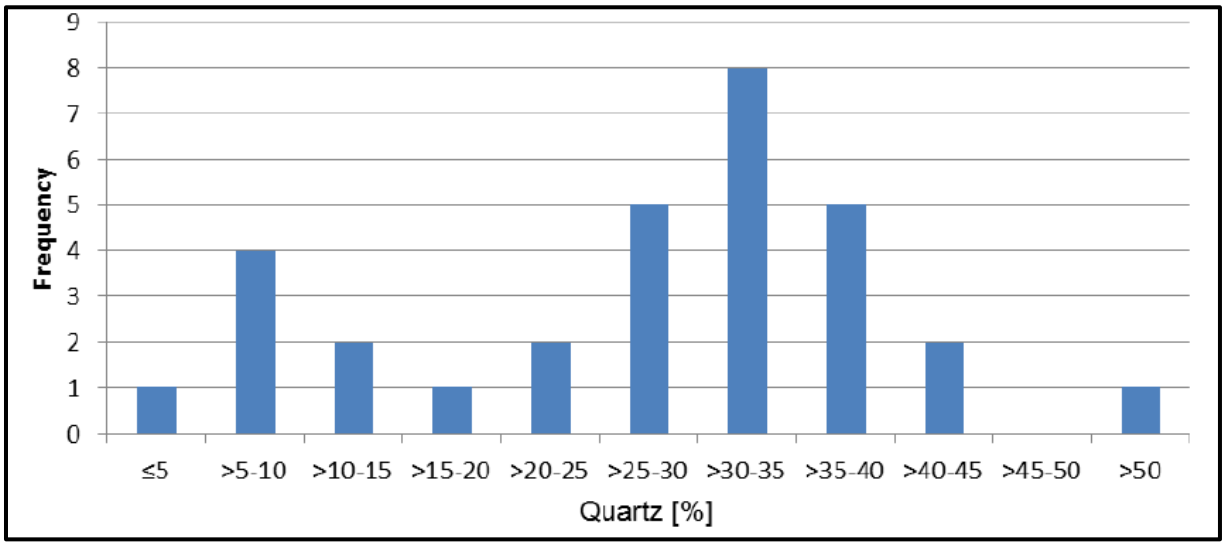

Figure 2.13 – *Histogram for quartz content along the tunnel alignment (Bane NOR, 2018a).*

Table 2.6 – *Classification of DRI, CLI and UCS based on standards by ISRM (1998).*

Category	DRI	CLI	UCS (MPa)
Extremely low	≤ 25	< 5	0.25 – 1
Very low	26 – 32	5.0 – 5.9	1 – 5
Low	33 – 42	6.0 – 7.9	5 – 25
Medium	43 – 57	8.0 – 14.9	25 – 50
High	58 – 69	15 – 34	50 – 100
Very high	70 – 82	35 – 74	100 – 250
Extremely high	≥ 83	≥ 75	> 250

3 Hard rock prediction models

In this chapter, several prediction models will be presented. This presentation includes information about the model's origin and their methods to calculate penetration rate. All the models alone are sufficient to estimate the penetration rate in hard rock conditions. Most of the information about the models comes from Wilfing (2016) and Macias (2016), along with other articles referred to in the specific chapters.

3.1 The NTNU model

The NTNU model originated from the Norwegian University of Science and Technology, and was first published in the 1970s (NTH, 1976). Several revisions have been done since, including the versions by Bruland (2000) and Macias (2016).

The NTNU model calculates performance predictions and cutter life assessments based upon empirical data from more than 300 km of tunnel from 40 different tunnel projects. In particular the model is based upon the intensive hydropower development in Norway during the 1970s and 1980s, where TBMs had a great impact (Jakobsen & Arntsen, 2014).

Among other empirical prediction models, the NTNU prediction model has good merits, and is widely accepted in the industry (Macias, 2016). The model retains its credibility by frequently being updated with additions obtained from new projects. The most well-known version of the NTNU model originate from Bruland (2000) and will be presented first, and then the revision by Macias (2016).

3.1.1 The NTNU model by Bruland

The net penetration rate (NPR) is defined as the advancement speed of the TBM while the cutterhead rotates with thrust against the face, expressed in meters per hour (Bruland, 2000). Bruland (2000b) has presented the following factors as influential on net penetration rate (Table 3.1).

Table 3.1 – *Machine and rock parameters influencing the net penetration rate (Bruland, 2000b)*

Geological parameters	Machine parameters
Fracture frequency	Gross average cutter thrust
Fracture orientation	Cutterhead velocity (RPM)
Drilling rate index (DRI)	TBM diameter
Porosity	Cutter spacing, shape and size

Rock mass fracturing

Starting with the geological parameters, the frequency and the orientation of the fractures are described by the fracturing factor (k_s). Rock mass fracturing is according to Bruland (2000b) the most important penetration rate parameter for tunnel boring. The less the distance between the fractures is, the greater is the influence it has on the penetration rate. Different types of fractures are described below:

- **Joints (Sp):** Continuous joints which can be followed all around the tunnel profile. They can be filled with clay or weak minerals, or they can be open just like bedding joints in granite (Bruland, 2000b).

- **Fissures (St):** Non-continuous joints which only can be followed partly around the tunnel profile. Such joints are typical fillings, joints of low shear strength or bedding plane fissures (Bruland, 2000b).

- **Homogenous Rock Mass (Class 0):** Massive rock without joints or fissures, typically found in intrusive dikes, sills and batholites. If the filled joints have high shear strength, they may be characterized as a homogenous rock mass (Bruland, 2000b).

For practical use while mapping in the tunnel, Bruland (2000b) has systematically divided the fractures into classes which are described by an associating distance between the weakness planes (Table 3.2).

Table 3.2 – *Fracture classes with distance between the planes of weakness (Bruland, 2000b)*

Fracture class (Joints = Sp / Fissures = St)	**Distance between planes of weakness [cm]**	
O	-	-
O-I	160	-
I-	80	90
I	40	80
II	20	40
III	10	20
IV	5	10

Angle of orientation (α)

In addition to the distances between the weakness planes, orientation to the tunnel axis also affect the rock mass fracturing factor (k_s), and hence the rate of penetration. The orientation of fractures relative to the tunnel axis is defined by the angle α. This angle is calculated by Equation 3.1.

$$\alpha = \arcsin{*}\ (\sin \alpha_f * \sin(\alpha_t - \alpha_s)) \tag{3.1}$$

where

α *angle between the planes of weakness and the tunnel axis [º]*

α_f *dip angle of the planes of weakness [º]*

α_t *tunnel direction [º]*

α_s *strike angle of the planes of weakness [º]*

Bruland (2000b) presented how the fracturing factor (k_s) depends on the α-angle and the fracture class, fissures and joints respectively (Fig. 3.1). A higher fracturing factor (k_s) will lead to a higher net penetration rate.

From the curves, one can observe:

- The weakness planes that are oriented at an angle of ~60° to the tunnel axis give the highest fracturing factor (k_s) for most of the fracture classes. In situations with very low distance between the planes of weakness (fissure class IV), 90° is the optimal angle for a high fracturing factor (k_s).

- Smaller distances between the weakness planes leads to a higher fracturing factor (k_s).

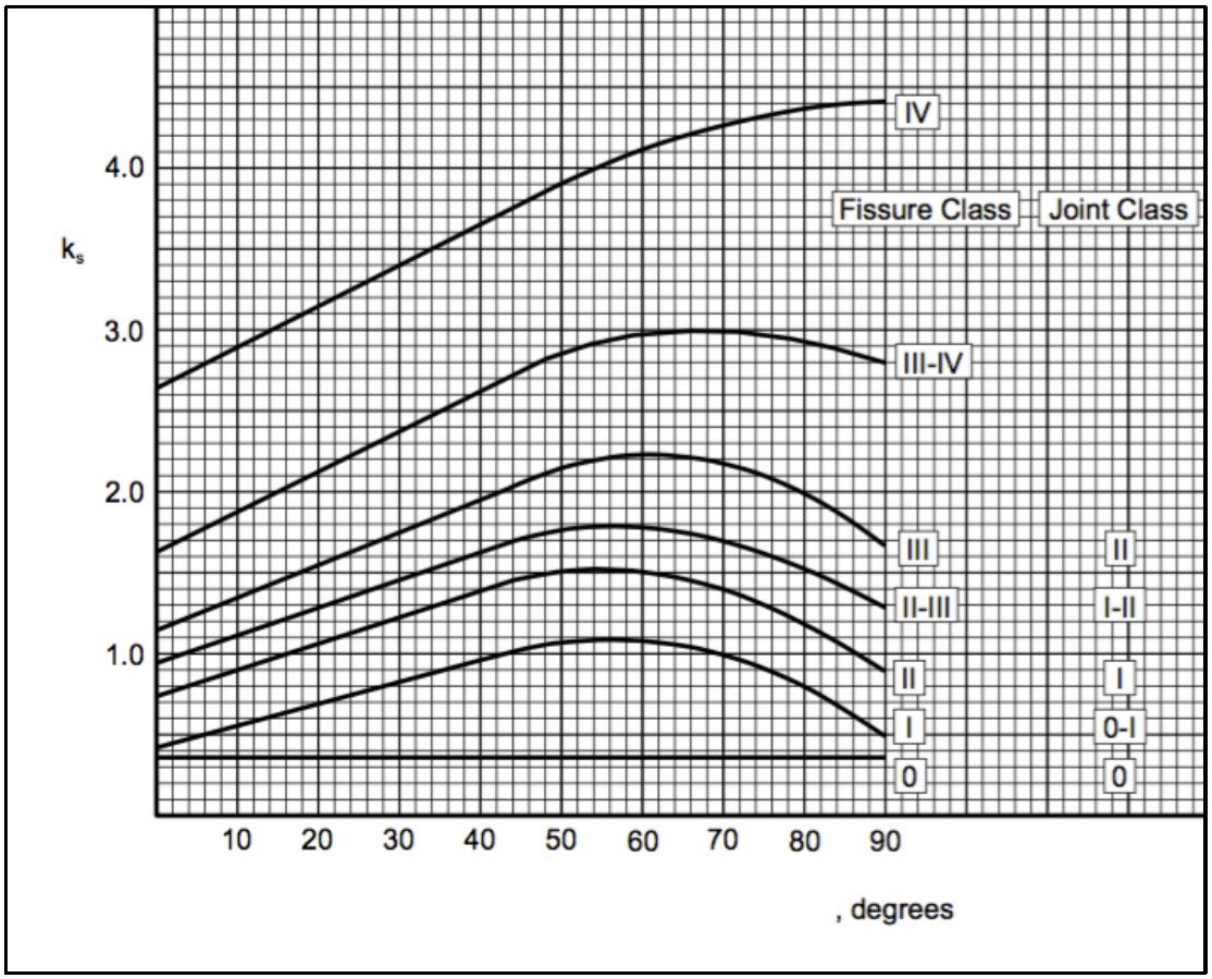

Figure 3.1 – *Fracturing factor (Bruland, (2000b).*

When there are more than one set of fractures present in a rock mass, the orientation angle and the degree of fracturing must be calculated for each set. To calculate the fracturing factor, the individual sets are combined into a total fracturing factor, $k_{s\text{-}tot.}$ (Eq. 3.2).

$$k_{s-tot} = \sum_{i=1}^{n} k_{si} - (n-1) * 0{,}36 \qquad (3.2)$$

where

$k_{s\text{-}tot}$	*total fracturing factor [-]*
k_{si}	*fracturing factor for set no. I [-]*
n	*number of fracturing sets [-]*

Drilling rate index (DRI)

The drilling rate index (DRI) is one of the geological parameters accounted for in the model, due to good correlations with field data regarding penetration rate from a number of TBM projects (Zare & Bruland, 2012). Bruland (2000b) has presented three curves representing different fracturing factors (Fig. 3.2). The curves show the relationship between DRI and the correction factor for DRI of the rock (k_{DRI}).

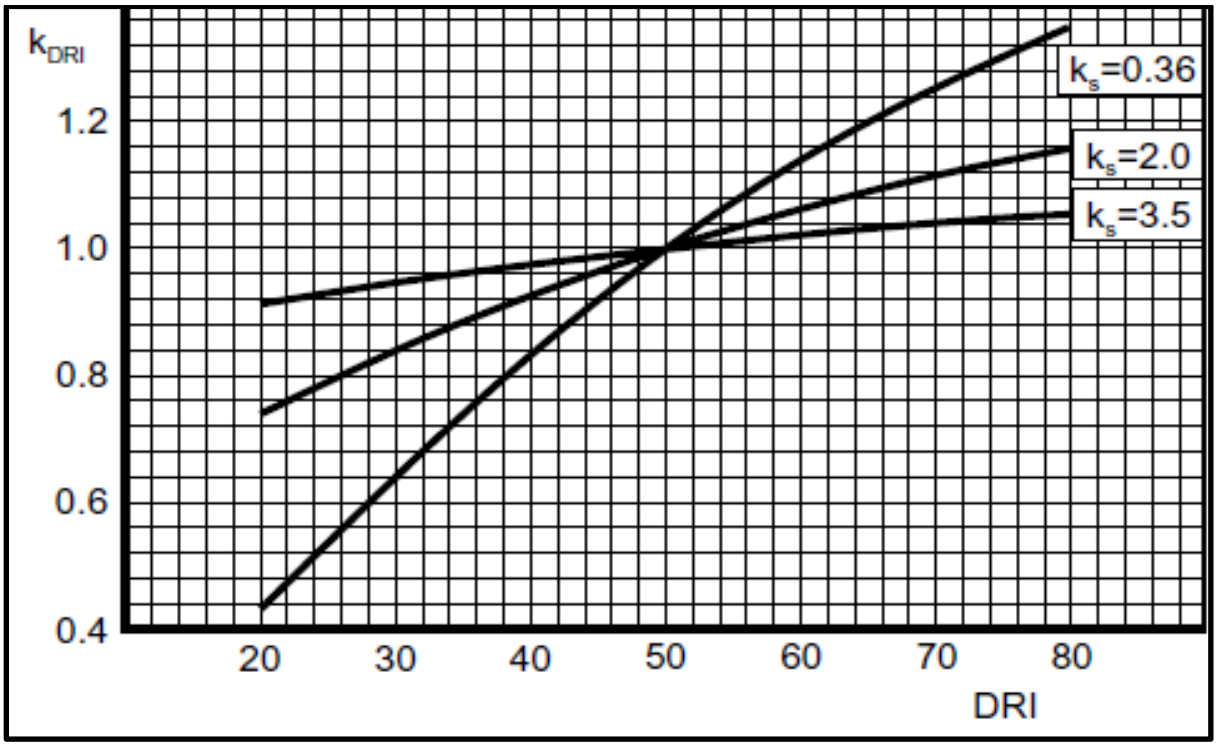

Figure 3.2 – *Correlation between drilling rate index (DRI) and correction factor (k_{DRI}), Bruland (2000b).*

Porosity

When the rock mass has a porosity of more than approximately 2% (volumetric), it is believed to have a significant impact on the rate of penetration (Macias, 2016). Figure 3.3 presents the correlation between the rock porosity and the correction factor for porosity of the rock (k_{por}) (Bruland, 2000b). The porosity of hard rocks is typically less than 2%, and it is expected that the correction factor for porosity (k_{por}) equals 1.0.

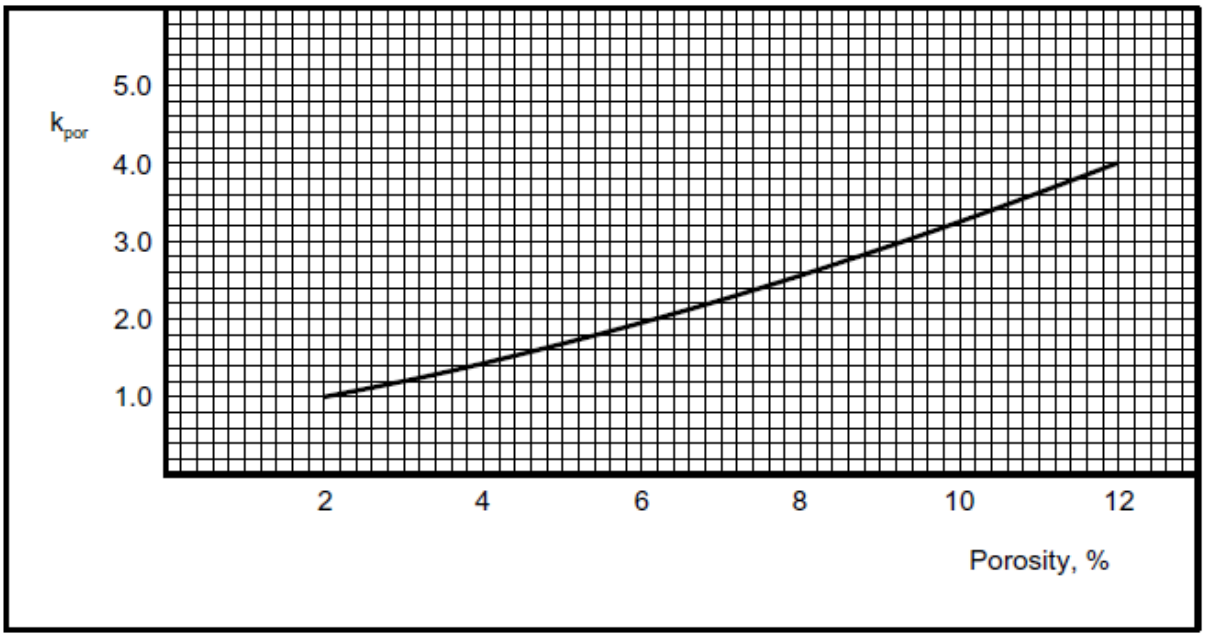

Figure 3.3 – *Correlation between porosity and the correction factor (k_{por}) (Bruland, 2000b).*

It is easily believed that the porosity was accounted for in the DRI, but the porosity's influence on the DRI is negligible for porosities less than 10-12 % (Bruland, 2000b). Porosity has therefore been included as an independent parameter in the NTNU model.

By multiplying the correction factors (k_{DRI} and k_{por}) with the total fracturing factor ($k_{s\text{-}tot}$), the equivalent fracturing factor can be found (Eq. 3.3).

$$k_{ekv} = k_{s-tot} * k_{DRI} * k_{por} \tag{3.3}$$

where

k_{ekv}	*equivalent fracturing factor [-]*
k_{s-tot}	*total fracturing factor [-]*
k_{DRI}	*correction factor for DRI of the rock [-]*
k_{por}	*correction factor for porosity of the rock [-]*

Gross average cutter thrust

In the NTNU-model, the gross average cutter thrust is defined as the total cutterhead thrust divided by the number of cutters. The thrust has a significant influence on the penetration rate. Higher thrust leads to a more efficient energy transfer from the cutterhead to the rock mass, which gives a deeper penetration (Bruland, 2000d). However, there are several factors limiting the applied thrust, as described by Macias (2016):

- Bad steel quality of the cutters.
- High machine vibration level and high instantaneous cutter loads during boring through highly fractured rock or marked single joints (MJS).
- Installed cutterhead power (torque) may limit the applicable thrust at high penetration rates or when boring in fractured rock. This is usually not a problem in modern TBMs.
- Boring in sharp curves or at steep gradients.

Figure 3.4 shows the gross average thrust per cutter as a function of TBM and cutter diameter.

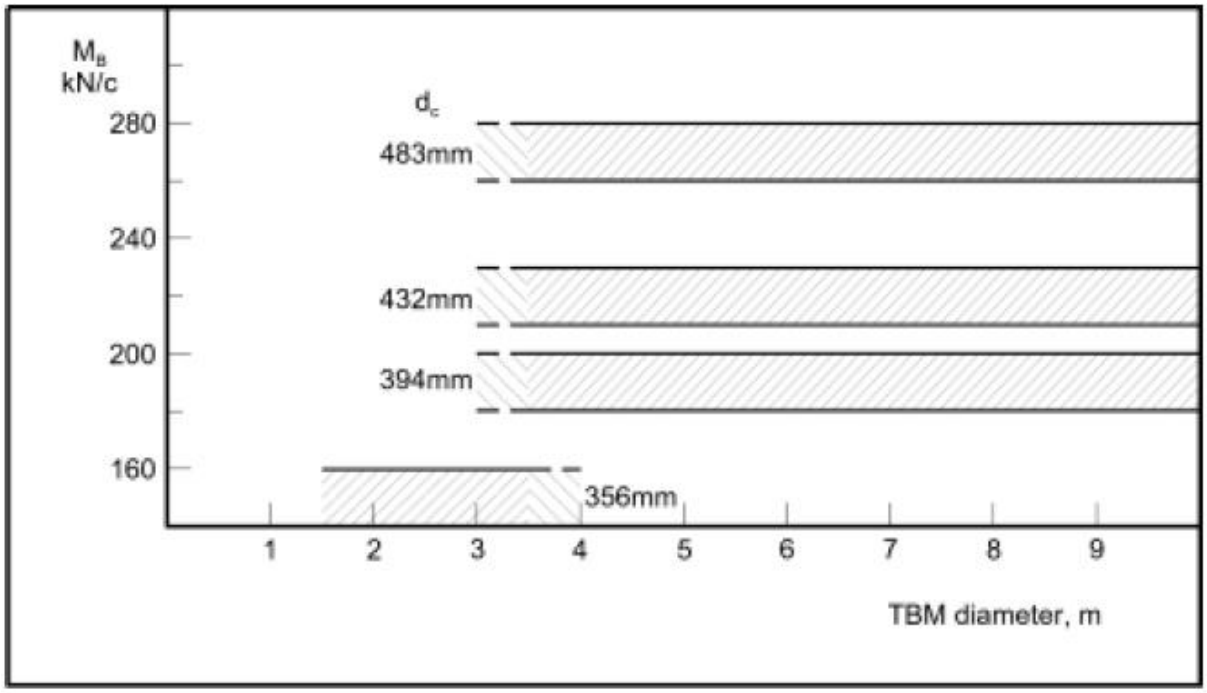

Figure 3.4 – *Recommended maximum gross average thrust per cutter. The upper limit indicated boring in homogenous rock mass, the lower limit indicates boring in medium to very fractured rock (Bruland, 2000b).*

The NTNU model is the only model using gross thrust as input parameter. The model does already account for the friction generated by the shield, which means that the measured friction not have to be subtracted.

Cutterhead velocity (RPM)

The cutterhead velocity (RPM) is measured as the number of revolutions per minute (rev/min), and can be determined from the cutter- and TBM diameter (Fig. 3.5). The NTNU model assumes that the rolling velocity of the outer gauge cutter has approximately the same value as the velocity of the cutterhead (RPM) (Bruland, 2000d). The potential of error in this assumption is great due to limited amount of field data (Bruland 2000d). A correction factor for the RPM has been added in the latest model version (Section 3.1.2).

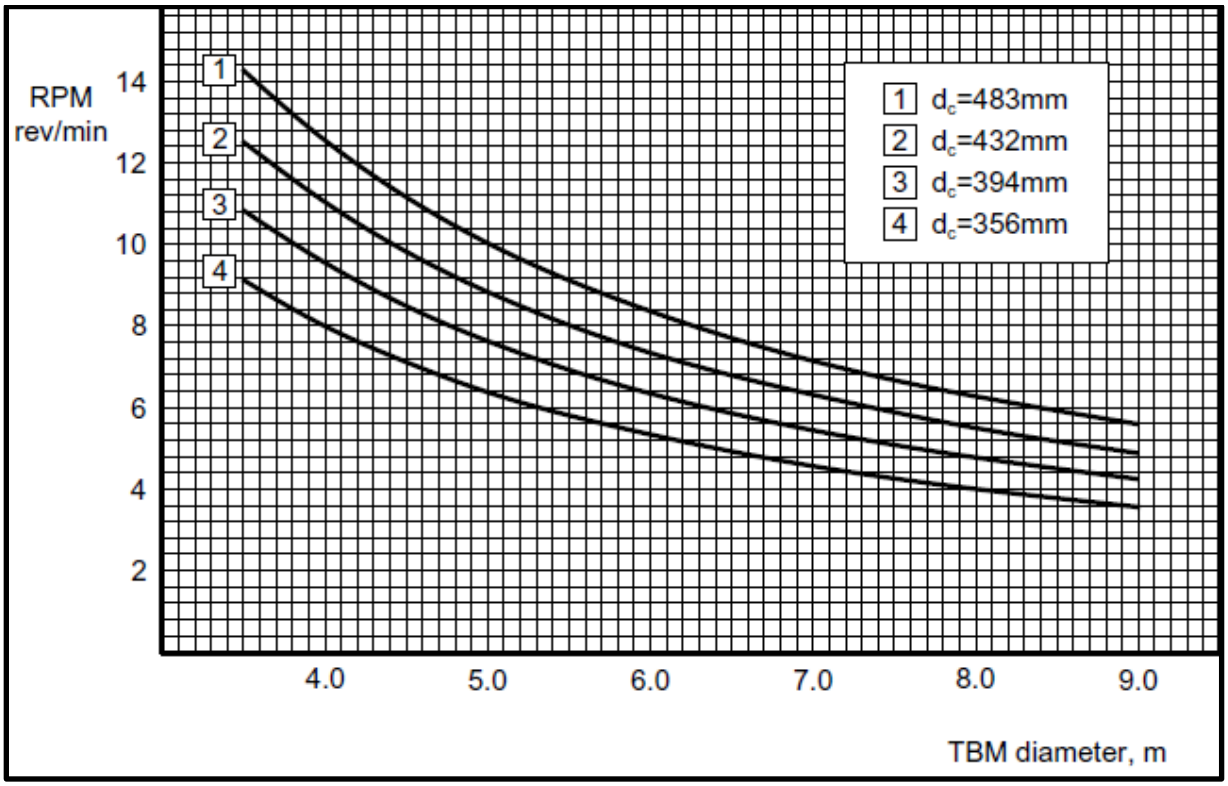

Figure 3.5 – *Relation between cutterhead velocity (RPM) and TBM diameter.*

Cutter diameter

For hard rock applications, Macias (2016) states that the most used cutter disc diameter nowadays is 19 inches (483 mm). This diameter is also the standard in the NTNU model. Over the recent years, cutter diameters have varied between 15,5 inches (394 mm) to 19-20 inches (~500 mm). A larger cutter diameter increases the contact between the cutter ring and the rock, which will demand a greater thrust to induce crack forming rock stresses (Bruland, 2000d).

Number of cutters on the cutterhead

The number of cutters can be determined by the cutter- and TBM diameter (Fig. 3.6). Experience shows that the number of cutters for tunnelling in extremely hard rock conditions correspond to an average cutter spacing of 70 mm (Bruland, 2000d).

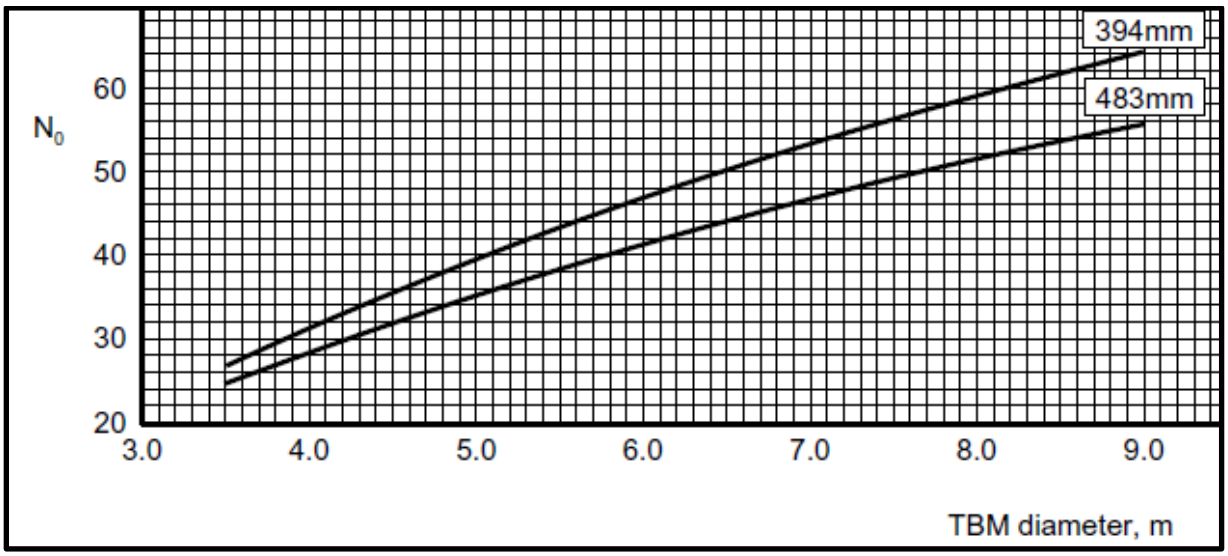

Figure 3.6 – *Relation between normal number of cutters and TBM diameter.*

Average cutter spacing

To calculate the average cutter spacing, the radius of the cutterhead is divided by the number of cutters. Bruland (2000d) shows that there is a linear relationship between the average cutter spacing and the penetration rate, where a reduction in cutter spacing increases the penetration rate. This does not apply if one operates with more than one cutter on each cutter track in the outermost tracks (Bruland 2000d).

Basic penetration rate

According to Bruland (2000d), the basic penetration rate is defined as the advancement of the TBM per revolution. This can be calculated with respect to the equivalent thrust per cutter (M_{ekv}), the critical cutter thrust (M_1) and the penetration coefficient (b). The equivalent thrust is given by the correction factors for cutter diameter and spacing to the applied cutter thrust. The critical cutter thrust is calculated from Figure 3.7 and the penetration coefficient from Figure 3.8.

The basic penetration rate is calculated in Equation 3.4.

$$i_o = \left(\frac{M_{ekv}}{M_1}\right)^b \tag{3.4}$$

where

i_o	*basic penetration rate [mm/rev]*
M_{ekv}	*equivalent cutter thrust [kN/cutter]*
M_1	*critical cutter thrust (necessary to achieve 1 mm/rev) [kN/cutter]*
b	*penetration coefficient [-]*

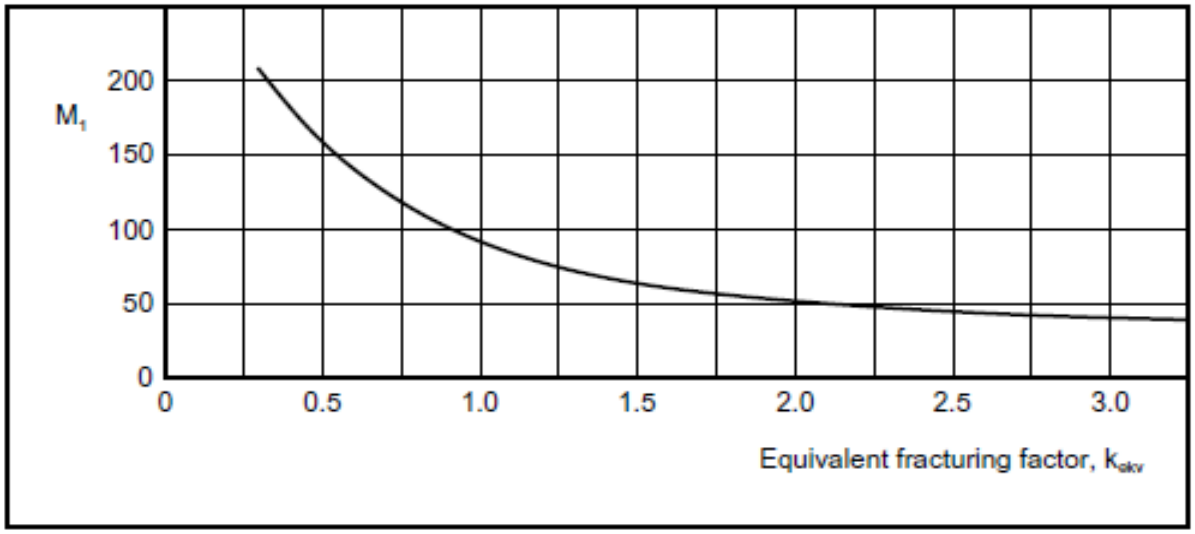

Figure 3.7 – *Critical thrust as a function of the equivalent fracturing factor.*

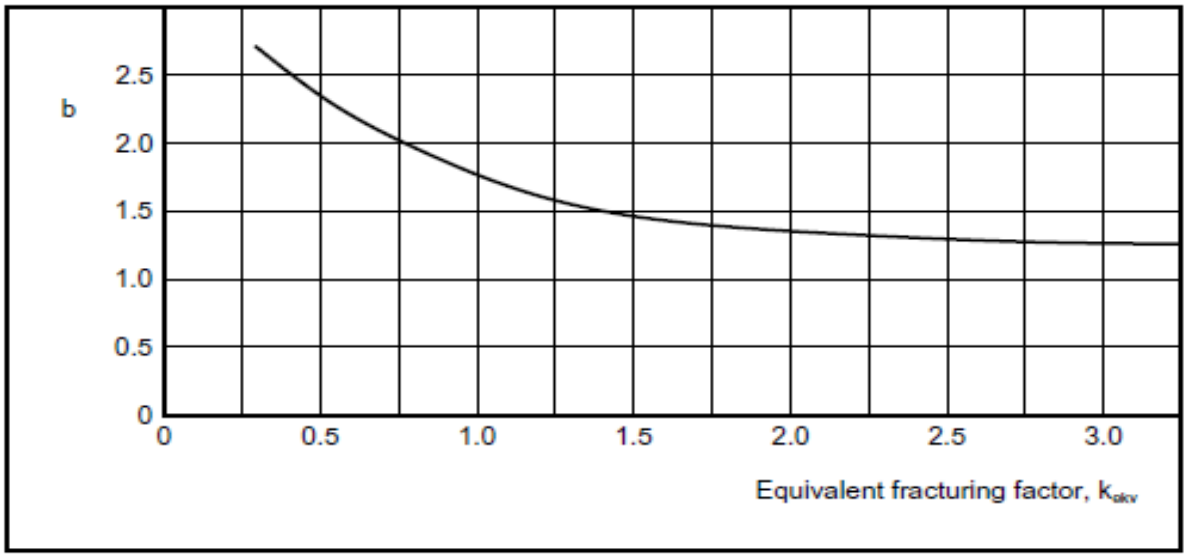

Figure 3.8 – *Penetration coefficient as a function of the equivalent fracturing factor.*

Basic net penetration rate

The basic net penetration rate can be calculated from Equation 3.5 (Bruland, 2000b).

$$I_o = i_o * RPM * \left(\frac{60}{1000}\right) \tag{3.5}$$

where

I_o	*basic net penetration rate [m/h]*
i_o	*basic penetration rate [mm/rev]*
RPM	*cutterhead velocity [rev/min]*

Figure 3.9 shows a flowchart of the procedure described above. The drillability, rock mass boreability, TBM operation and TBM specifications form the basis for calculating the basic net penetration rate.

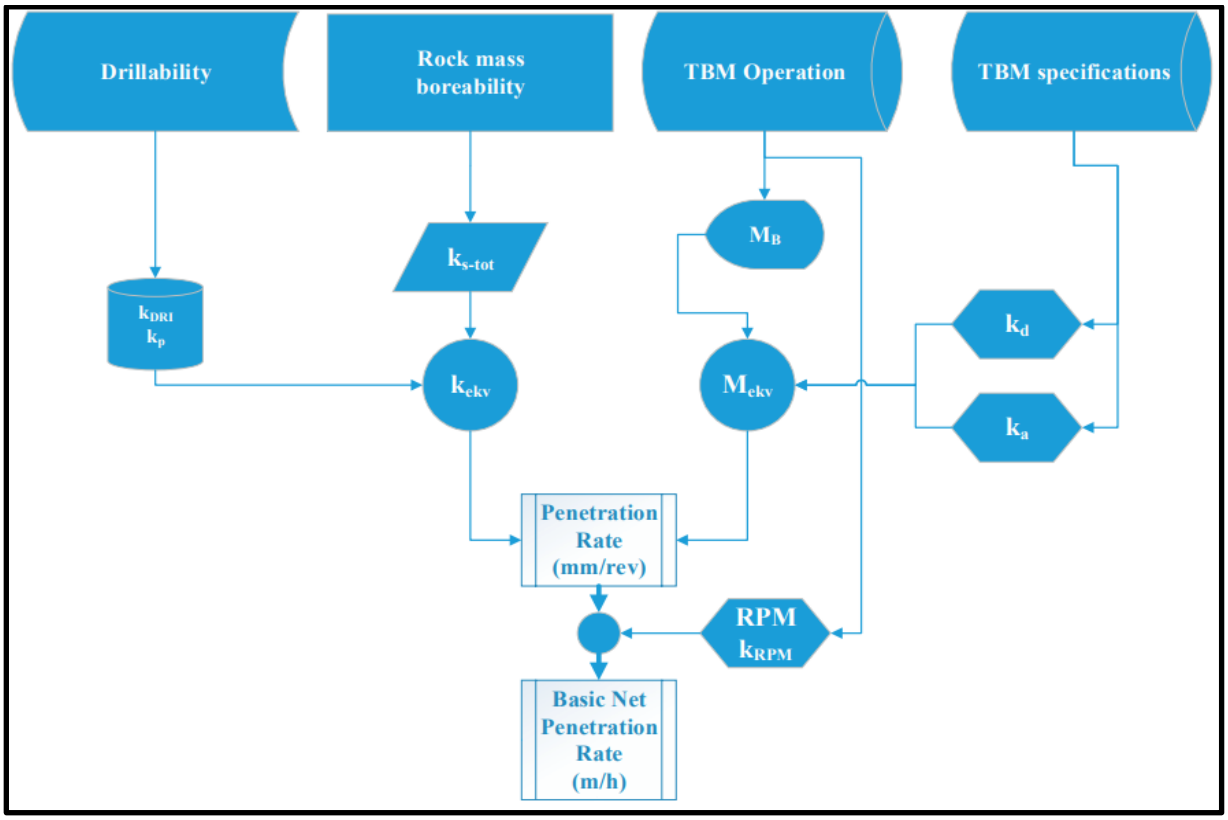

Figure 3.9 – *Performance prediction flowchart generated by the latest version of the NTNU model (Macias, 2016).*

3.1.2 The NTNU model by Macias

Macias (2016) revised the NTNU model. The update includes data from new projects, which increases the empirical basis of the data.

The following factors that impact on the penetration rate have either been revised or extended:

- Standard number of cutters.
- Cutter diameter.
- Installed cutterhead power.
- Recommended applied gross cutter thrust.
- Cutterhead velocity (RPM).
- Intervals for calculating DRI.
- Fracture classes, inclusion for rock masses with low degree of fracturing.
- Graph for estimating the rock mass fracturing factor ($k_{s)}$.
- The DRI correction factor (k_{DRI}).
- The penetration coefficient (b) and the basic penetration (i_0).
- RPM impact on the penetration rate and corresponding correction factor (k_{rpm}).

Rock mass fracturing

Macias (2016) updated the fracture classification, classifying both joints and fissures as "fractures" (Table 3.3).

Table 3.3 – *Fracture classes defined by the spacing between planes of weakness (Macias, 2016)*

Fracture class (Sf)	Average spacing between fractures a_f (cm)	Range class (cm)		Degree of fracturing
0	∞	480	∞	Non-fractured
1	320	240	480	Extremely low
2	160	120	240	Very low
3	80	60	120	Low
4	40	30	60	Medium
5	20	15	30	High
6	10	7.5	15	Very high
7	5	4	7.5	Extremely high

The equivalent fracturing factor (k_{ekv}) is calculated in a similar manner as earlier (Eq. 3.3), using the fracturing factor (k_s) determined from Figure 3.10 and Figure 3.11.

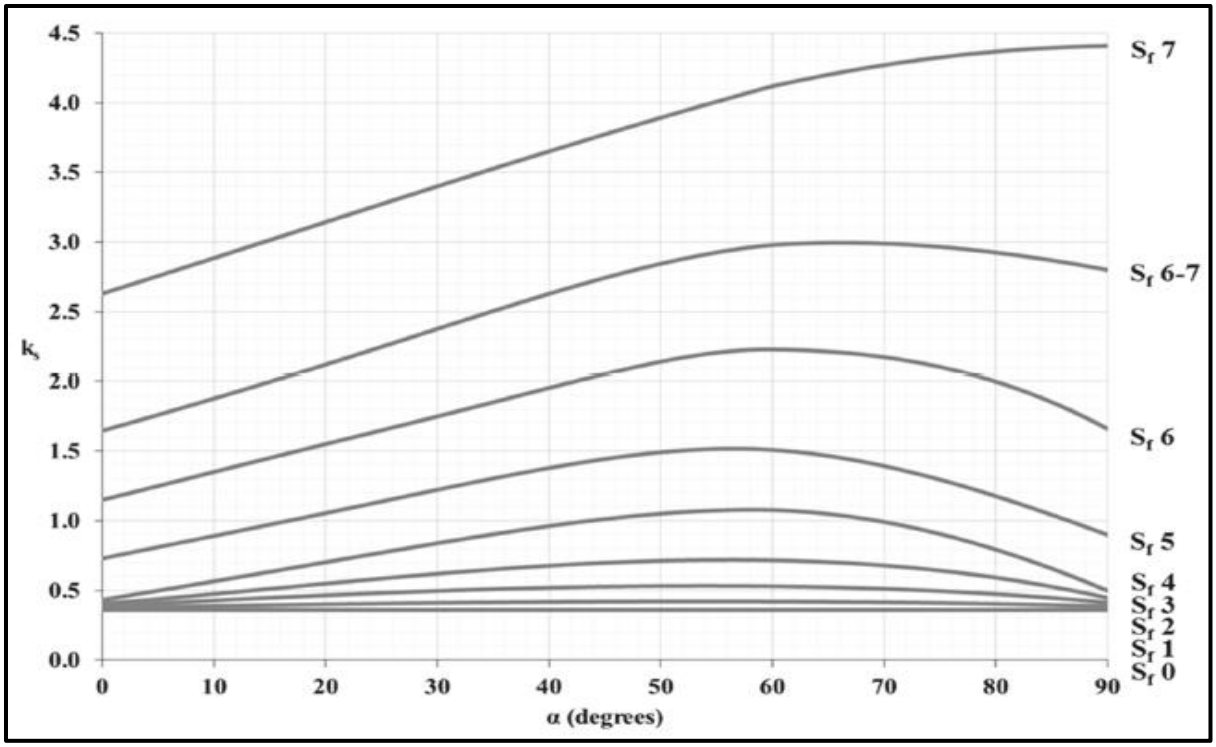

Figure 3.10 – *Rock mass fracturing factor (k_s) as a function of the angle between the tunnel axis and the fractures (Macias, 2016).*

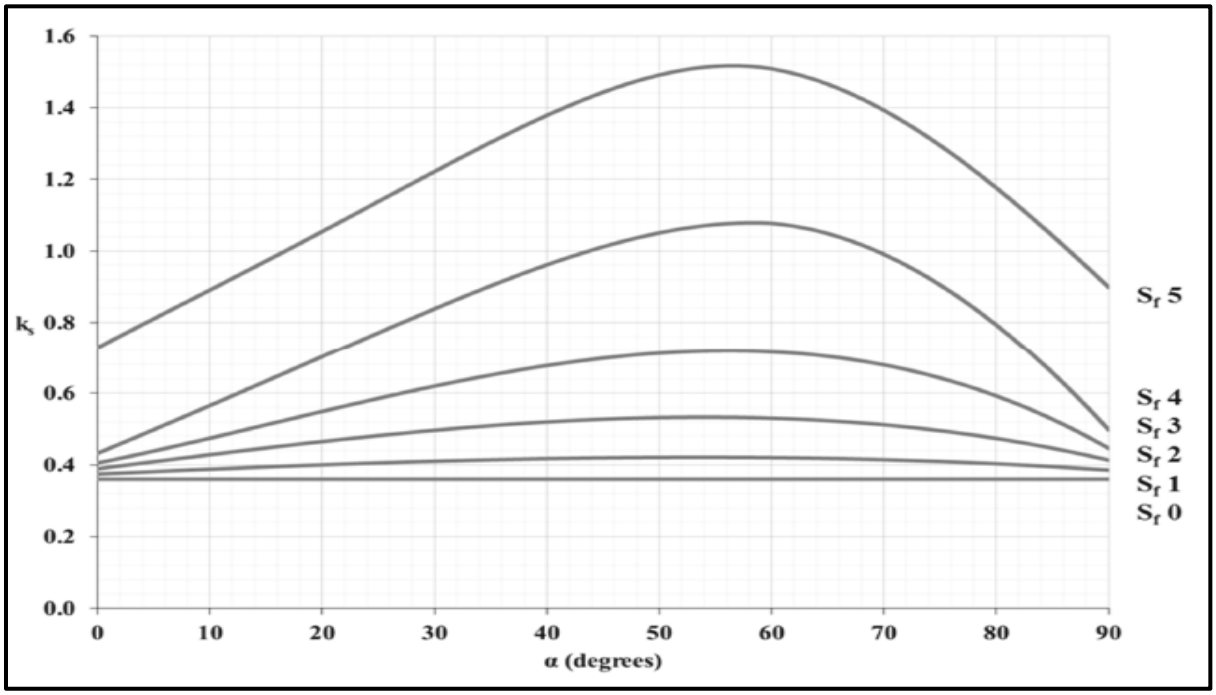

Figure 3.11 – *Rock mass fracturing factor (k_s) as a function of the angle between the tunnel axis and the fractures (for detailed calculations of rock masses with low degrees of fracturing) (Macias, 2016).*

Basic net penetration rate

With the exception of an added correction factor for applied cutterhead velocity (RPM), the calculation of the basic net penetration rate in this version is similar to the calculation described in Equation 3.5. The updated formula is presented in Equation 3.6.

$$\mathrm{I_o} = \mathrm{i_o} * \mathrm{RPM} * \left(\frac{60}{1000}\right) * \mathrm{k_{RPM}} \tag{3.6}$$

where

I_o	*basic net penetration rate [m/h]*
i_o	*basic penetration rate [mm/rev]*
RPM	*cutterhead velocity [rev/min]*
k_{RPM}	*correction factor for applied cutterhead rpm [-]*

Macias (2016) found a correlation between the relative RPM and a correction factor for the applied cutterhead RPM (Fig. 3.12). This correction factor is based on limited amount of empirical data and Macias (2016) recommend using this correlation with caution.

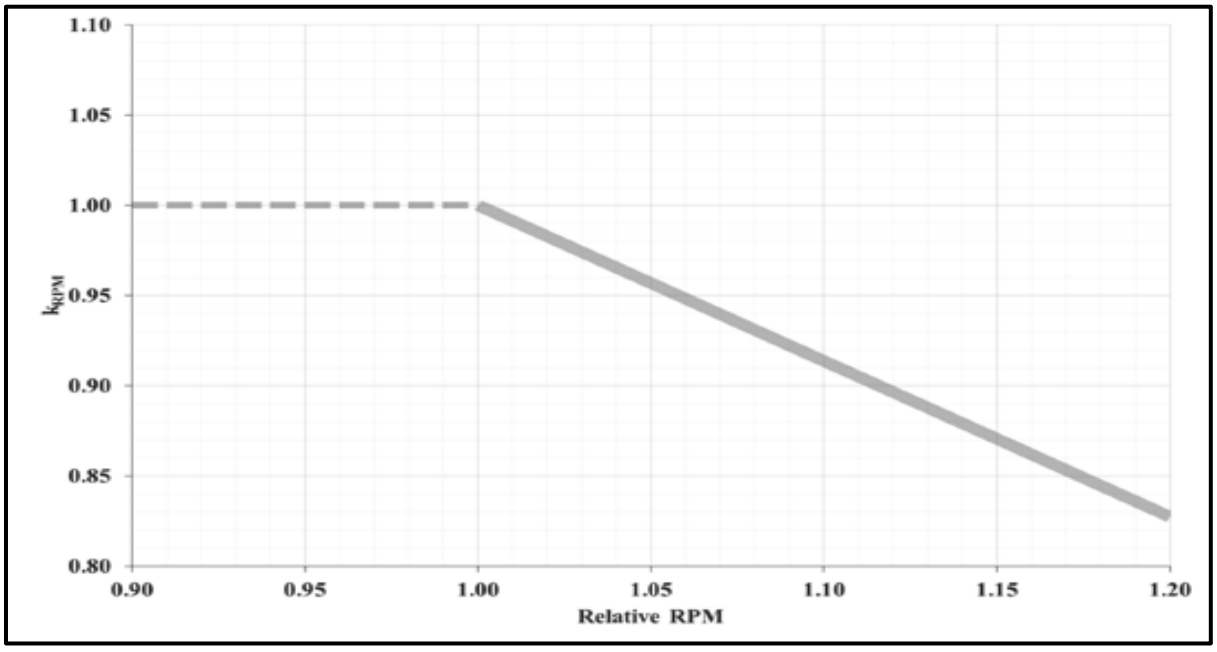

Figure 3.12 – *Correction factor for cutterhead velocity (rpm) illustrating where it differs from the recommended value (Macias, 2016).*

3.1.3 Advantages and disadvantages

The NTNU model by Bruland (2000) and the modified NTNU model by Macias (2016) have both advantages and disadvantages regarding the prediction of penetration rates. Pros and cons regarding these two models are presented in the following:

The NTNU model by Bruland:

+ Accounting for both rock mass and TBM parameters (Farrokh et. al., 2012).
+ Relying on a wide range of empirical data (Farrokh et. al., 2012).
+ Fracturing of rock mass is of major importance (Wilfing, 2016).
- Rely on outdated data, which may reduce their potential for performance prediction (Macias, 2016).
- Some of the parameters are commonly not determinable outside of Norway (e.g. cutter life index CLI) (Wilfing, 2016).
- The model does not cover the entire range of rock mass types that occur in nature, e.g. issues regarding degrees of fracturing, rock-breaking processes and influence of groundwater or rock mass stress on boreability (Macias, 2016).

The NTNU model by Macias:

+ Same as pros described regarding the NTNU model by Bruland (2000).
+ More field data from recent tunnel projects implemented in the empirical database, which led to updates, revisions and extensions (Macias, 2016).
- Same cons described regarding the NTNU model by Bruland (2000).
- More data from actual tunnelling projects are required in order to verify the influence of the corrosion on the rock`s abrasion rates (Macias, 2016).

3.2 The Colorado School of Mines (CSM) model

The Colorado School of Mines (CSM) model was first published in 1977 by Ozdemir et.al. The model was designed to be an analytical penetration prediction model based on performing laboratory tests at the Earth Mechanics Institute in Golden, Colorado. Results from these tests have been compared with TBM field data in order to include practical findings. In 1997, Rostami updated the original model and created the most established version of the model. He revised several formulas and gathered new data with constant cross-section cutters (Wilfing, 2016).

The philosophy behind this model is to first start from the individual cutter forces acting on the rock mass, then determine the overall cutterhead thrust- and power requirements to obtain the maximum rate of penetration (Rostami & Ozdemir, 1993). By comparing these estimated values with the installed machine parameters, the maximum obtainable rate of penetration will be achieved (Yagiz et al., 2012).

3.2.1 The CMS model by Rostami

To find the total force per cutter (Eq. 3.9), the angle and pressure of the contact area need to be calculated from Equation 3.7 and Equation 3.8.

$$\Phi = \cos^{-1} * \left(\frac{\mathrm{R} - \mathrm{P}}{\mathrm{R}}\right) \tag{3.7}$$

where

Φ	*angle of contact [rad]*
R	*cutter radius [mm]*
P	*penetration rate [mm/rev]*

$$P^0 = C * \sqrt[3]{\frac{S * \sigma_u^2 * \sigma_t}{\Phi * \sqrt{R * T}}} \tag{3.8}$$

where

P^0	*pressure of contact area [MPa]*
C	*cutting coefficient (approx. 2.12) [-]*
S	*spacing of cutters [mm]*
σ_u	*uniaxial compressive strength [MPa]*
σ_t	*brazilian tensile strength [MPa]*
T	*cutter tip width [mm]*

$$F_t = \left(\frac{T * R * \Phi * P^0}{(1 + \Psi) * 1000}\right) \tag{3.9}$$

where

F_t	*total thrust per cutter [kN/cutter]*
Ψ	*stress distribution factor (usually between 0.2 to -0.2) [-]*

When knowing the total force, the normal- and rolling force can be calculated from Equations 3.10 and 3.11.

$$F_n = F_t * \cos(\frac{\Phi}{2}) \tag{3.10}$$

$$F_r = F_t * \sin(\frac{\Phi}{2}) \tag{3.11}$$

where

F_n	*normal thrust per cutter [kN/cutter]*
F_r	*rolling thrust per cutter [kN/cutter]*

As mentioned, the model is based on comparing estimated thrust- and power requirements with machine values. To estimate these values, the following steps have to be performed:

$$\mathrm{Th}^* = \sum_{1}^{N} \mathrm{F_n} \approx \mathrm{N} * \mathrm{F_n} \tag{3.12}$$

$$\mathrm{Tq}^* = \sum_{1}^{N} \mathrm{F_r} \approx 0{,}3 * \mathrm{D} * \mathrm{N} * \mathrm{F_r} \tag{3.13}$$

$$\mathrm{RPM} = \frac{\mathrm{V}}{\pi * \mathrm{D}} \tag{3.14}$$

$$\mathrm{P}^* = \frac{\pi}{30} * \mathrm{Tq}^* * \mathrm{RPM} \tag{3.15}$$

where

Th^*	*total thrust requirement [kN]*
Tq^*	*total torque requirement [kNm]*
D	*TBM diameter [m]*
N	*number of cutters [-]*
RPM	*rotational speed [rev/min]*
V	*linear velocity limit of the cutters [-]* *(160 m/min for 482 mm diameter cutter)*
P^*	*power requirement [kW]*

The penetration rate can be found by adjusting the penetration parameter in Equation 3.7 until one of the requirements have been reached. This is considered as the maximum penetration per revolution that is possible to achieve with the present rock and machine parameters (Yagiz et. al, 2012).

3.2.2 The MCSM model by Yagiz

In 2002, Yagiz introduced new aspects to the CSM model, known as the modified CSM model (MCSM). This model calculates the rate of penetration using a brittleness index (BI), the distance between weakness planes (F_s) and the angle between the weakness planes (α). According to Yagiz (2009), one can predict the brittleness index using density-, UCS- and BTS values (Eq. 3.16)**.** In an ideal situation, one would perform a laboratory test to find this parameter.

$$\mathrm{BI_P} = (0.198 * \sigma_u) - (2.174 * \sigma_t) + (0.913 * \rho) - 3.807 \qquad (3.16)$$

where

BI_P	*predicted brittleness [kN/mm]*
ρ	*density [kN/m^3]*
σ_u	*uniaxial compressive strength [MPa]*
σ_t	*brazilian tensile strength [MPa]*

The penetration rate from the MCSM model can be calculated from Equation 3.17.

$$\mathrm{ROP} = 0.272 + \left(0.027 * \mathrm{BI_p}\right) - (0.225 * \mathrm{F_s}) + (0.437 * \log(\alpha)) + (0.097 * \mathrm{CSM_{ROP}}) \qquad (3.17)$$

where

ROP	*rate of penetration [m/h]*
CSM_{ROP}	*result from CSM-model [m/h]*
BI_P	*predicted brittleness [kN/mm]*
F_s	*distance between planes of weakness [m]*
α	*angle between the plane of weakness and TBM driven direction [°]*

3.2.3 Advantages and disadvantages

The Colorado School of Mines (CSM) model, as well as the modified model (MCSM), have both advantages and disadvantages regarding the prediction of penetration rates. Pros and cons regarding these two models are presented in the following:

CSM model by Rostami:

+ Accounts for both rock mass and TBM parameters (Farrokh et. al., 2012).
+ Relies on good database (Farrokh et. al., 2012).
+ Good estimations for massive rock conditions where the rock strength has the greatest impact on the rate of penetration (Yagiz, 2012).
- Several parameters and complex relationships (Farrokh et. al., 2012).
- Bad predictions for heavily fractured rock mass conditions (Farrokh et. al., 2012).
- No parameters which describe the rock mass fracturing are included (Rostami, 1997).

MCSM model by Yagiz:

+ Same pros as described regarding the CSM model.
+ Based on a database obtained from several mechanical tunnelling projects, which takes rock mass fracturing into account (Yagiz, 2012).
- Needs to perform punch penetration tests to determine brittleness index (BI), which is commonly not used in European rock mechanic laboratories (Wilfing, 2016).

3.3 The Gehring model

The Gehring model was first published by Karlheinz Gehring in 1995 and has since been updated several times. The model is based on empirical data with data gathered from four projects: two in South-Africa and two in South-Korea (Brino et al., 2015). From these analyses, a number of correction factors have been created and later implemented in the formula. The correction factors take rock mass properties, as well as cutterhead types and geometries, into consideration.

In 2016, Wilfing compared the Gehring model and the CSM model with the results from 30 penetration tests and geological mapping at two tunnel projects. It was found that the model needed to be updated. The updates included incorporations of a critical y-axis offset, as well as correcting factors for rock toughness and discontinuous pattern result. The result was a new prognosis tool called the "Alpine model", which is based on the existing Gehring model (Wilfing, 2016). The acquisition of the original version of the model by Gehring (1995) has not been successful. Therefore, the model by Wilfing (2016) has been used to describe both the model by Gehring and Wilfing.

3.3.1 The Gehring model by Gehring

To calculate the penetration rate (which represents the maximum penetration for a given normal force per cutter), Equation 3.18 needs to be followed (Wilfing, 2016).

$$p = \frac{F_N}{\sigma_u} * k_i \tag{3.18}$$

where

p	*penetration rate [mm/rev]*
F_N	*net thrust per cutter [kN/cutter]*
σ_u	*uniaxial compressive strength [MPa]*
k_i	*correction factors [-]*

The k_i parameter from Equation 3.18 includes the following correction factors:

k_0	*basic penetration [-]*
k_1	*specific failure energy [-]*
k_2	*rock mass fabric [-]*
k_3	*state of stress in rock mass [-]*
k_4	*cutter diameters ≠ 432 mm (17") [-]*
k_5	*cutter spacing ≠ 80 mm [-]*

These six factors are described in the following (Wilfing, 2016):

k_0 = basic penetration

To generalize a more complicated formula presented by Gehring in 1995, the basic penetration factor is set to 4.0 for machines with a certain setup of 17" (432 mm) cutters and 80 mm spacing. Equation 3.19 shows how the basic penetration factor is calculated. The penetrating coefficient a = 800 and exponent b = 1 originates from different approaches, such as Gehring, Farmer, Sanio and NTH (Wilfing, 2016).

$$k_0 = a * \sigma_u^{-b} = 800 * 200^{-1} = 4.0 \tag{3.19}$$

where

k_0	*correction factor for basic penetration [-]*
a	*penetration coefficient (=800) [-]*
b	*penetration exponent (=1) [-]*
σ_u	*uniaxial compressive strength (set to ~200 kN/c) [MPa]*

According to TBM experts at the Follo Line Project, a basic penetration factor of 4.0 is sufficient to use in the calculations, although the machine setup is different.

k_1 = specific failure energy

Documented data shows that fracture energy (W_f) is a parameter that influences the penetration rate of rock masses. The fracture energy that is needed to cause failure of a specimen under uniaxial compression is called the specific failure energy (w_f), and is of importance regarding the penetration of a rock. This is accounted for in the k_1 correction factor, calculated by Equation 3.20 and 3.21.

$$w_f = \frac{W_f}{\sigma_u} \tag{3.20}$$

where

w_f	*specific failure energy [m^3 10^{-6}]*
W_f	*failure energy [Nm]*
σ_u	*uniaxial compressive strength [MPa]*

$$k_1 = 0{,}475 * w_f^{-0{,}56} \tag{3.21}$$

where

k_1	*correction factor for specific failure energy [-]*
w_f	*specific failure energy [m^3 10^{-6}]*

k_2 = rock mass fabric

The rock mass fabric is accounted for in the third correction factor. Spacing and orientation of schistosity, foliation, joints or other planes of weaknesses is considered as important regarding the rate of penetration (Gehring, 1995). Regarding the distances between the planes of weaknesses, only the distances smaller than 50 cm are expected to influence the penetration rate (Wilfing, 2016).

The orientation is calculated by the dip angle, strike angle and tunnel direction, and is defined as the smallest angle between the tunnel axis and the discontinuity (Eq. 3.22).

$$\alpha = \sin^{-1}\left(\sin \alpha_f * \sin\left(\alpha_t - \alpha_s\right)\right) \tag{3.22}$$

where

α	*smallest angle between tunnel axis and discontinuity [°]*
α_f	*dip angle discontinuity [°]*
α_t	*strike angle discontinuity [°]*
α_s	*tunnel direction [°]*

When the orientation and the spacing of the weakness planes are known, the k_2 correction factor can be found from Table 3.4:

Table 3.4 – *Correction factor k_2 depending on spacing and orientation of discontinuity relative to tunnel axis in terms of α-angle (Wilfing, 2016).*

Spacing of discontinuity	Correction factor k_2 at α			
	0°	30°	60°	90°
> 50 cm	1.0	1.0	1.0	1.0
10 – 50 cm	1.2	1.3	1.6	1.3
5 – 10 cm	1.4	1.8	2.3	1.6
< 5 cm	1.7	2.3	3.0	2.0

k_3 = state of stress in rock mass

This correction factor is especially important in projects with high horizontal stresses (Wilfing, 2016). Because of the relatively low overburden at the Follo Line Project, it is not expected that there will be any stress regime worth correcting for.

k_4 = cutter diameters ≠ 432 mm (17")

When Gehring (1995) made his formula, he based his calculations on a machine setup of 432 mm cutter diameter. To correct for deviating sizes, a linear correlation between cutter diameter and penetration rate was made (Eq. 3.23).

$$k_4 = \frac{430}{d_c} \tag{3.23}$$

where

k_4	*correction factor for cutter diameters ≠ 432 mm [-]*
d_c	*cutter diameter [mm]*

k_5 = cutter spacing ≠ 80 mm

For the same reason there exists a correction factor for cutter diameter, there also exists a correction factor for cutter spacing ≠ 80 mm. This is shown in Figure 3.13.

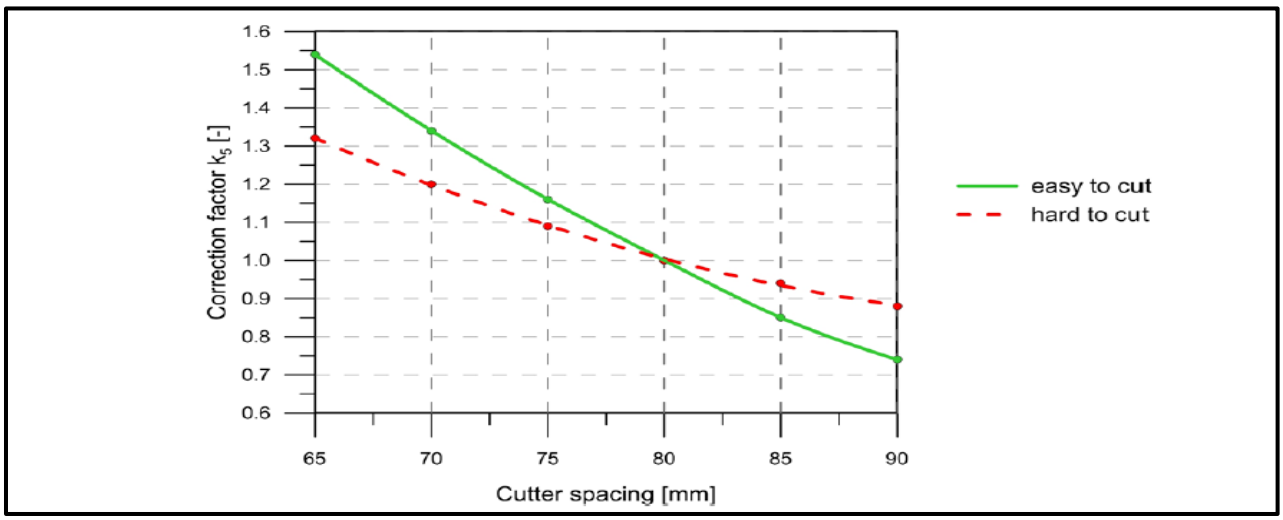

Figure 3.13 – *Correction factor k_5 and cutter spacing as a function of drillabillity (Wilfing, 2016).*

3.3.2 The Alpine model by Wilfing

The Alpine model presented by Wilfing in 2016 is based on the already described model by Gehring (1995). Some revisions and extensions have been made, where the most important ones are presented in the following. The Alpine model formula (modified Gehring model) is presented in Equation 3.24**,** and the y-intercept BTS approach is presented in Equation 3.25.

$$p = \frac{F_N - b_{BTS}}{\sigma_u} * k_0 * k_2 * k_i + 3 \tag{3.24}$$

$$b_{BTS\ 3mm} = e^{0.08 * \sigma_t + 4.1} = y - intercept_{BTS\ 3mm} \tag{3.25}$$

where

p	*penetration rate [mm/rev]*
F_N	*net thrust per cutter [kN/cutter]*
$b_{BTS\ 3mm}$	*y-intercept BTS approach at penetration 3 mm/rev [-]*
k_0	*correction factor for basic penetration (=4.0) [-]*
k_2	*correction factor for discontinuity pattern [-]*
k_i	*further correction factors for geotechnical/machine parameters [-]*
σ_t	*brazilian tensile strength [MPa]*

See Chapter 3.3.1 for detailed description of the correction factors.

According to Wilfing (2016), it must be noted that the correction factor for the state of stress is not yet defined. The basic correction factor (k_0) and correction factor for discontinuity pattern (k_2) is implemented into the modified model, to prevent too steep gradients (Wilfing, 2016). Wilfing (2016) demonstrates that the Alpine model strongly improves the version by Gehring, especially since the y-intercept is of major importance to reflect the actual relation between the applied force and resulting penetration.

3.3.3 Advantages and disadvantages

The Gehring model and the Alpine model have both advantages and disadvantages regarding the prediction of penetration rates. Pros and cons regarding these models are presented in the following:

The Gehring model by Gehring

+ Accounts for both rock mass and TBM parameters (Farrokh et. al., 2012).
+ Empirical origin leads to results close to the reality (Wilfing, 2016).
+ Easy to determine the input parameters (Wilfing, 2016).
+ Flexible revision potential because of the modular structure, where each correction factor can be considered independent from one another (Wilfing, 2016).
- Small data set for original regression analyses (Wilfing, 2016).
- Based on literature and data from before 1995 (Wilfing, 2016).
- Correction factors do not reflect actual conditions, since only one discontinuity system is considered and the effect of intersecting systems in the penetration is neglected (Wilfing, 2016).

The Alpine model by Wilfing

+ Same as pros described regarding the Gehring model.
+ Bigger dataset and more empirical data for the analyses (Wilfing, 2016).
+ Revision of correction factors that take the effect of intersection systems into consideration (Wilfing, 2016).
- Investigations are based on only one tunnel project with narrow range of rock types, and must be validated by further data (Wilfing, 2016).
- Low regression coefficient of the Brazilian tensile strength (Wilfing, 2016).
- Still need for an extended determination table for proposed correction factors k_2 (Wilfing, 2016).

3.4 The Q_{tbm} model by Barton

The Q_{tbm} model by Barton (2000) is based on the already developed and well-known Q-system for rock mass classification (Eq. 3.26). In Norway, the Q-system is widely used in drill & blast projects to classify rock masses with respect to stability of underground openings. Based on the estimations of six parameters, a Q-value can be estimated, where different Q-values are related to different types of permanent support (NGI, 2015).

$$Q = \frac{RQD}{J_n} * \frac{J_r}{J_a} * \frac{J_w}{SRF} \tag{3.26}$$

where

RQD	*degree of fracturing (rock mass designation) [%]*
J_n	*joint set number [-]*
J_r	*joint roughness number [-]*
J_a	*joint alteration number [-]*
J_w	*joint water reduction factor [-]*
SRF	*stress reduction factor [-]*

When applying this Q-value to a TBM project, Barton (2000) had to modify the RQD to a tunnelling oriented direction (RQD_0). The Q_0-value is calculated from Equation 3.27.

$$Q_0 = \frac{RQD_0}{J_n} * \frac{J_r}{J_a} * \frac{J_w}{SRF} \tag{3.27}$$

The RQD_0-parameter is assumed identical to RQD, which had to be mapped in the cross passages. The RQD-mappings done by OTV (Chapter 4.3.1.4) are directly transferrable to the correct RQD_0-value.

In addition to the Q_0-value, Barton (2000) has added other parameters when modifying the Q-value to a Q_{TBM} model. One of these are the parameter called SIGMA, which is dependent on the joint inclination angle (β). When the inclination is unfavorable, $SIGMA_{cm}$ is applied (Eq. 3.28). When the inclination is favorable, SIGMAtm is applied (Eq. 3.29).

$$\mathrm{SIGMA_{cm}} = 5\gamma \mathrm{Q_c^{1/3}}, \text{where } \mathrm{Q_c} = \mathrm{Q_0} * \frac{\sigma_c}{100} \tag{3.28}$$

where

$SIGMA_{cm}$	*rock mass strength with unfavorable inclination [MPa]*
γ	*density [g/cm^3]*
σ_c	*uniaxial compressive strength [MPa]*

$$\mathrm{SIGMA_{tm}} = 5\gamma \mathrm{Q_t^{1/3}}, \text{where } \mathrm{Q_t} = \mathrm{Q_0} * \frac{\mathrm{I_{50}}}{4} \tag{3.29}$$

where

$SIGMA_{tm}$	*rock mass strength with favorable inclination [MPa]*
γ	*density [g/cm^3]*
I_{50}	*point load index [-]*

The final Q_{TBM} model is presented in Equation 3.30.

$$\mathrm{Q_{TBM}} = \mathrm{Q_0} * \frac{\mathrm{SIGMA}}{\mathrm{F^{10}}/_{20^9}} * \frac{20}{\mathrm{CLI}} * \frac{\mathrm{q}}{20} * \frac{\sigma_\theta}{5} \tag{3.30}$$

where

F	*net thrust per cutter [tnf/cutter]*
CLI	*cutter life index [-]*
q	*quartz content [%]*
σ_θ	*biaxial stress on tunnel face [MPa]*

According to Barton (2000), the net penetration rate (NPR) can be calculated using the Q_{TBM}-value (Eq. 3.31):

$$NPR \approx 5 * Q_{TBM}^{-1/5} \quad (3.31)$$

where

NPR *net penetration rate [m/h]*

3.4.1 Advantages and disadvantages

The Q_{tbm} model by Barton (2000) has both advantages and disadvantages regarding the prediction of penetration rates. Pros and cons regarding the model are presented in the following:

+ Empirical origin based upon 145 TBM tunnels leads to results close to the reality (Barton, 2000)
+ Easy to determine most of the input parameters (Wilfing, 2016).
+ The model is modified with respect to a TBM-excavated tunnel, e.g. introduction of the RQD_0-value (Barton, 2000).
- Based on the Q-system which originally is made for classification of rock masses excavated by drill & blast (NGI, 2015).
- Fewer joints visible in tunnels excavated by TBM will influence the RQD-value. The joint roughness number (J_r) and joint alteration number (J_a) will also be influenced, which will have further influence on the Q-value (NGI, 2015).
- Some of the parameters are commonly not determinable outside of Norway (e.g. cutter life index CLI), or are not strictly defined (e.g. rock mass strength SIGMA) (Wilfing, 2016)
- It is not common to perform stress tests along the tunnel alignment. Calculations by using the overburden are therefore necessary.

3.5 The prediction model by Yagiz

Yagiz presented in 2008 a study that was attempted to develop a more accurate and practical predictive equation. This was especially adapted to jointed/faulted hard rock conditions. The formula is based on data from only one tunnel project; the Queens Water Tunnel in New York:

$$\mathrm{ROP} = 1.093 + 0.029 * \mathrm{PSI} - 0.003 * \mathrm{UCS} + 0.437 * \log(\alpha) - 0.219 * \mathrm{DPW} \qquad (3.32)$$

where

PSI	*peak slope index (Eq. 3.16) [kN/mm]*
UCS	*uniaxial compressive strength [MPa]*
α	*smallest angle between tunnel axis and discontinuity [°]*
DPW	*distance between planes of weakness [m]*

3.5.1 Advantages and disadvantages

+ Easy to calculate and few lab tests need to be performed (Yagiz, 2008).
+ The empirical obtained formula has a good correlation coefficient (r = 0.82).
- No applied machine data included.
- Equation was achieved based on only one project (Yagiz, 2008).

3.6 The prediction model by Hassanpour et al.

In 2011, Hassanpour, Rostami and Zhao published "a new hard rock TBM performance prediction model for project planning" in the journal *Tunnelling and Underground Space Technology*. This new model is based on a database of actual machine performance from different hard rock TBM tunnelling projects. Relationships between different geological- and TBM operational parameters have been investigated and further analyzed using both single- and multi-variable regression techniques (Hassanpour et al., 2011).

158 tunnel sections have been selected for the study, originating from three water conveyance tunnels in Iran as well as Manapouri Second Tailrace Tunnel. These tunnels have been constructed in different rock types including sedimentary, igneous and metamorphic rocks with a wide range of rock strengths (Hassanpour et al., 2011).

Equations calculating the Field Penetration Index (FPI) and the Rate of Penetration (ROP) have been developed on an empirical basis. The equations are presented below (Eq. 3.33 and 3.34).

$$\mathrm{FPI} = e^{((0.008*\mathrm{UCS})+(0.015*\mathrm{RQD})+1.384} \tag{3.33}$$

where

FPI	*field penetration index [kN/cutter/mm/rev]*
UCS	*uniaxial compressive strength [MPa]*
RQD	*degree of fracturing (rock quality designation) [MPa]*

Further, the rate of penetration (ROP) can be calculated from Equation 3.31.

$$\mathrm{ROP} = \frac{0.06 * \mathrm{F_N} * \mathrm{RPM}}{\mathrm{FPI}} \tag{3.34}$$

where

ROP	*rate of penetration [MPa]*
F_N	*average disk cutter load [kN]*
RPM	*rotational speed [rev/min]*
FPI	*field penetration index [kN/cutter/mm/rev]*

Hassanpour et al. (2011) presented a FPI chart that can be used for a quick estimation of FPI values in different rock conditions. The chart is presented in Figure 3.14.

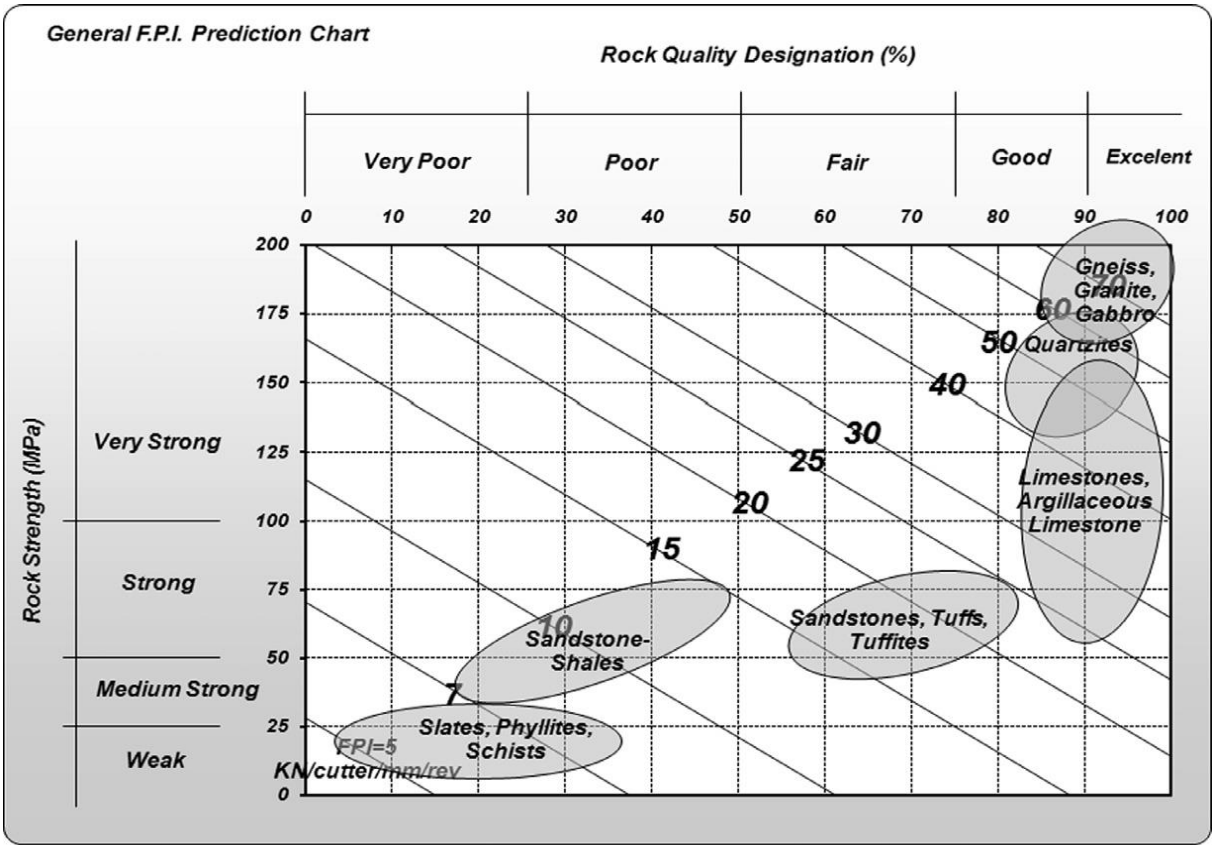

Figure 3.14 - *Chart for estimating Field Penetration Index (FPI) based on rock mass properties derived from Equation 3.33. (Hassanpour et al., 2011).*

3.6.1 Advantages and disadvantages

The model by Hassanpour et al. (2011) has both advantages and disadvantages regarding the prediction of penetration rates. Pros and cons regarding the model are presented in the following:

+ Both single and multi-variable regression analyzes were used to develop empirical equations (Hassanpour et al., 2011).

+ Applicable at a wide range of geological conditions (Hassanpour et al. 2011).

- Based on only four tunnel projects (Hassanpour et al. 2011).

- The model must be applied with caution in highly fractured rock masses and water sensitive rocks like marlstones and mudstones (Hassanpour et al. 2011).

3.7 The prediction model by Farrokh et al.

Farrokh, Rostami and Laughton discuss the development of new models to support an improved level of predictive accuracy in penetration rate estimation (Farrokh et al. 2012).

A new prediction model was generated based on data from more than 300 TBM projects, and contains several formulas calculating the rate of penetration. The results from these formulas were compared with actual projects, to ensure the model's capability for predicting penetration rates (Farrokh et al., 2012).

Farrokh et al. (2012) presented two methods to calculate the rate of penetration:

- Regression analysis with PRev as the objective parameter. PRev is defined as the penetration rate per revolution (mm/rev).

- Provide the PR directly. PR is defined as the penetration rate (m/h).

The first method has been applied in this thesis, in which it gave the most promising results.

Both methods include numerical codes for rock type (RT_c) and rock quality designation (RQD_c). The rock type categorization is presented in Table 3.5.

Table 3.5 – *Rock type categorization (RT_c) in database, modified from Farrokh et al. (2012).*

Rock Type (RT)	Code	Numerical code (RT_c)
Claystone, mudstone, marl, slate, phyllite, argillite	C	5
Sandstone, siltstone, conglomerate, quartzite	S	3
Limestone, chalk, dolomite, marble	L	3
Karstic Limestone	K	3
Metamorphic rocks such as gneiss and schist	M	2
Coarse igneous such as granite and diorite	G	1
Fine volcanic such as basalt, tuff and andesite	V	2

The rock quality designation classification (RQD_c) is presented in Table 3.6.

Table 3.6 – *RQD categorization (RQD_c) in database (Farrokh et al. 2012).*

CFF	Code	Description	Corresponding RQD range
Less than 8 fractures/m	S or 1	Low frequency	90 - 100
8-12 fractures/m	M or 2	Medium frequency	60 - 90
12-16 fractures/m	H or 3	High frequency	< 60

PRev as the objective parameter

Multivariable regression analyses with PRev as the objective parameter were performed using Minitab 16. By finding the PRev-value, one can easily find the PR by multiplying with the cutterhead velocity (RPM) of the TBM. The calculations are presented in Equations 3.35 and 3.36.

$$\mathrm{PRev} = e^{0.41 + (0.404 * \mathrm{D}) - (0.027 * \mathrm{D}^2) + (0.0691 * \mathrm{RT_c}) - (0.00431 * \mathrm{UCS}) + (0.0902 * \mathrm{RQD_c}) + (0.000893 * \mathrm{F_n})} \quad (3.35)$$

where

PRev	*penetration rate per revolution [mm/rev]*
D	*tunnel diameter [mm]*
RT_c	*rock type numerical code (Table 3.5) [-]*
UCS	*uniaxial compressive strength [MPa]*
RQD_c	*rock quality designation numerical code (Table 3.6) [-]*
F_n	*disc cutter normal force [kN]*

$$\mathrm{PR} = \frac{\mathrm{PRev} * \mathrm{RPM} * 60}{1000} \quad (3.36)$$

where

PR	*penetration rate [m/h]*
RPM	*rotational speed [rev/min]*

PR directly

The penetration rate (PR) can according to Farrokh et al. (2012) be calculated directly from Equation 3.36.

$$PR = \frac{F_n^{0.186} * RQD_c^{0.133} * RT_c^{0.183} * RPM^{0.363} * D^{5.47} * e^{(0.046*D^2)}}{5.64 * UCS^{0.248} * e^{(1.58*D)}} \quad (3.36)$$

where

PR	*penetration rate [m/h]*
F_n	*disc cutter normal force [kN]*
RQD_c	*rock quality designation numerical code (Table 3.6) [-]*
RT_c	*rock type numerical code (Table 3.5) [-]*
RPM	*rotational speed [rev/min]*
D	*tunnel diameter [m]*

3.7.1 Advantages and disadvantages

The model by Farrokh et al. (2012) has both advantages and disadvantages regarding the prediction of penetration rates. Pros and cons regarding the model are presented in the following:

+ Adequately distinguish between the ground conditions and job constraints that control TBM performance, which other models do not include (Farrokh et al., 2012).

+ A database of TBM field performance works as a subject to a statistical analysis, which generates better accuracy than other models (Farrokh et al., 2012).

- Despite that the model is based on data from more than 200 projects, the equation that predicts the NPR has a regression coefficient of 63%, which is rather low (Farrokh et al., 2012).

- Due to the model's limitations, it is strongly recommended to use this model in combination with other models, especially in more complex project situations (Farrokh et al., 2012).

4 Methodology

This chapter presents the research methodology used to obtain the results and acquire relevant field data. It describes how the field data was collected, processed and systemized, and hence gives the reader an understanding of how the input parameters regarding the prediction models have been carried out. Laboratory tests, field mappings and data analyses are performed from the inbound north tunnel (TBM 1).

4.1 Literature studies

Before starting to carry out results, a literature study was performed. The aim of this literature study was to obtain detailed knowledge about all the models, as well as information about tunnel boring in general. Excavation of tunnels with TBMs in Norway have in recent times been quite rare. Therefore, it was necessary to obtain a good insight in the different aspects of such a big project in order to carry out reasonable results.

The literature studies have mainly been focused on existing articles from previous projects, such as The Ulriken tunnel project, the Røssåga tunnel project and the Koralm tunnel project. The main sources for the NTNU models, the MCSM model, the Alpine model and the Q_{tbm} model have been used to gather information about these models. For the remaining models, journals, articles and websites have been of great help.

Several databases have been used, especially the university database of NTNU, called *Oria*. In addition, *Scopus* and *Science Direct* (both from Elsevier) have been widely used. *Tunnelling and Underground Space Technology*, a journal in *Science Direct,* have been especially helpful.

4.2 Personal communication

In addition to the literature studies, personal communication with workers at the Åsland site has been performed. The workers are key people in the project and possess knowledge of different topics. These people have been pointed out in Table 4.1.

Table 4.1 – *Colleagues who have been particularly important regarding this thesis.*

Name	Profession
Fredrikke Sofia Grønlund Syversen	Assisting site manager / external supervisor
Bjørnar Gammelsæter	Chief geologist
Marcus Fritzøe Lawton	Geologist
Agnethe Hoff Finnøy	Geologist
Guro Isachsen	Geologist
Arnulf Hansen	Special advisor TBM
Thor Skjeggedal	Special advisor TBM
Artyom Andreev	Former student (MSc)

4.3 Geological data

Before starting the data collection, it was an advantage to know what kind of geological input parameters that was needed in order to calculate the penetration rates from the prediction models. This information is presented in Table 4.2 (Macias, 2016).

Table 4.2 – *Performance prediction models and their geological input parameters (Macias, 2016).*

Performance prediction model	Geological input parameters	Reference
NTNU model Modified NTNU model	DRI, porosity, rock mass fracturing,	Bruland (2000) Macias (2016)
CSM model MCSM model	UCS, BTS, rock mass fracturing, brittleness, density	Rostami (1997) Yagiz (2002)
Gehring model Alpine model	UCS, rock mass fracturing, BTS, abrasivity/breakability	Gehring (1995) Wilfing (2016)
Q_{tbm} model	Q-value, UCS, PLT, density, porosity, induced biaxial stress	Barton (2000)
Model by Yagiz	UCS, brittleness, rock fracturing	Yagiz (2008)
Model by Hassanpour et al.	UCS, RQD	Hassanpour et al. (2011)
Model by Farrokh et al.	UCS, RQD	Farrokh et al. (2012)

4.3.1 Field work

Most of the geological data originate from mappings performed by Bane NORs geologists on site. In addition, the author has had the opportunity to perform own mappings during the period from August 2017 to April 2018, which was limited to some cross-passage mappings and OTV-analyses. According to Bruland (2000c), back-mapping of a TBM bored tunnel should consist of:

- Continuous detailed mapping of rock mass fracturing.
- Continuous and detailed mapping of rock type distribution.
- Rock sampling and laboratory testing of rock properties.

Due to the doubled-shielded TBMs at the Follo Line Project, back-mapping is rather difficult to perform. The tunnel is immediately lined with concrete elements after excavation, which leaves the geologist with few opportunities to map the rock surface. Because of this, face inspections, cross passage (CP) inspections, inspections in the escape tunnel and optical teleview (OTV) inspections have been performed. Macias (2016) pointed out that determination of the rock type, as well as identification of marked single joints, intrusions, mixed face, water and degree of fracturing, are the most important steps to follow up regarding the mapping.

According to Bruland (2000c), the measurements recorded should represent the average of the tunnel sections in question. The sections may be subdivided for measurement purposes if changes in rock type or other factors dictate (Macias, 2016). The subdivisions are described in Chapter 4.5.1. Appendix B illustrates the CPs and the escape tunnel in relation to the sections.

4.3.1.1 Face inspections

Face inspections through the cutterhead have been (and are still being) performed, and gives a visual documentation of the geology at the tunnel face. One can roughly document whether the face is highly fractured or not, as well as making a visual overview of the rock type(s), weathering and possible mixed face conditions. The fractures are often challenging to map correctly through a cutterhead inspection, due to narrow workspace and relatively poor light conditions. In addition to the limited view through the cutterhead, there are only two dimensions visible at the tunnel face, which in combination with a non-functioning compass (reacting with the TBMs metals) makes it difficult to map the fractures accurately.

In this thesis, the face inspections are only used as a supplement to confirm or disconfirm assumptions regarding rock type and/or fractures (Fig. 4.1). As pointed out in Table 4.1, the rock type is not an input parameter to any of the performance prediction models. Figure 4.2a shows how the face mapping report provided by the geologists looks like. Figure 4.2b shows how it looks like when mapping through the cutterhead.

Figure 4.1 – *Example of a face inspection with different rock types and degree of fracturing. Notice the high fracture frequency in the amphibolite (marked in red). Photo: Bane NOR (2018).*

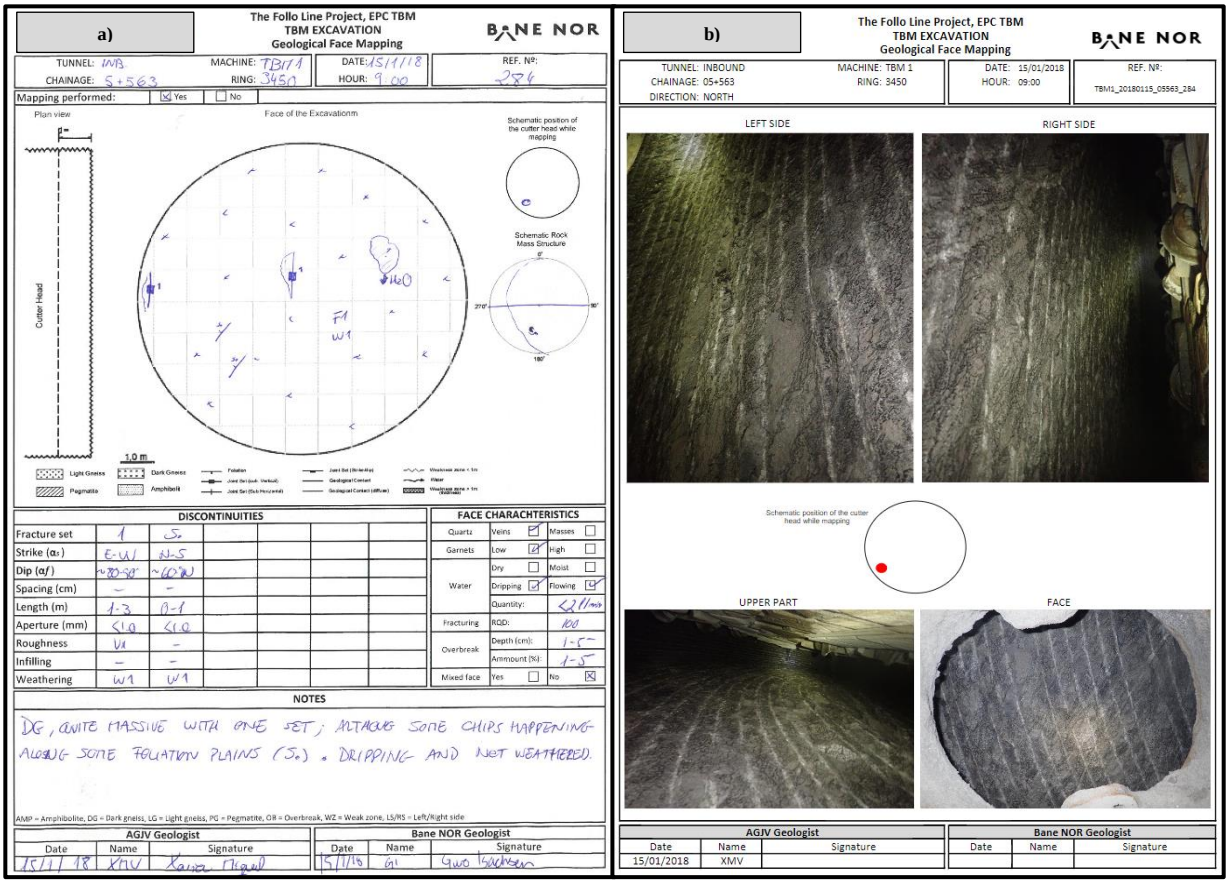

Figure 4.2 – *Face inspection. a) Rock face mapping report, provided by geologists from contractor and company (15.01.2018). b) Inspection which indicates dark and narrow conditions (Bane NOR, 2018b).*

4.3.1.2 Cross-passage (CP) inspections

Between the inbound and the outbound tunnels, cross passages (CPs) are made. These are excavated a few hundred meters behind the TBMs by drill & blast, and leave the rock surface open for the geologists to perform mappings. This is one of few possibilities to map the rock mass in three dimensions, even though the CPs are not exactly in the tunnel trace. The CPs are mapped with the Q-system in order to find the type and quantity of rock support, in addition to make a documentation of the rock mass quality. The Q-system is described in Chapter 3.4. For more detailed information about the mapping procedure and the guidelines in rock support design decisions, see NGI's handbook *Using the Q-system* (NGI, 2015).

The cross-passage mappings are performed for documentation. In addition, the Q_{tbm}-performance prognosis model described in Chapter 3.4 is dependent on the Q-values acquired from the CPs. Figure 4.3 shows how the cross-passage mapping report provided by the geologists look like. Figure 4.4 illustrates how it can look like during mapping in the CPs. If there has been performed several mappings in the same CP, the average value of the three mappings closest to the tunnel are being used. During the first 2700 meters, mapping from an additional escape tunnel have been a supplement to the main data (Chapter 4.3.1.3).

4.3.1.3 Escape tunnel inspections

Before the TBMs started to excavate, a 2.7 km long escape tunnel was excavated northwards using D&B. At one point, the two north going tunnels are crossing each other, which makes it impossible to build a cross passage. Therefore, an escape tunnel was built. This tunnel is perfect for performing geological investigations and to collect RQD- and Q-values. Figure 4.5 illustrates excavation of the face.

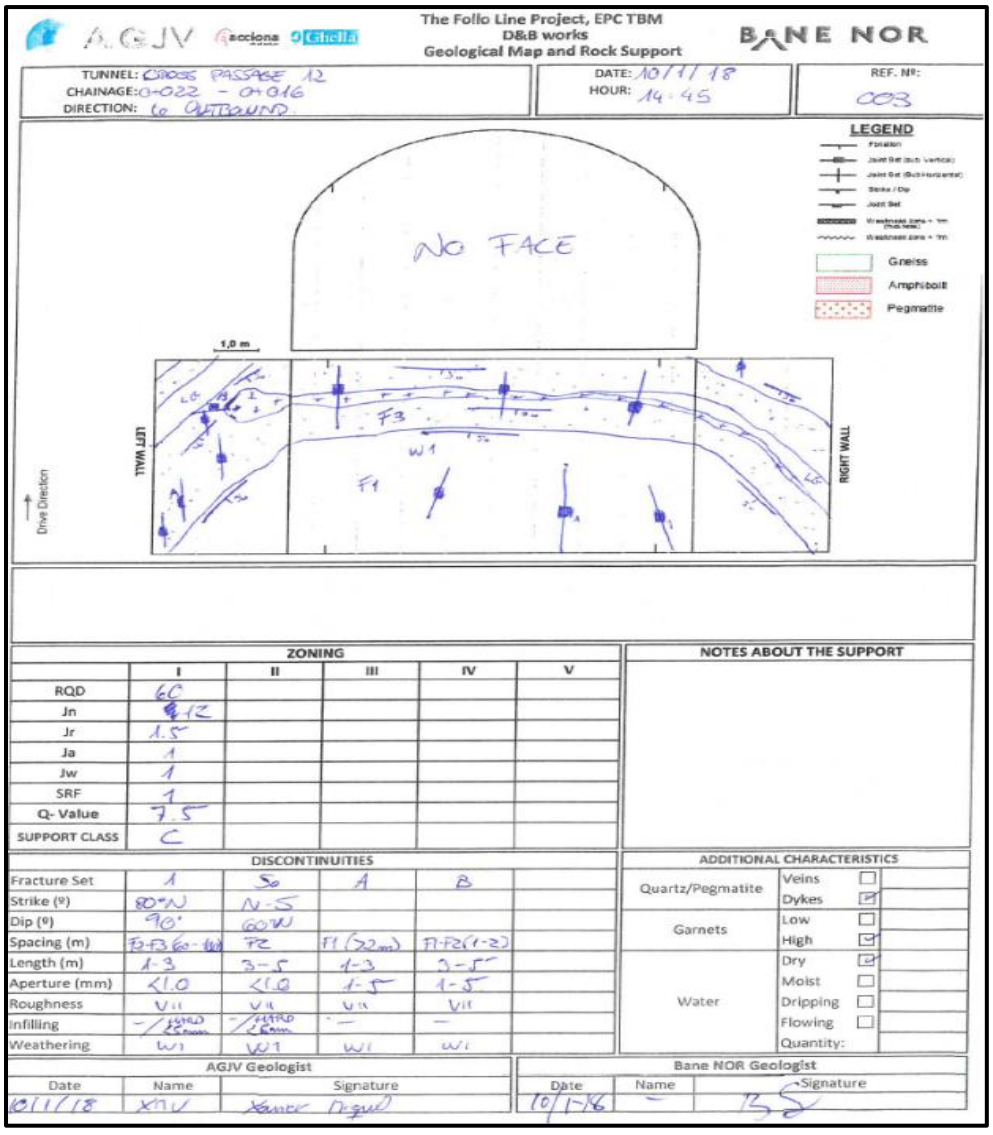

The Follo Line Project, EPC TBM
D&B works
Geological Map and Rock Support

BANE NOR

TUNNEL: CROSS PASSAGE 12
CHAINAGE: 0+022 - 0+016
DIRECTION: to OUTBOUND

DATE: 10/11/18
HOUR: 14:45

REF. Nº: 003

LEGEND
Gneiss
Amphibolit
Pegmatite

NO FACE

1,0 m
LEFT WALL
RIGHT WALL
Drive Direction
F3
W1
F1

ZONING

	I	II	III	IV	V
RQD	60				
Jn	9-12				
Jr	1.5				
Ja	1				
Jw	1				
SRF	1				
Q- Value	7.5				
SUPPORT CLASS	C				

NOTES ABOUT THE SUPPORT

DISCONTINUITIES

Fracture Set	1	So	A	B
Strike (º)	80°N	N-S		
Dip (º)	90°	60W		
Spacing (m)	F2-F3 60-100	F2	F1 (>2m)	F1-F2(1-2)
Length (m)	1-3	3-5	1-3	3-5
Aperture (mm)	<1.0	<1.0	1-5	1-5
Roughness	VII	VII	VII	VII
Infilling	- / HARD 25mm	- / HARD 25mm	-	-
Weathering	W1	W1	W1	W1

ADDITIONAL CHARACTERISTICS

Quartz/Pegmatite	Veins	☐
	Dykes	☑
Garnets	Low	☐
	High	☑
Water	Dry	☑
	Moist	☐
	Dripping	☐
	Flowing	☐
	Quantity:	

AGJV Geologist

Date	Name	Signature
10/11/18	XMV	

Bane NOR Geologist

Date	Name	Signature
10/11/18	—	

Figure 4.3 –*Cross passage mapping report. b) CP 40 from inside. c) Overbreak between gneiss and amphibolite in CP 40 (Bane NOR, 2018b). Photos taken by the author.*

Figure 4.4 – *CP 40 from inside.*

Figure 4.5 – *Excavation of escape tunnel*

4.3.1.4 Optical Teleview (OTV) inspections

The back-mapping of the rock mass fracturing is on the Follo Line Project (EPC TBM) performed with optical televiewing (OTV). OTV is being used as a back-mapping method mainly because of double shielded and closed TBMs used at the project, which makes it impossible to perform a continuous mapping along the tunnel in a traditional way. For instance, this is important to establish a rock mass fracturing factor ($k_{s\text{-}tot}$). In addition, other values like RQD and Q-values can be found with this method. This is especially helpful in tunnel sections where cross-passages are missing.

An optical televiewer (OTV), also called an optical borehole imager, is according to Williams & Johnsen (2004) a tool used to generate a "continuous oriented 360 degrees image of the walls inside a predrilled borehole". To obtain information on geological conditions ahead of the TBM drive, continuous probe drilling is performed. The probe holes are normally drilled to a length of about 40 meters, with an overlap of approximately 10 meters (Fig. 4.7). While these probe holes are drilled, measurement while drilling (MWD) are carried out. MWD data mainly gives information about weakness zones and water seepages, and is not suited for detailed fracture mapping. The instrument for televiewing has a compass and a gyro to keep track of borehole orientation. The result is a high-resolution picture where fractures and lithology can be mapped in detail (Bane NOR, 2018b).

This high-resolution picture is illustrated in Figure 4.6.

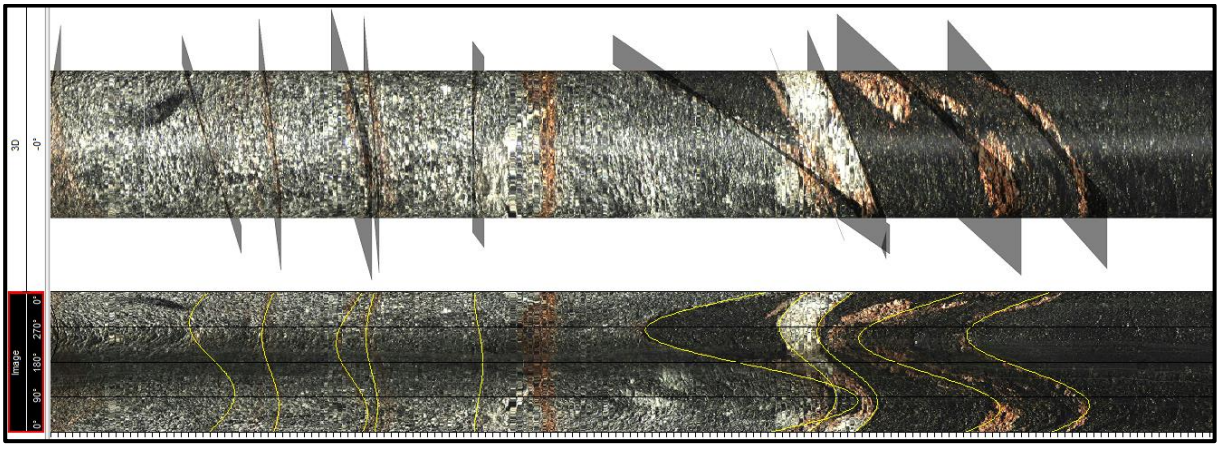

Figure 4.6 – *High-resolution picture of probe drilled borehole generated from an optical televiewer (OTV). The fractures are mapped in WellCAD. The uppermost picture illustrates the bore hole in 3D, while the other illustrates the bore hole in 2D (Bane NOR, 2018b).*

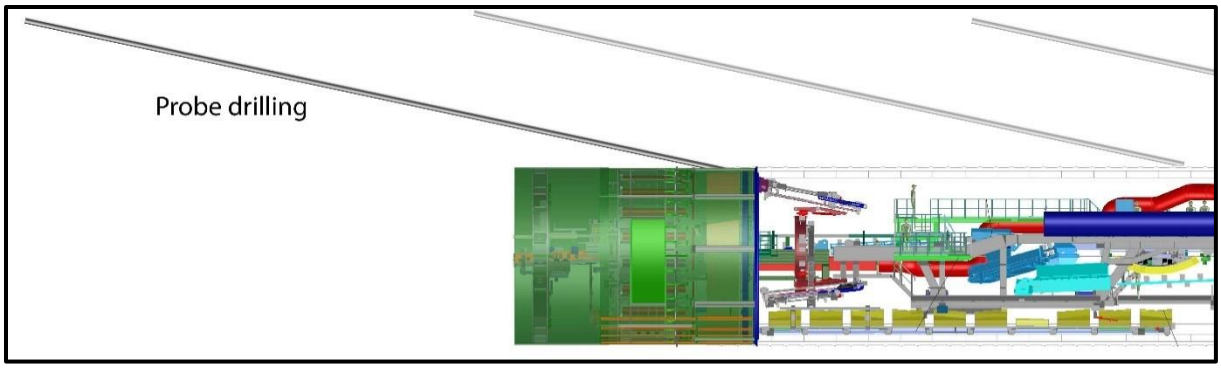

Figure 4.7 – *Probe drillings (40 m) from a double shielded TBM. Approximately 10 meter overlap. Illustration modified from Bane NOR (2018b).*

The image file generated from the OTV is imported to a log composite software called WellCAD, where it processes the data. Fractures are defined manually along the image, and the software draws the best fitting sine wave (Fig. 4.6). Open fractures are often easy to detect, while closed fractures are more difficult to observe. When the fractures are marked, one can decide strike and dip of the weakness planes. Fracture spacing and angles, as well as RQD, are easy to obtain from the software. These parameters are important in almost all the performance prediction models described in Chapter 3.

When all the fractures are defined, the software generates a pole plot. This can also be imported to another software, called *Dips* (Fig. 4.8). From this pole, one can group fractures into different fracture sets by allocating contour lines around the black dots in the plot. According to Bruland (2000c), the NTNU model, recommends using a maximum of three fracture sets when back-mapping is performed.

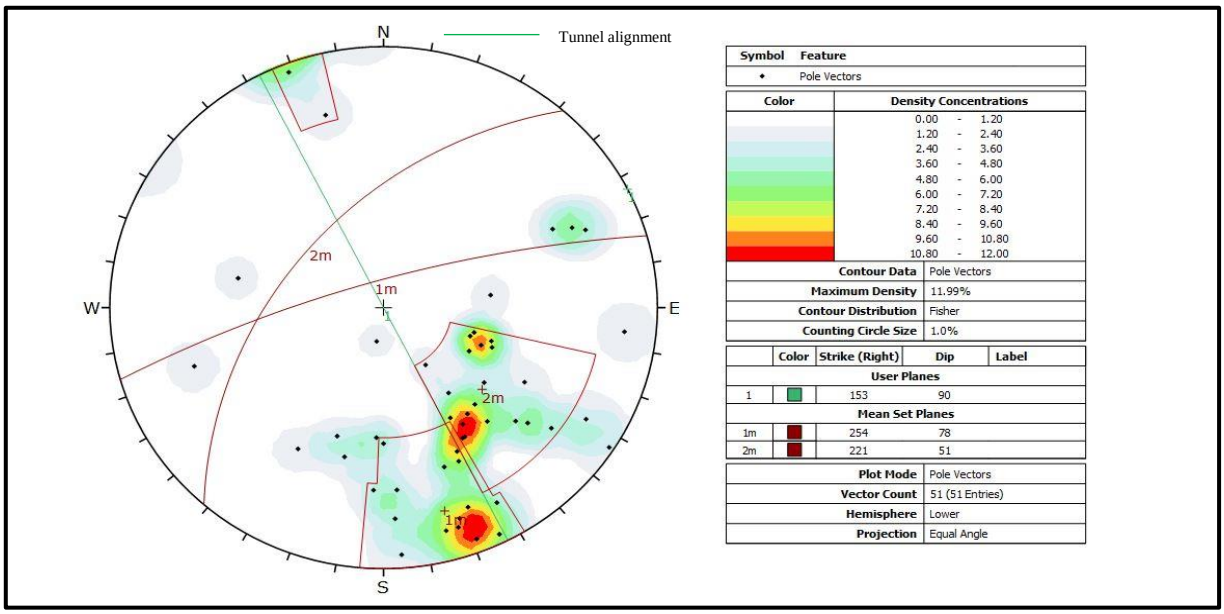

Figure 4.8 – *Two fracture sets imported to Dips from the OTV-analysis in WellCAD (Bane NOR, 2018b).*

4.3.2 Laboratory tests

There has been performed several laboratory tests at SINTEF's laboratory located in Trondheim. Rock samples have been collected perpendicular to the tunnel alignment with a 250 meter interval, and tested at the laboratory.

The results are presented in Chapter 5.1, and detailed laboratory test reports and a summary template are presented in Appendix D.

Table 4.3 shows the executed tests, what calculations the test results have been used for and which model the test results are included in. The procedures are based on well-known standards, and are therefore not described in detail. The related standards are presented in Table 4.3.

Table 4.3 – *Laboratory tests executed for this thesis.*

Test method	Used to calculate	Used in model	Procedure standard
Density (ρ)	Density Brittleness value (S_{20})	NTNU Q_{tbm} MCSM Yagiz	NTNU/SINTEF test (Dahl et al., 2012)
Brittleness value (S_{20})	Drilling Rate Index	NTNU	NTNU/SINTEF tests (Dahl et al., 2012)
Sievers'J-value (SJ)	Drilling Rate Index Cutter Life Index	NTNU Q_{tbm}	NTNU/SINTEF tests (Dahl et al., 2012)
Abrasion Value Cutter Steel (AVS)	Cutter Life Index	Q_{tbm}	NTNU/SINTEF test (Dahl et al., 2012)
Uniaxial Compressive Strength (UCS)	Brazilian Tensile Strength	CSM MCSM Gehring Alpine Q_{tbm} Yagiz Hassanpour et al. Farrokh et al.	ISRM (1978)
Mineralogical composition (XRD)	Quartz content	Q_{tbm}	Chemical/Mineralogical Laboratory (Dahl, 2011)

In addition to UCS tests executed in the pre-investigation phase, new UCS values have been obtained for every 250th meter along the tunnel alignment. This has been performed to reflect the local variations within the tunnel alignment. Unfortunately, these UCS values are low and are assumed not to be representative for the present geology in the project. This assumption is based upon the big deviation from the results from the pre-investigations, and there is a common understanding of this among the geologists at site. The reasons for the low values are discussed in Chapter 6.4.

To increase the reliability of the results, a combination of the results from the pre-investigations and from the latest results have been made. The values from the pre-investigations, which is assumed representative, have been adjusted up or down based upon the latest UCS-values. By doing so, the local variations will be included in the calculations. This is done by adding the deviation in percentage from the mean value of the latest UCS values to the pre-investigation value. This method has been confirmed and supported by the geologists at site. The method concept is exemplified in Table 4.4:

Table 4.4 – *Example of method used when UCS values have been calculated.*

Imaginary section	1	2	3	4	**Average value:**
Results from pre-investigation (MPa)		180	220		
Results from tests along the tunnel alignment (MPa)	100	78	87	130	98.75
Percentage deviation from the average value	1.27%	- 26.60%	- 13.51%	31.66%	
Total calculated UCS (MPa)	180 * 1.127% = 202.86	180 / 1.266% = 142.86	220 / 1.135% = 193.83	220 * 1.317% = 289.74	

In order to compensate for missing BTS-values, several correlations between UCS and BTS have been made. Correlations by Nilsen et al. (2000), Kahraman et al. (2012) and Altindag & Guney (2010) among others are frequently used. According to Nazir et al. (2013), the correlation formula by Altindag and Gunay (2010) shows the best correlation. The correlation is calculated to be 79% for "different rock types including limestone". This formula has been used to calculate missing BTS-values.

The formula by Altindag and Gunay (2010) is presented in Equation 4.9.

$$\mathrm{BTS} = (\mathrm{UCS}/12.38)^{(1.00/1.0725)} \tag{4.9}$$

Possible errors connected to the use of correlation formulas are presented in Chapter 4.6.2 and discussed in Chapter 6.4.

4.4 Machine data

In order to compare the calculated results with the actual situation, the machine data has to be acquired and systemized. The process regarding data download and data processing is described in detail below. The machine data include both how the machines operate and how they perform. The TBMs at the Follo Line Project have an electronic data logging system, where several sensors record various parameters every 10th second. Downloaded machine data are presented in Chapter 5.1.

4.4.1 Data download

4.4.1.1 Software and web application

A software called PROCON II provided by Maidl Tunnelconsultants (MTC, 2018) treats the recorded parameters and make them available through a web application. From this web application, one can either download unprocessed data (raw format), or one can download processed and summarized data in reports. Specific parameters can also be monitored in real time through this application (Fig. 4.9).

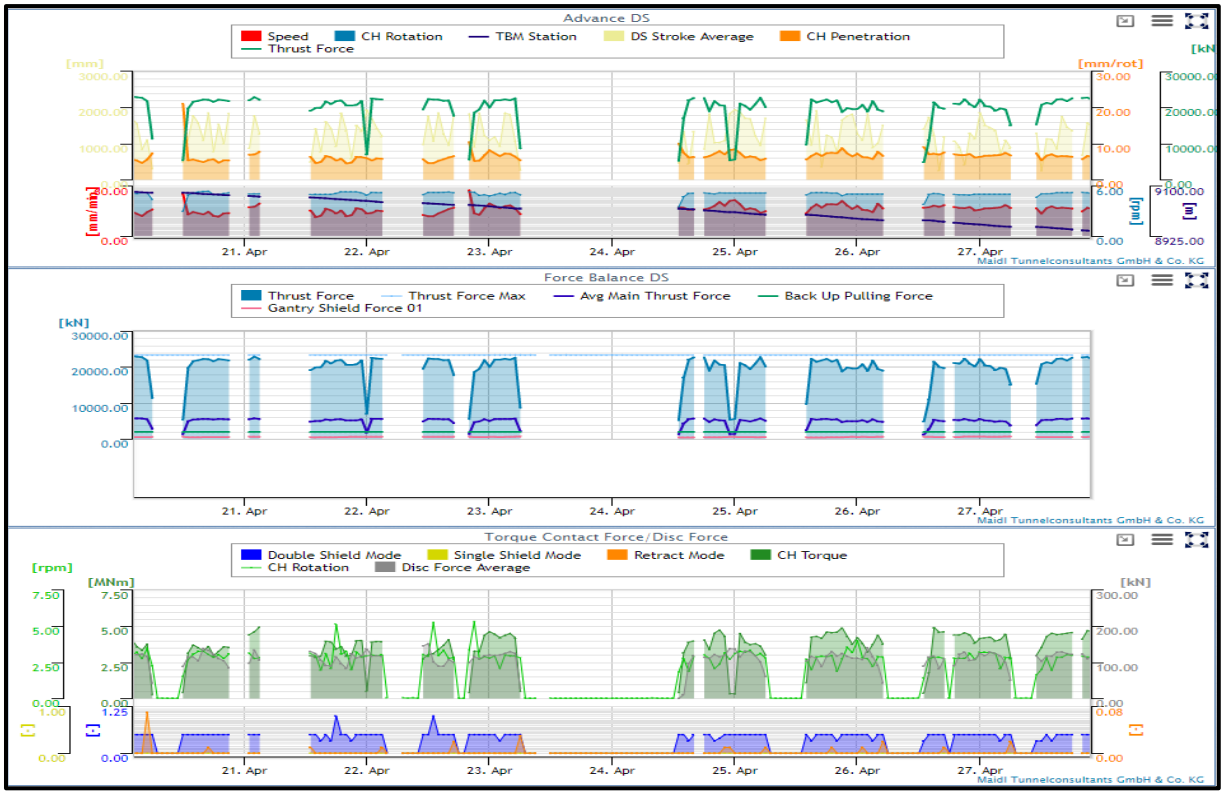

Figure 4.9 – *Extraction from the web application provided by MTC (2018). The figure shows specific parameters monitored in real time for TBM 1 (ring 1500 to 1575, april 2017).*

4.4.1.2 Data acquisition

From the electronic data logging system, relevant data have been downloaded in a raw format. Some of the parameters have been directly relevant to the performance, while others have been irrelevant. However, the irrelevant parameters are relevant for the interpretation of the results, and is an important supplement. Both the performance data and the supplementary data have been listed in Table 4.5.

Table 4.5 – *Parameters downloaded from the software. The parameters are listed in the order that fit the filtering spreadsheet presented in Appendix F. Inspired by Andreev (2017).*

Parameter	Data type	Unit
Date and time	Supplementary data	
Stroke length	Supplementary data	mm
Penetration rate	Performance data	mm/rev
Advance speed	Performance data	mm/min
Cutterhead velocity (RPM)	Performance data	rev/min
Torque	Supplementary data	kNm
Boring time	Supplementary data	h
Ring build time	Supplementary data	h
Chainage	Supplementary data	m
Remaining excavation	Supplementary data	m
Thrust	Performance data	kN

The acquisition of the data parameters listed above has been performed with intervals of 25 concrete lining rings. The web application does not support intervals by chainage or tunnel meters, only by defining ring numbers or dates. One ring has a width of 1.8 meters, which equals 45 meters for 25 rings. However, the lengths vary between 41 and 49 meters due to a flaw with the logging system.

The acquired machine data are presented in Appendix F. For the inbound north tunnel (TBM 1), data from ring number 3 – 2500 have been acquired, which equals approximately 4500 meters of tunnel (Table 4.6).

4.4.2 Data processing

After downloading machine data for the relevant tunnel chainages, the raw data was processed. The methodology described in this chapter is based on descriptions compiled in the doctoral thesis written by Macias (2016)-

The main reason for processing data is to filter and then calculate the average values for the relevant machine performance parameters. Filtration is important in order to exclude data recordings that not represent an excavation phase (e.g. cutter inspections or other delays). The data logging system records 24/7.

By using the standard reports of summarized data generated by the software, the workload could have been reduced significantly. It was established that such reports do not provide the required level of detail. In addition, these reports did not indicate how the automatic filtration are performed.

The following filtering criteria have been set:

1. **Removal of penetration rates (mm/rev) that equal "0"**

By removing the penetration rates that equal "0", one excludes the recorded data when the TBMs are standing still. The machine data are recorded every 10^{th} second no matter if the machines are excavating or not (Fig. 4.11).

2. **Removal of cutter thrusts (kN/cutter) smaller or similar to "100"**

By removing cutter thrusts smaller or similar to "100", one excludes values often related to either regripping phases or cutterhead movement towards the face without excavation. This filter will remove values from activities linked to other operations than excavation, that was not removed by the first filter. Macias (2016) states that such low cutter thrusts might be a result of excavation in high concentrated fault zones. It is important to mention that this criterion involves a risk of removing realistic values from the data set, hence there are discussions if the number is appropriate (Macias, 2016).

All the figures are generated with the templates presented in Appendix F. Remarks behind the filtering process based on Macias (2016) are presented in the following:

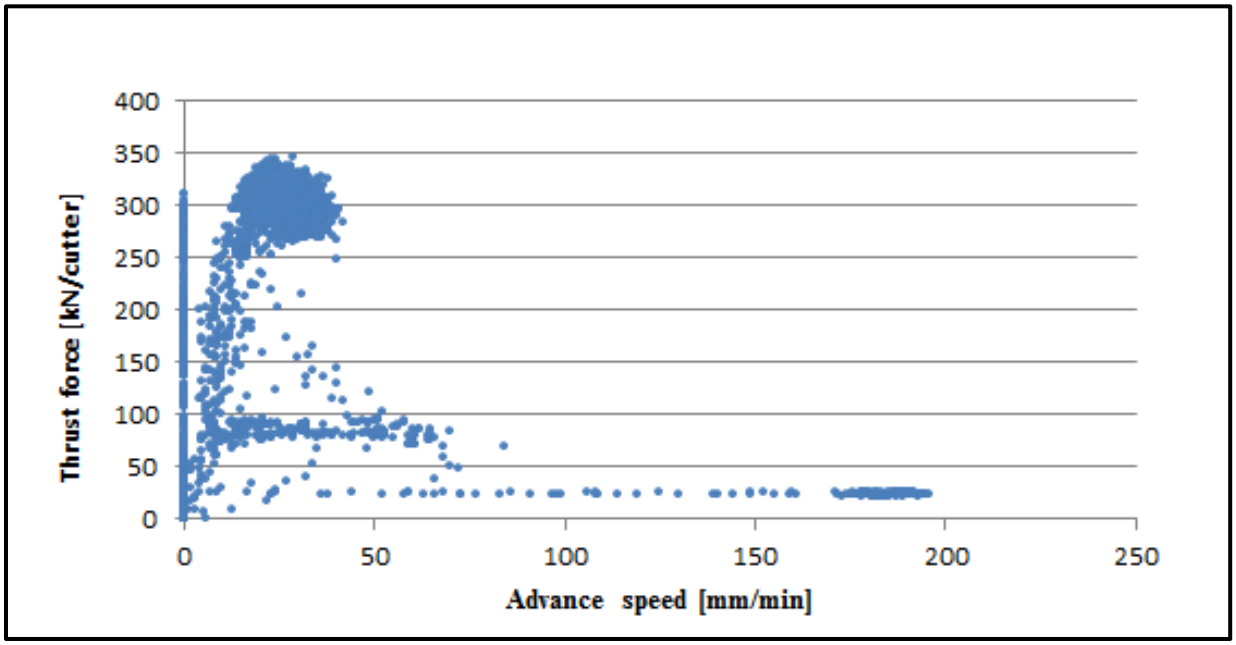

Figure 4.10 – *Unfiltered values of penetration rate and cutter thrust for a tunnel section generated from ring 850 to ring 875 in the inbound north tunnel (TBM 1).*

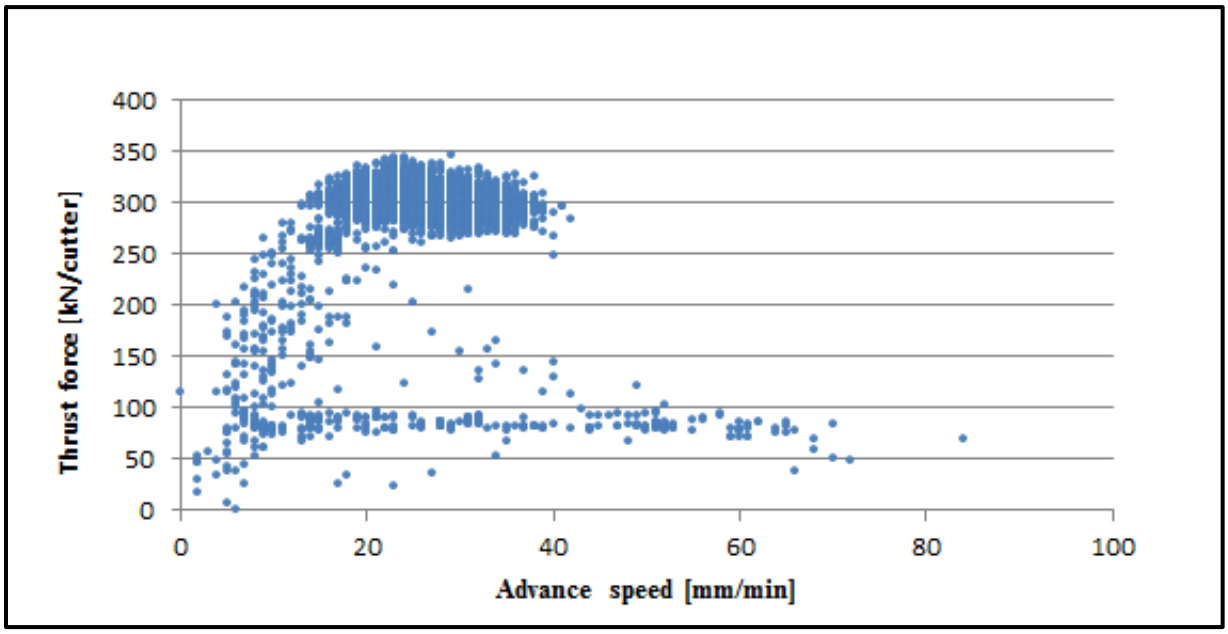

Figure 4.11 – *Filtered values of penetration rate and cutter thrust for the similar data from Figure 4.10. Filtered for "mm/rev > 0", generated from ring 850 to ring 875 in the inbound north tunnel (TBM 1).*

Figure 4.10 shows the unfiltered distribution of values from advance speed (mm/min) and cutter thrust. The values are gathered from one of the tunnel sections of 45 meters (25 rings) in the inbound north tunnel (TBM 1). Below a cutter thrust of 50 kN, most values appear to be unrealistic. There is an accumulation of values concentrated around 80 kN/cutter, which is a result of forward movement of the cutterhead without any excavation taking place. Such accumulations have been observed for thrust levels varying from 40 – 170 kN/cutter.

Figure 4.11 shows the same distribution of data as presented in Figure 4.10, filtered for "mm/rev > 0", and shows atypical advance speed recordings around 25 kN/cutter. These are removed when the penetration rate is filtered for values that equal "0". These recordings represent non-excavation periods (e.g. regripping).

Figure 4.12 shows the same distribution of data presented earlier, where both filtering criteria earlier described have been applied.

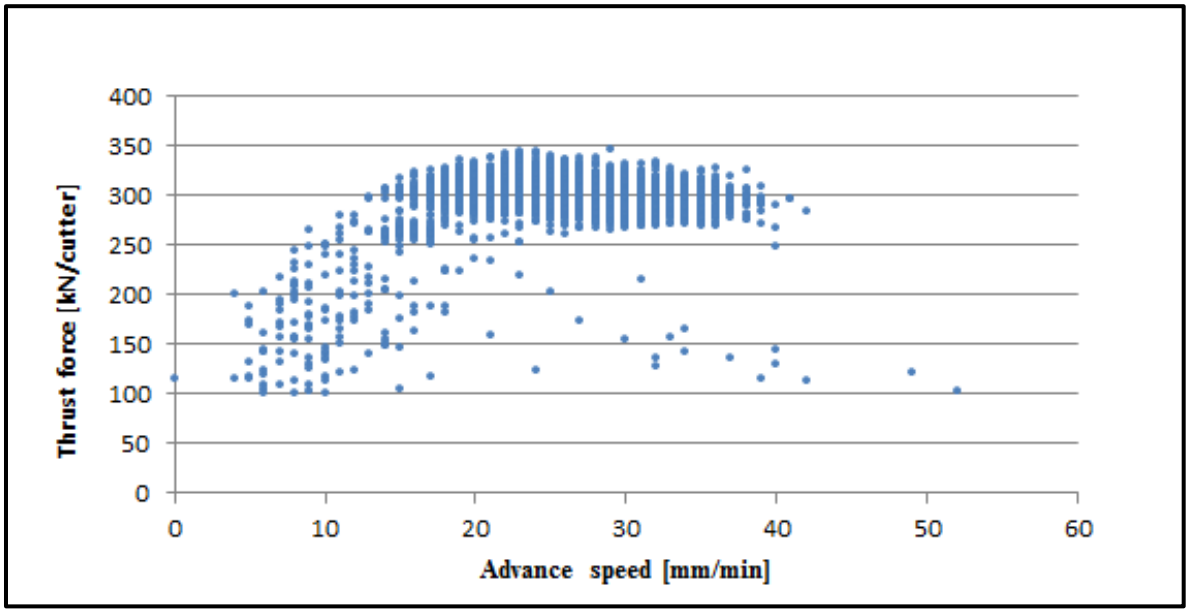

Figure 4.12 – *Filtered values of penetration rate and cutter thrust for the similar data from Figure 4.10 and 4.11. Filtered for both filter criteria presented earlier.*

Inspired by Macias (2016), a systematic filtration table has been made (Table 4.6). This table presents the average values of the machine performance data presented in Table 4.5, in order to illustrate how the average values change between the filtering steps. The first criterion has been applied in step 2 and the second criterion has been applied in step number 3. Both filter mechanisms have simultaneously been applied in step 3 to 5, with variation in cutter thrust.

Table 4.6 – *Step by step filtration.*

Step no.	Filtering criteria	Thrust [kN/cutter]	Penetration Rate [mm/rev]	Advance Speed [mm/min]	RPM [rev/min]
1	**Unfiltered**	156.92	2.28	21.41	2.55
2	**> 0 mm/rev**	295.68	4.80	24.02	5.07
3	**> 50 kN/cutter**	296.16	4.79	24.03	5.07
4	**> 100 kN/cutter**	303.02	4.67	23.80	5.11
5	**> 150 kN/cutter**	303.94	4.67	23.84	5.11

The largest difference in averaged values appears between step 1 and step 2, where all the "zeros" have been removed. Most of the advance speed (mm/min) recordings below 50 kN/cutter have been filtered away with the first filter criterion (step 2). This can be explained by the regripping phases where the penetration rate (mm/rev) is recorded as "0"-values.

By applying step 4, significant differences in the averaged values occur. By applying step 5, almost no changes are observed. Therefore, cutter thrusts under 100 kN/cutter were set as the filtering criteria in this thesis. Andreev (2017) agrees that such criteria would be sufficient in most cases:

> *"Observations show that the majority of advance speed values that are recorded during a forward movement of the cutterhead (without excavation taking place) are generated for thrust levels in the range of 60 – 100 kN/cutter"* **(Andreev, 2017:40)**

He also presented an example from a tunnel section that includes a weakness zone (Fig. 4.13). By analyzing the raw data from this zone, it has been confirmed that the recordings above 100 kN/cutter represent actual excavation. This, together with earlier mentioned reasons, underlines that a removal of cutter thrust below or similar to 100 kN/cutter is appropriate.

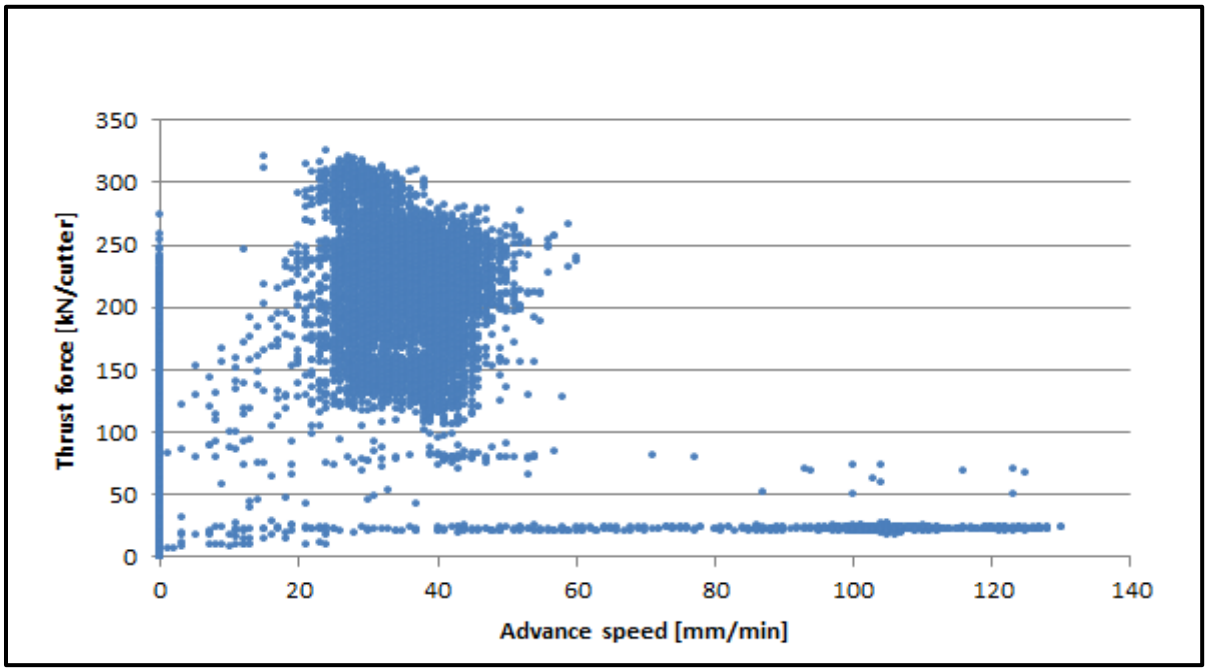

Figure 4.13 - *Unfiltered values of penetration rate and cutter thrust for a tunnel section generated from ring 1788 to ring 1814 in the inbound north tunnel (TBM 1). This includes a weakness zone.*

It is important to mention that the changes in average values can vary for different data sets, and each data set should be treated separately. A more detailed investigation in order to draw a conclusion is needed. A general recommendation is to use such filtering criterion with caution.

4.5 Data analyses

Calculations of penetration rates from the prediction models and analyses of data have been systemized, calculated and analyzed. All the analyses are presented in the appendices.

4.5.1 Tunnel section division

In order to compare calculated penetration rates to the actual penetration rate, sufficient tunnel segments had to be chosen. Based on the available data from December 2017, a 4500-meter long segment in the inbound north tunnel (TBM 1) has been studied.

For a more precise calculation of the different rates of penetration, the tunnel has been divided into sections. The division of these sections are based on the frequency of the laboratory tests, as well as other available geological data. As described in Chapter 4.3.2, the core sampled for the laboratory tests are taken out every 250th meter. Therefore, these sections are varying between 219 and 316 meters of length, due to geological variations based on the $k_{s\text{-}tot}$ values. The sections are presented in Table 4.7.

The back-mapping shall ideally be performed every 10th meter. However, Bruland (2000c) states that:

> *"Back-mapping in tunnels lined with concrete elements or shotcrete at the cutterhead is very difficult to perform with the purpose to establish a continuous geological model. In such tunnels the back-mapping must be improvised and done at points wherever the rock surface is available"* **(Bruland, 2000c:64).**

In order to meet this statement, continuous OTV-analysis and pointwise geological mappings have been performed (Chapter 4.3).

Table 4.7 shows how the tunnel sections are divided.

Table 4.7 – *Section divisions studied in this thesis.*

Section no.	Chainage [m]	Tunnel meters [m]
1	11778 - 11559	219
2	11559 - 11289	270
3	11289 - 10973	316
4	10973 - 10703	270
5	10703 - 10472	231
6	10472 - 10252	220
7	10252 - 9982	270
8	9982 - 9756	226
9	9756 - 9530	226
10	9530 - 9306	224
11	9306 - 9080	226
12	9080 - 8810	270
13	8810 - 8584	225
14	8584 - 8268	316
15	8268 - 8043	225
16	8043 - 7773	270
17	7773 - 7548	225
18	7548 - 7278	270
Total		**4500**

In Appendix B, an illustration of the northbound tunnels with connecting cross passages, escape tunnel and section division is presented. This is made to get an overview of the tunnels stretch towards Oslo.

4.5.2 Prediction model calculations

To calculate the theoretical penetration rates with the different prediction models, procedures described in Chapter 3 are used. Both the calculations and the resulting graphs are presented in the same spreadsheets, with different sheet numbers. These are presented in Appendix G.

In addition to presenting one spreadsheet per prediction model, a final spreadsheet comparing the different results has been carried out (Appendix I)**.** This includes the penetration rates calculated from averaged values for the whole tunnel alignment and the achieved NPR. The results are presented in Chapter 5.2**.**

4.5.3 Mapping fractures

The fracturing factor ($k_{s\text{-}tot}$) linked to the NTNU model has been calculated with OTV-analyses, and is based upon calculations by Bane NOR`s geologists. These analyses have given information about the fracture spacing and orientation, which further leads to different fracture classes. In addition, the number of fractures have been counted for each section, which together provides a RQD-value. The information about the fractures are presented in Appendix C. The percentage distribution of each fracture class is presented in Chapter 5.1.

By mapping the fractures with OTV, a continuous representation of the fractures is obtained. The probe holes are overlapping and the results from the overlapping part closest to the tunnel are chosen as the most valid results. Therefore, the last part of probe hole 1 in Figure 4.14 has been removed for each case. **"A"** denotes the length of probe hole 1, which is the distance that the OTV fracturing factor actually represents. **"B"** denotes the distance after the overlapped area furthest away from the tunnel has been removed. The average of several "B-distances" comprises the total tunnel length analyzed with OTV.

Figure 4.14 gives an illustration of the two subsequent probe holes.

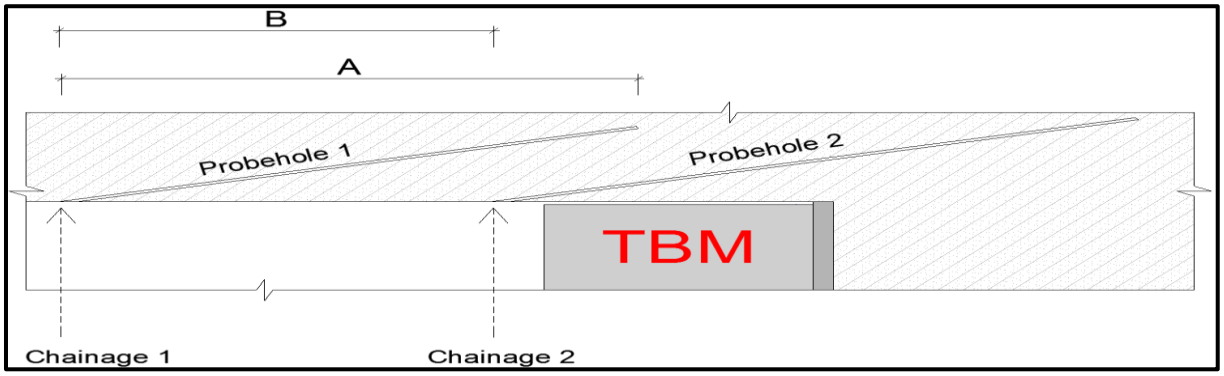

***Figure 4.14** – Two subsequent probe holes. Distance B is used to calculate average $k_{s\text{-}tot}$ for 45 m sections. Distance A is the actual length of the probe hole used to establish the $k_{s\text{-}tot.}$ (Andreev, 2017).*

4.5.4 Machine performance

The machine performance data that has been downloaded are described in Chapter 4.4. The raw data for each 45 m have been averaged and presented in Appendix F. This includes values of thrust (kN), cutterhead velocity RPM (rev/min) basic penetration rate (mm/rev) and net penetration rate (mm/min).

4.5.5 Frictional drag

Both Herrenknecht (the TBM supplier) and the contractor agree with the calculation of TBM shield friction (drag). The drag force has to be deducted from the TBM propel system thrust (the gross total cutterhead thrust) in order to estimate the actual cutter thrust. Based on a drag test performed at the inbound north tunnel (TBM 1) in 2017, the company arrived at the following conclusion:

Static front shield friction (6 400 kN) x Dynamic factor (0.5) = TBM shield drag 3 200 kN

Several prediction models require the net thrust value as an input parameter. To calculate the net thrust, the applied thrust (gross) must be subtracted by 3200 kN.

4.5.6 Influential parameters

To determine the most influential parameters, comparisons and sensitivity analyses have been performed. To fully understand model's behavior, it is important to have knowledge about the input parameters. The most influential parameters have been found both regarding the achieved and predicted NPRs:

Parameters influencing the achieved NPR

Determining the parameters influencing the achieved NPR can be helpful to understand why some of the models give better results than others. To determine these parameters, a comparison between the specific parameter values and the achieved NPR have been performed. In addition to a visual graphical illustration of the two parameters, a coefficient of correlation (r^2) have been calculated. By doing so, one can easily see the visual relationship between the parameters for each section, as well as determine the influence by a percentage number.

The calculations are done in Appendix H1 and the results are presented in Chapter 5.3.1.

Parameters influencing the predicted NPR

The most influential parameters in the various models may not be the same parameters as in reality. To identify the parameters influencing the predicted NPR the most, a sensitivity analysis of each model has been performed. One can determine the most sensitive parameter by changing one parameter at the time in order to achieve the predicted NPR. This has been done by trial and error. The percentage difference between the calculated value and the original value defines the sensitivity of the parameter. A lower percentage value corresponds to a higher sensitivity, and thus, the parameter is of high importance in the model. The percentages have not been compared from one model to another, only within each model.

In addition, the variation of parameter influence on the predicted NPR is presented for each model (Appendix H2). This has been done to illustrate that a parameter may be influential in other geological conditions, even if it is not influential in the present geological setting at this project.

The calculations are done in Appendix H2 and the results are presented in Chapter 5.3.2.

4.6 Method uncertainties

The methods described in Chapter 4 are related to a number of possible errors, which may influence the predicted results. The most influential errors are presented in the following subchapters.

4.6.1 Field work

The data acquired from the field work are related to some sources of error, especially due to the difficulties regarding the mapping in a circular TBM tunnel covered with segments. Further uncertainties regarding the penetration rates are discussed in Chapter 6.4.

- It is difficult to distinguish between fractures induced from blasting and tectonic induced fractures when mapping in the CPs. The mapped Q-values and fracture information can therefore be wrong. However, educated and experienced geologists have performed the cross-passage mappings.

- When processing the raw borehole images in WellCAD (Chapter 4.3.1.4), the user must define each individual fracture manually and assign the fractures to different sets. The degree of subjectivity may affect the reliability and accuracy of the obtained results.

- The size of the drilled probe hole is a potential uncertainty. It can be difficult to know if observed fractures intercept with the actual tunnel cross section or not. In a worst-case scenario, the borehole may be drilled parallel to a certain fracture set and will consequently not be recorded by the OTV. This is though highly unlikely.

- When determining RQD from OTV-analyses, the values tend to be slightly higher than values gathered from regular mappings in CPs or the escape tunnel (Bane NOR, 2018a). This may also affect the Q-values in section 13, 15 and 17, which have been mapped with OTV.

4.6.2 Laboratory tests

The laboratory tests are all performed at the certified laboratory at SINTEF. The trademarked acronyms and terms Drilling Rate Index™, Cutter Life Index™ (DRI™ and CLI™) are unique for test results and calculated indices originates from the NTNU/SINTEF laboratory, and can only be obtained by testing samples at their reference laboratory (Dahl et al., 2012).

It is important to treat the results from the laboratory testings with caution and vigilance. Small errors can have a large impact on the test results. The most decisive uncertainties regarding the execution of laboratory tests are:

- According to the standard, UCS test samples shall be taken perpendicular to the foliation angle (ISRM, 1978). At the Follo Line Project, the samples takings are not always performed perpendicular, which may affect the UCS-values. For that reason, the gathered values are believed to be lower than it should be and therefore not representative for the rock mass along the tunnel alignment. This issue has partly been solved by implementing the UCS values from the pre-investigation phase, described in Chapter 4.3.2.

- The correlation between BTS and UCS is found by a conversion formula, which has a correlation coefficient of 0.79 (Eq. 4.9). Such correlations shall be used with caution, and might not be as accurate as if a lab test was performed for each section.

4.6.3 Data download and analyses

There is a huge amount of data that is downloaded and analyzed. The organization and categorization of this data can potentially be a source of error. To reduce the risk for such uncertainties, actions such as double downloads, control calculations have been done.

An accurate removal of values not representing excavation is hard perform. The filtering criterion must therefore be treated with caution.

5 Results

In this chapter, the results of the work carried out will be presented. Compiled geological- and machine related data will be presented first. Then, the results gathered from the various models will be presented, which include predictions for the whole tunnel alignment and for each section. Lastly, an evaluation of the most influential parameters will be presented, both connected to the achieved NPR and to the predicted NPR.

5.1 Compilation of data

The fieldwork performed at the Follo Line Project are, as mentioned, limited to cross passage and OTV-inspections, as well as face inspections. As described in Chapter 4.3.1.1, the face inspections are only used as a supplement to confirm or disconfirm the other results. Laboratory tests are also executed, and a compilation of this data is presented in the following. A cumulated averaged graph is presented in their associated diagram.

Rock mass fracturing

Information about the fractures have mainly been collected from the OTV-analyses. This includes averaged fracture spacing and orientation, as well as some RQD-values. Most of the RQD-values are collected from the CPs and the escape tunnel. Chapter 4.3.1.2 and Chapter 4.3.1.3 describe the methods in detail. All the results are presented in Appendix C.

The frequency of the different fracture sets has been presented in Figure 5.1.

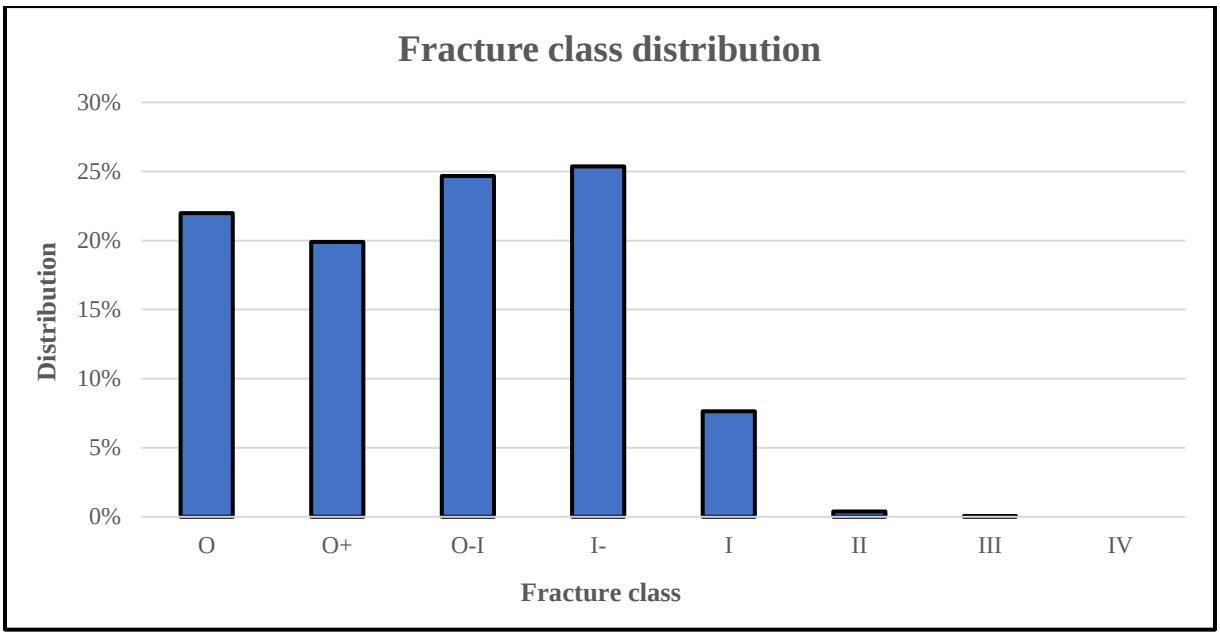

Figure 5.1 – *Distribution of fracture classes throughout the whole tunnel length. The class division originates from the NTNU model by Bruland (2000).*

In addition to presenting the fracture classes, Bruland (2000) introduced a fracturing factor ($k_{s\text{-}tot}$). The calculated fracturing factor is plotted for each section (Fig. 5.2). Both the fracture classes and the fracturing factor represent the overall fracturing trend, in which they are based on the spacing and orientation of the fractures.

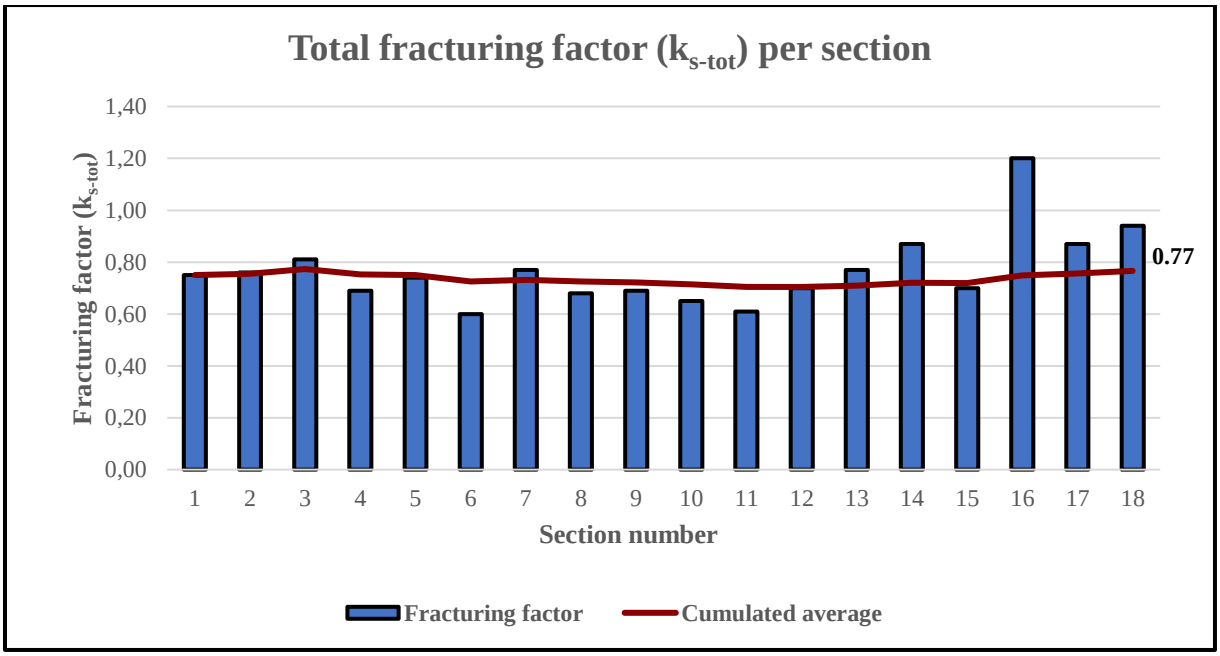

Figure 5.2 – *Averaged total fracturing factor calculated for each section with a weighted average value of 0.77.*

In addition to the NTNU model, information about the fractures are essential in the other prediction models. This information is typically related to spacing and orientation of the fractures, as well as the rock quality designation (RQD).

The fracturing parameters are plotted with averaged values for each section and with a total cumulated average. Figures 5.3 to 5.5 illustrate the fracturing parameters.

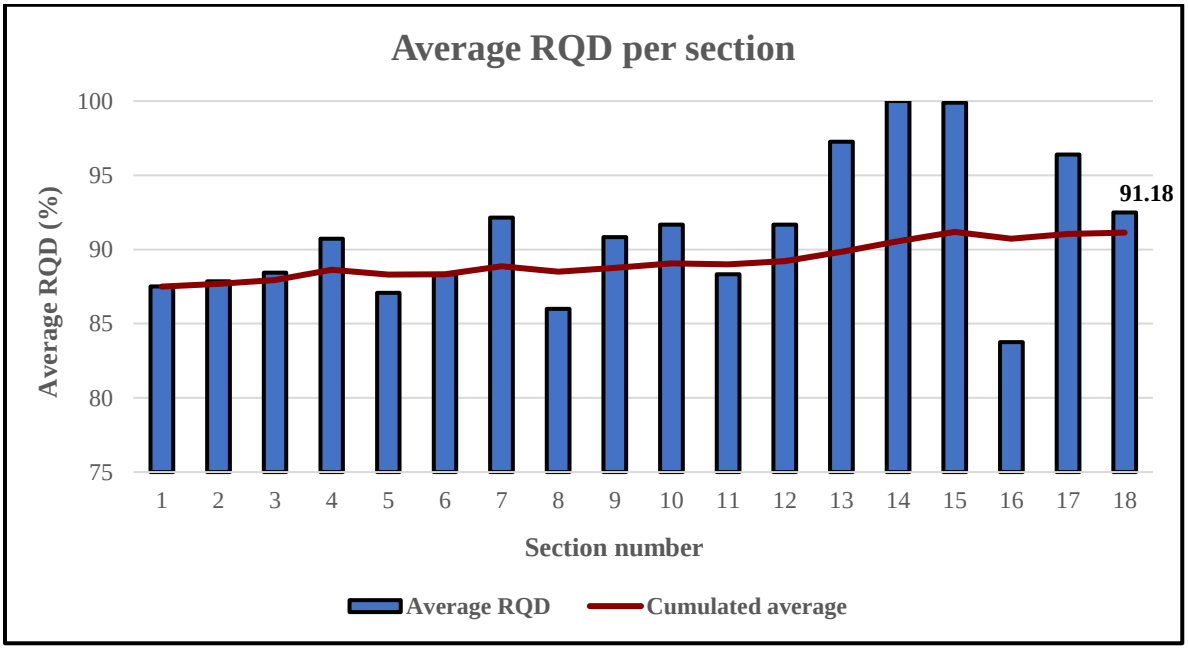

Figure 5.3 – *Averaged RQD for each section with a weighted average value of 91.18 %.*

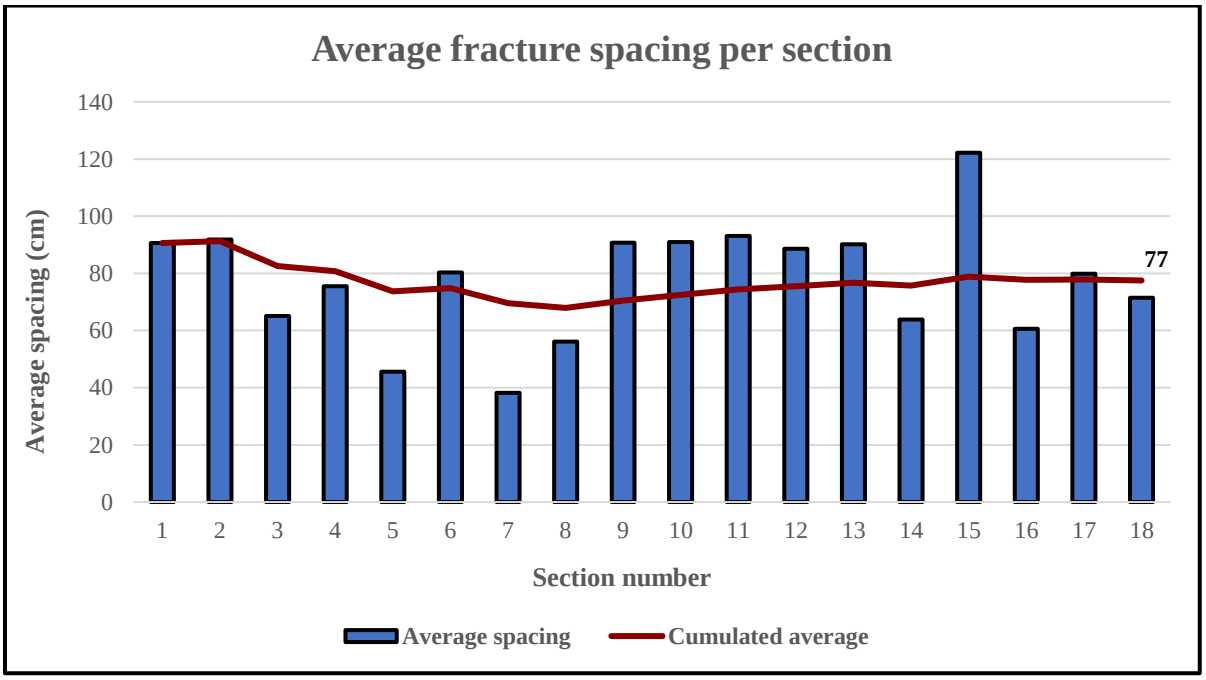

Figure 5.4 – *Averaged fracture spacing for each section. Notice the total weighted average value of 77 cm.*

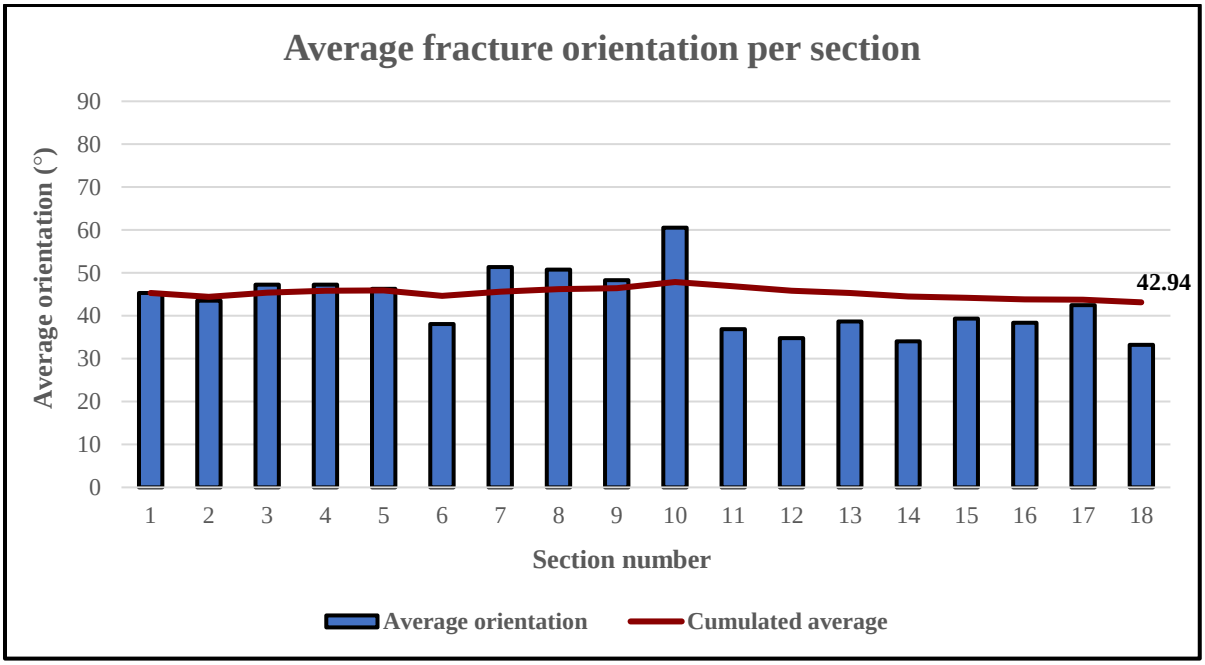

Figure 5.5 – *Averaged angles between fractures and TBM driven direction for each section. Notice the total weighted average value of 42.94 °.*

Q-values

From the cross-passage (CP) inspections and inspections in the escape tunnel, parameters included in the Q-method have been collected. Due to missing cross-passages in section 13, 15 and 17, the Q-values in these sections have been determined from OTV-analyses. All the results are presented in Appendix E.

Figure 5.6 displays the averaged Q-values and the associated cumulated average.

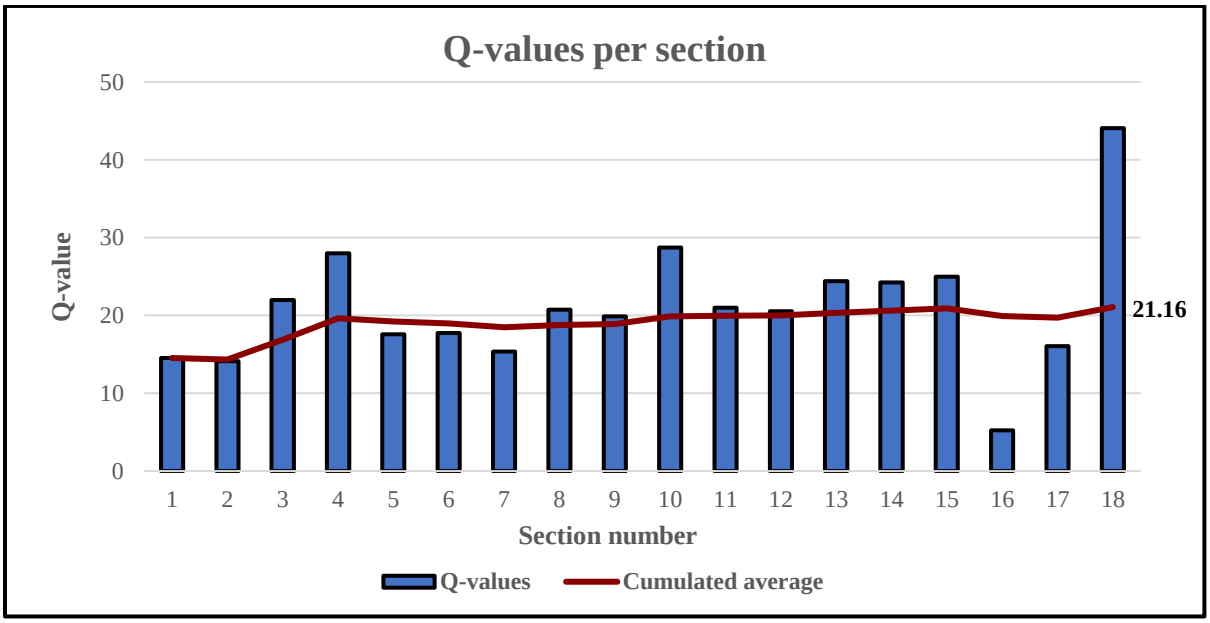

Figure 5.6 – *Averaged Q-values for each section. Notice the total weighted average value of 21.16.*

Laboratory tests

Results from a representative selection of parameters obtained from the laboratory tests are presented in the following. Figure 5.7 shows the averaged DRI for each section and the associated cumulated average.

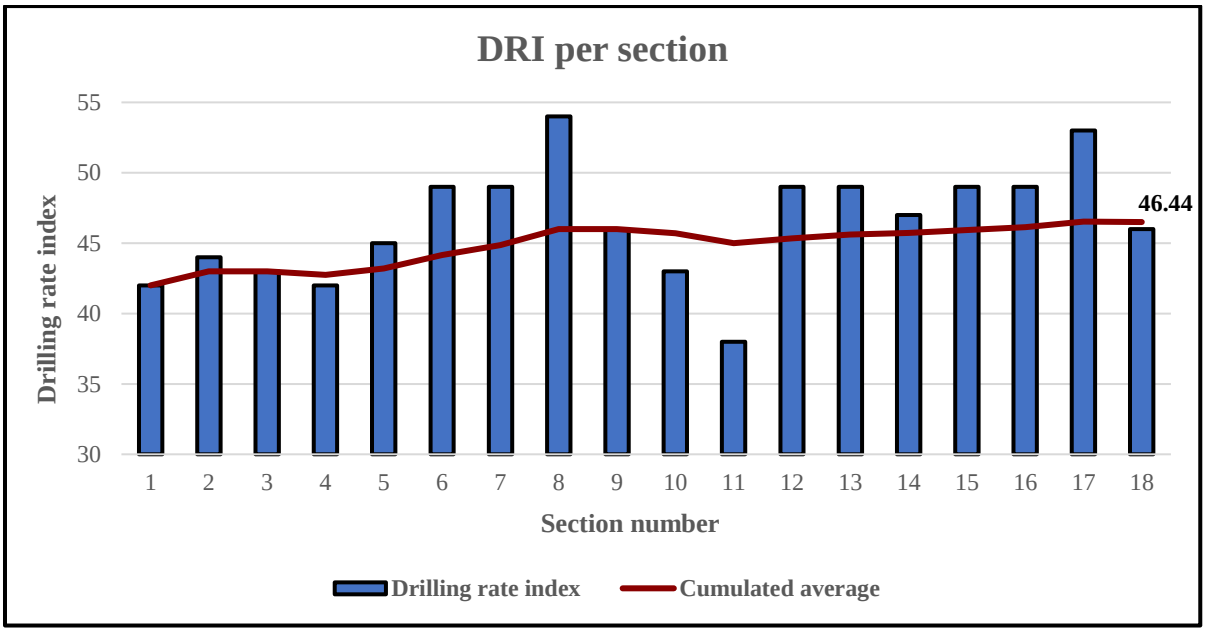

Figure 5.7 - *Averaged DRI-values for each section. Notice the total weighted average value of 46.44.*

Figure 5.8 shows the averaged CLI for each section and the associated cumulated average.

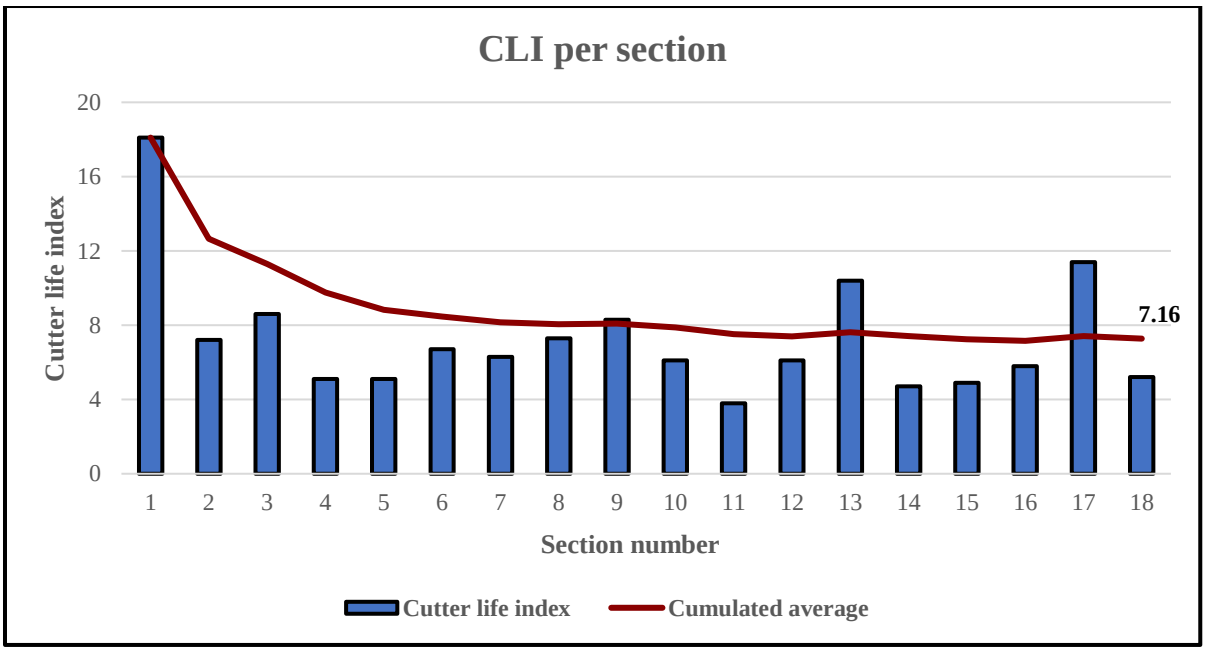

Figure 5.8 – *Averaged CLI-values for each section. Notice the total weighted average value of 7.16.*

Figure 5.9 shows the averaged quartz content for each section and the cumulated average.

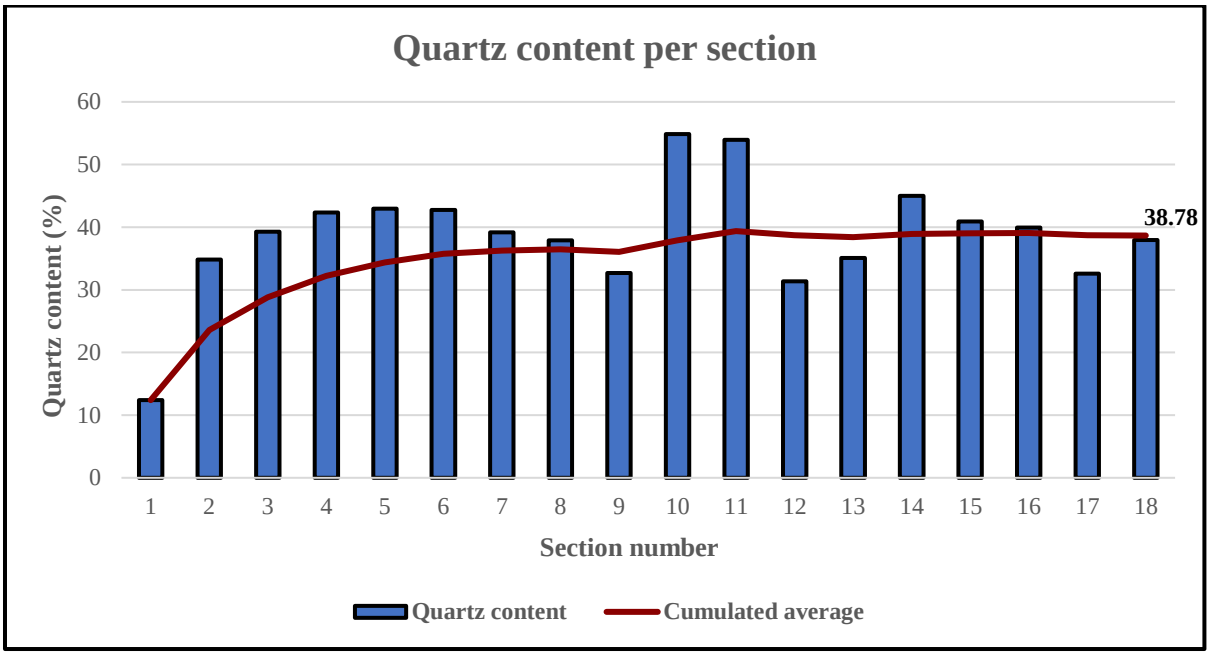

Figure 5.9 - *Averaged quartz content for each section. Notice the total weighted average value of 38.78 %.*

Figure 5.10 illustrates the averaged UCS values for each section and the cumulated average.

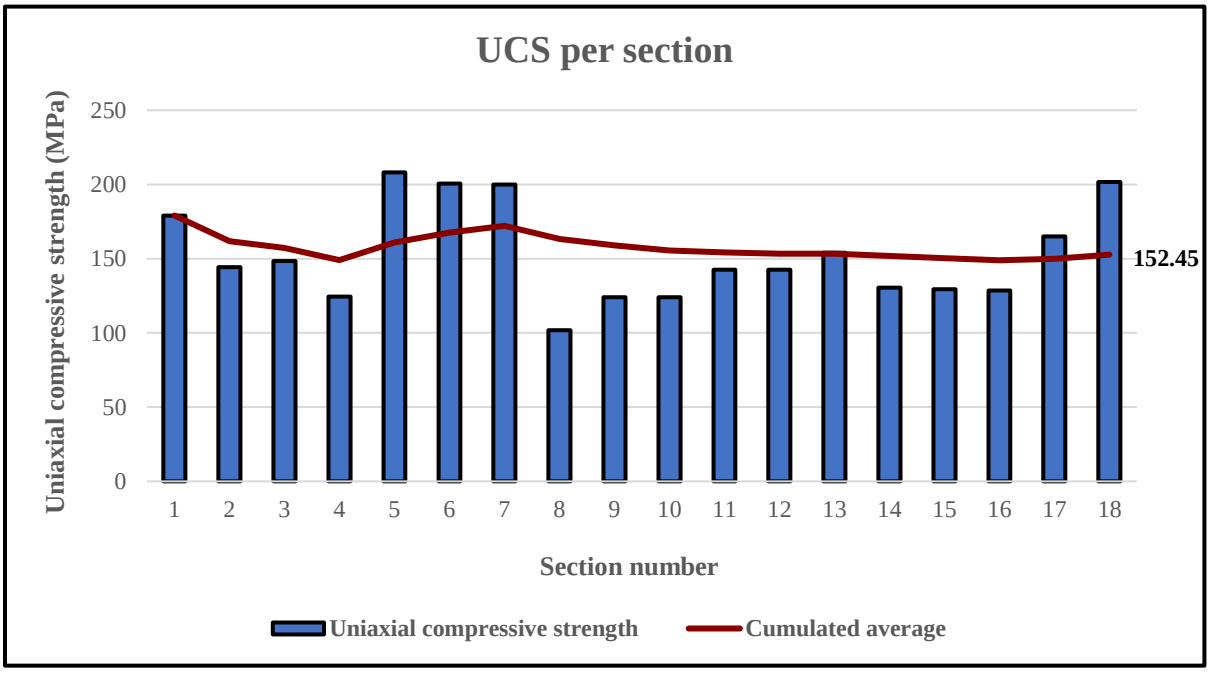

Figure 5.10 - *Averaged UCS values for each section. Notice the total weighted average value of 152.45 MPa.*

Figure 5.11 illustrates the averaged BTS values for each section and the associated cumulated average. Because the BTS values are based on the UCS values, the trend of these are similar (Fig. 5.10),

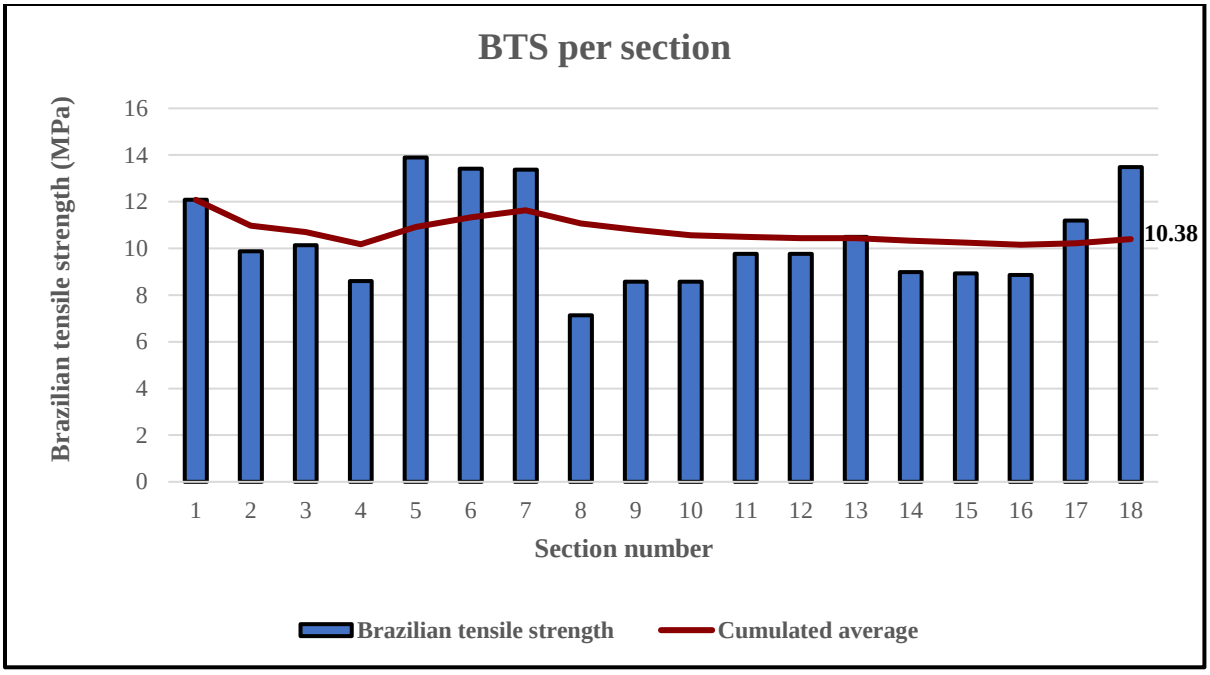

Figure 5.11 - *Averaged BTS values for each section. Notice the total weighted average value of 10.38 MPa.*

Machine data

The data presented in this chapter are downloaded according to the methods described in Chapter 4.4. The data are presented as averaged values per section**.** The comparisons and calculations are done with data from every 25th ring, which corresponds to every 45th meter. As pointed out in Table 4.7, the section lengths vary between 219 and 316 meters. The data in this chapter are presented as box plots with an attached standard deviation line. This is further discussed in Chapter 6.1.

Figures 5.12 to 5.14 illustrate the machine data and the associated cumulated averages.

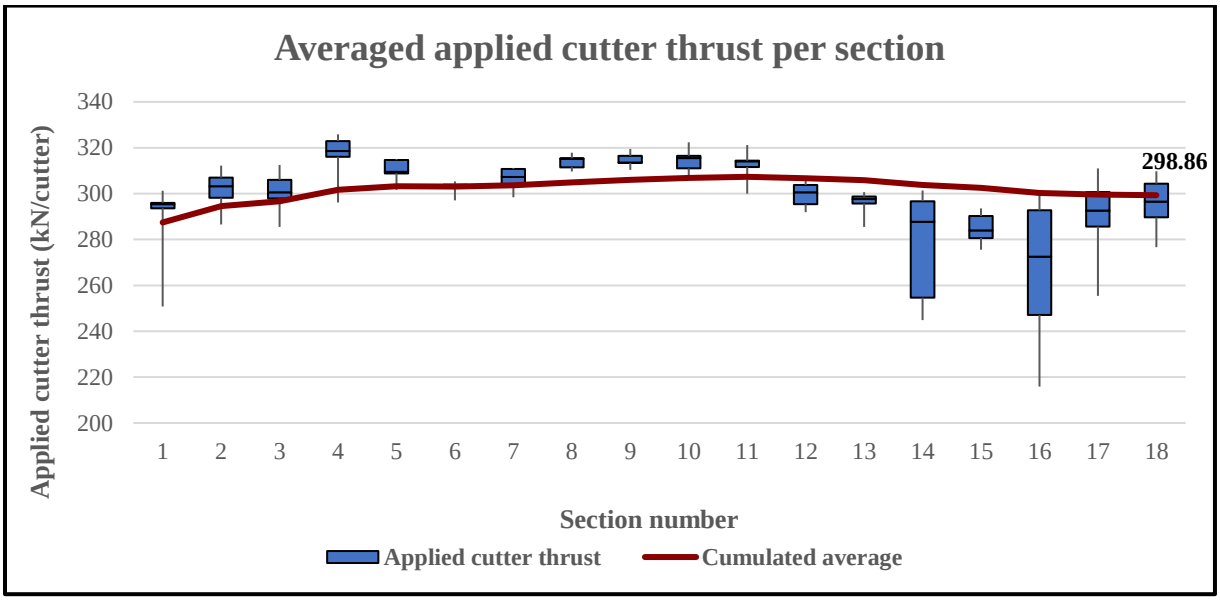

Figure 5.12 - *Averaged cutter thrust for each section. Notice the total weighted average value of 298.86.MPa.*

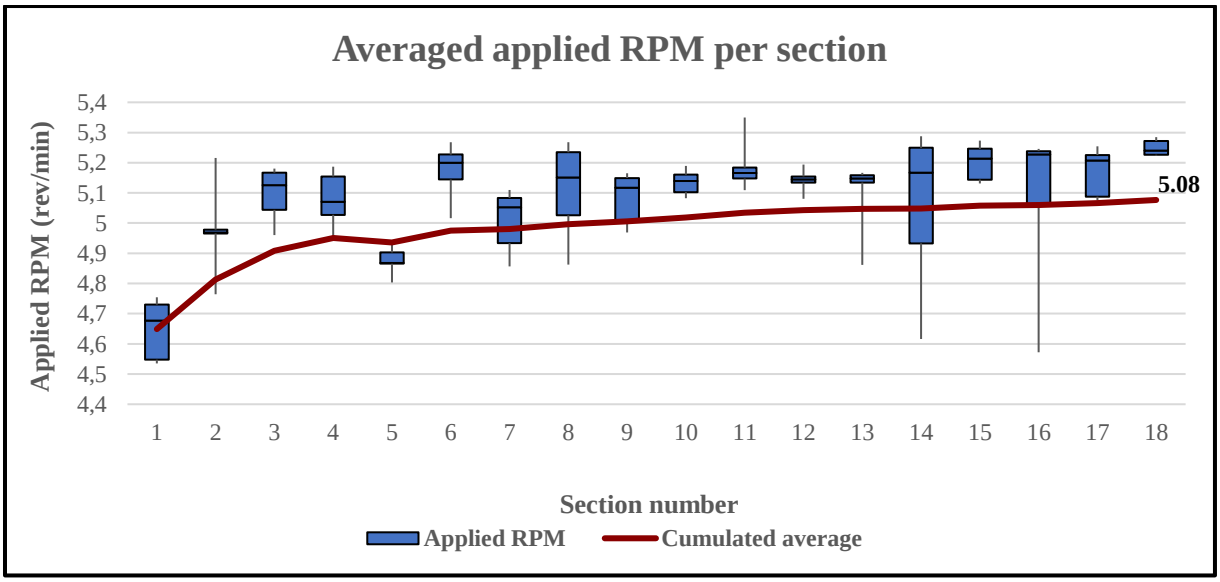

Figure 5.13 – *Averaged RPM for each section. Notice the total weighted average value of 5.08 rev/min.*

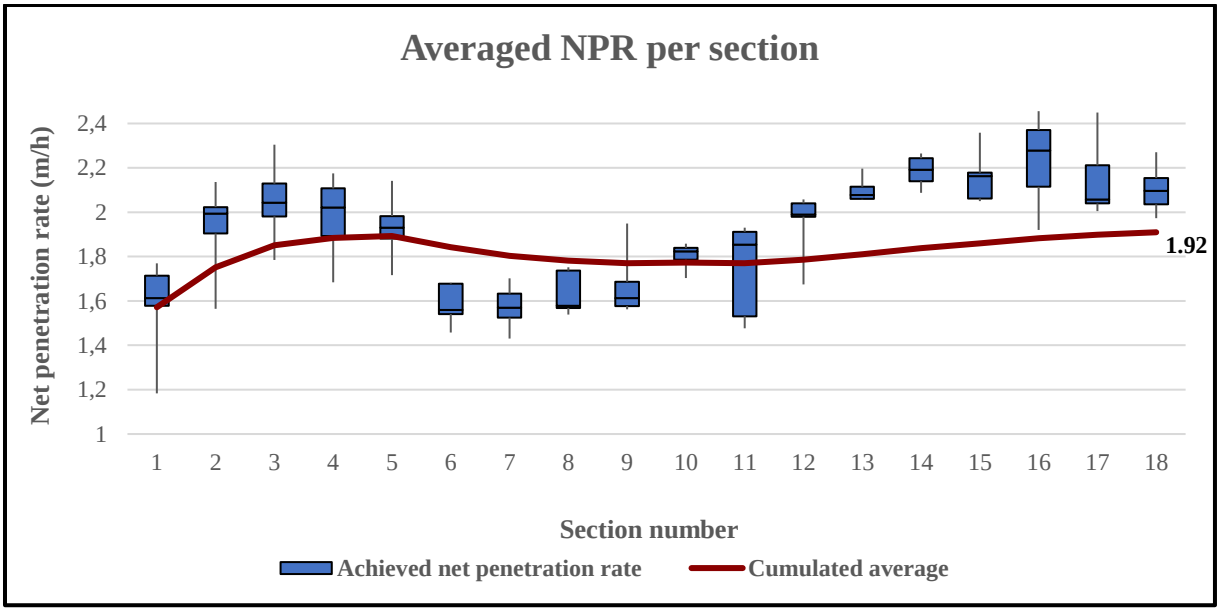

Figure 5.14 – *Averaged achieved NPR for each section. Notice the total weighted average value of 1.92 (m/h).*

The weighted averages of the downloaded machine data are presented in Table 5.1 with their related standard deviation.

Table 5.1 – *Weighted averages and standard deviations for the downloaded machine parameters.*

	RPM (rev/min)	**Total advance force (kN)**	**Cutter force (kN/cutter)**	**Basic penetration rate (mm/rev)**	**Net penetration rate (m/h)**
Total weighted average	5.08	21216.91	298.83	6.32	1.92
Standard deviation	0.18	1343.51	18.91	0.87	0.26
Deviation %	3.45%	6.33%		13.78%	13.71%

5.2 Prediction model results

This chapter presents the predicted NPRs from the different performance models. The results are presented in two different ways:

- Weighted average over the complete 4.5 km long tunnel alignment.
- Weighted average divided into 18 sections based on available data.

All the models are presented with both gross- and net thrust values as input parameters. The gross thrust is the applied thrust downloaded from the logged machine data, while the net thrust is defined as the gross thrust minus frictional drag. The frictional drag is set to 3200 kN, which is described in Chapter 4.5.5. It is important to distinguish between the terms gross-/net penetration rate and gross-/net thrust. The differences are described in Table 5.2.

Table 5.2 – *Terms important to distinguish when the results are presented.*

Terms	Definition
Gross penetration rate (GPR)	Penetration rate expressed in mm/rev
Net penetration rate (NPR)	Penetration rate expressed in m/h
Gross thrust	Applied thrust downloaded directly from the machine data
Net thrust	Gross thrust minus frictional drag

The NTNU model is the only prediction model using gross thrust as input parameter when the penetration rates are predicted. All the other performance prediction models use net thrusts as input, except the Q_{tbm} model and the model by Farrokh et al., where it is not stated whether gross or net thrust are used. Due to the different approaches of using thrust as input, the model calculations are presented in both ways.

All the results regarding the model calculations are presented in Appendix G.

5.2.1 The NTNU model

Results from the NTNU model by Bruland (2000) will be presented first. Thereafter, the results from the modified NTNU model by Macias (2016) will be presented. Information about these models are presented in Chapter 3.1.

5.2.1.1 The NTNU model by Bruland

The results calculated by this model are presented and compared to the achieved penetration rate in Figures 5.15 and 5.16.

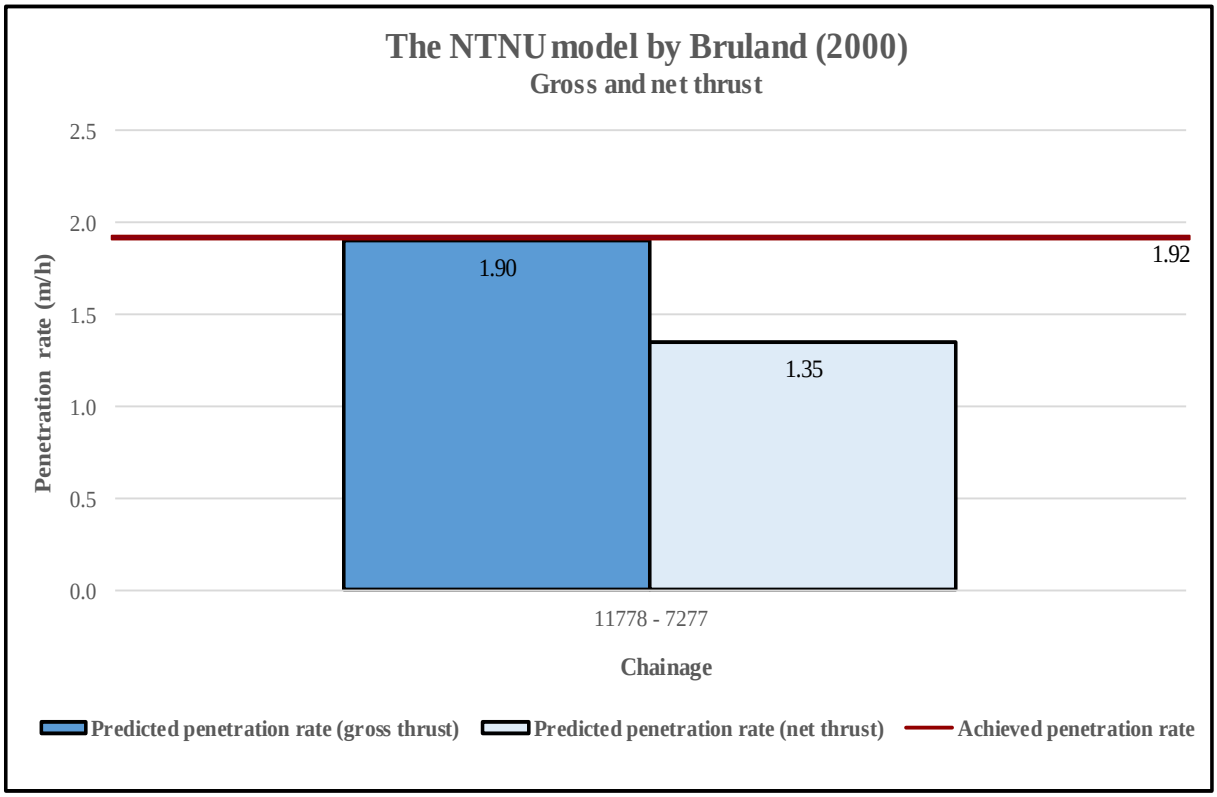

Figure 5.15 – *Weighted average penetration rate over the complete 4.5 km tunnel calculated with the NTNU model by Bruland (2000). The results are compared to the achieved penetration rate (red line).*

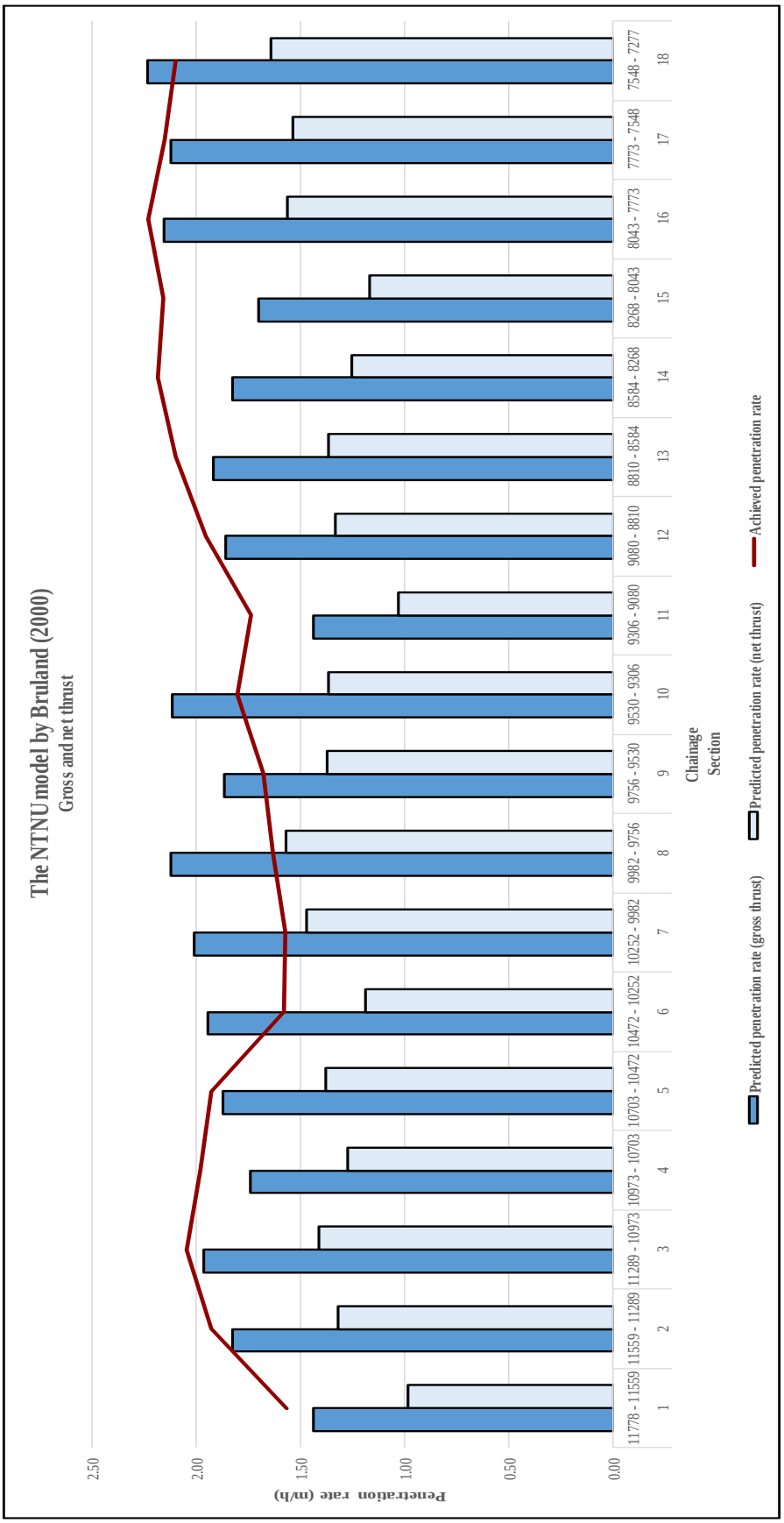

Figure 5.16 - *Average penetration rates for each section calculated with the NTNU model by Bruland (2000). The results are compared to the achieved penetration rate (red line).*

5.2.1.2 The NTNU model by Macias

The results calculated by this model are presented and compared to the achieved penetration rate in Figures 5.17 and 5.18.

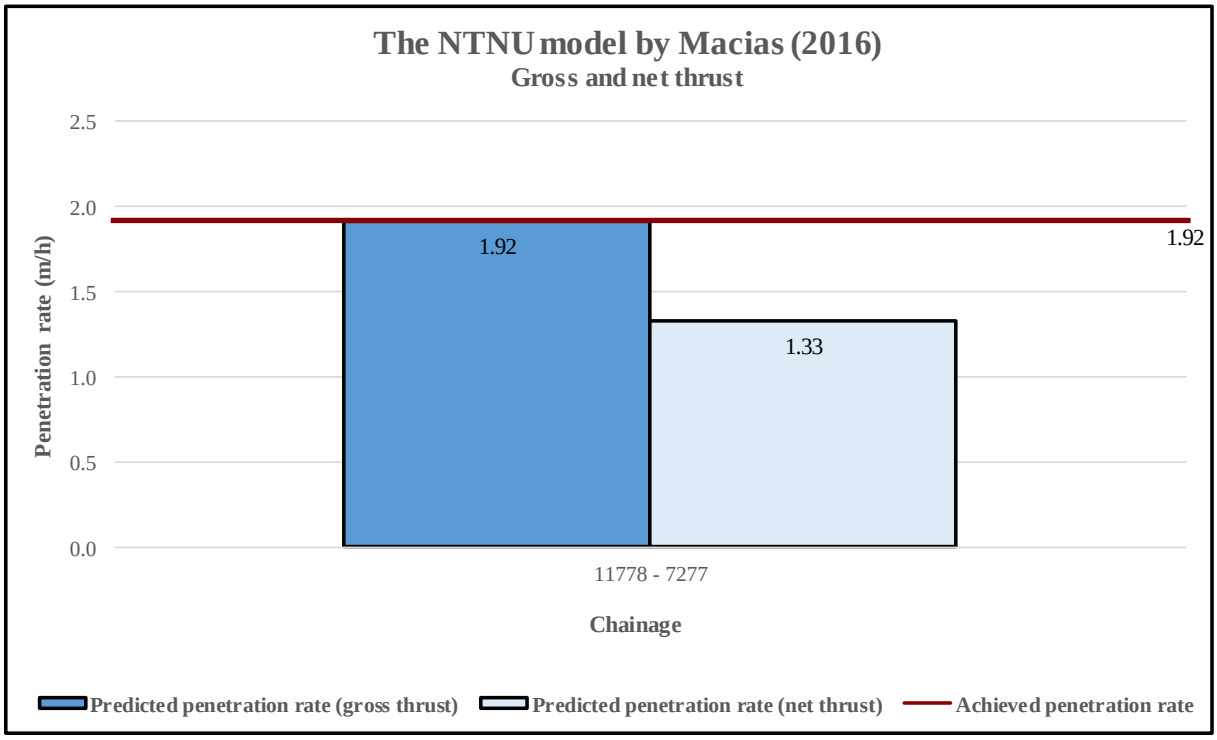

Figure 5.17 – *Weighted average penetration rates over the complete 4.5 km tunnel calculated with the NTNU model by Macias (2016). The results are compared to the achieved penetration rate (red line).*

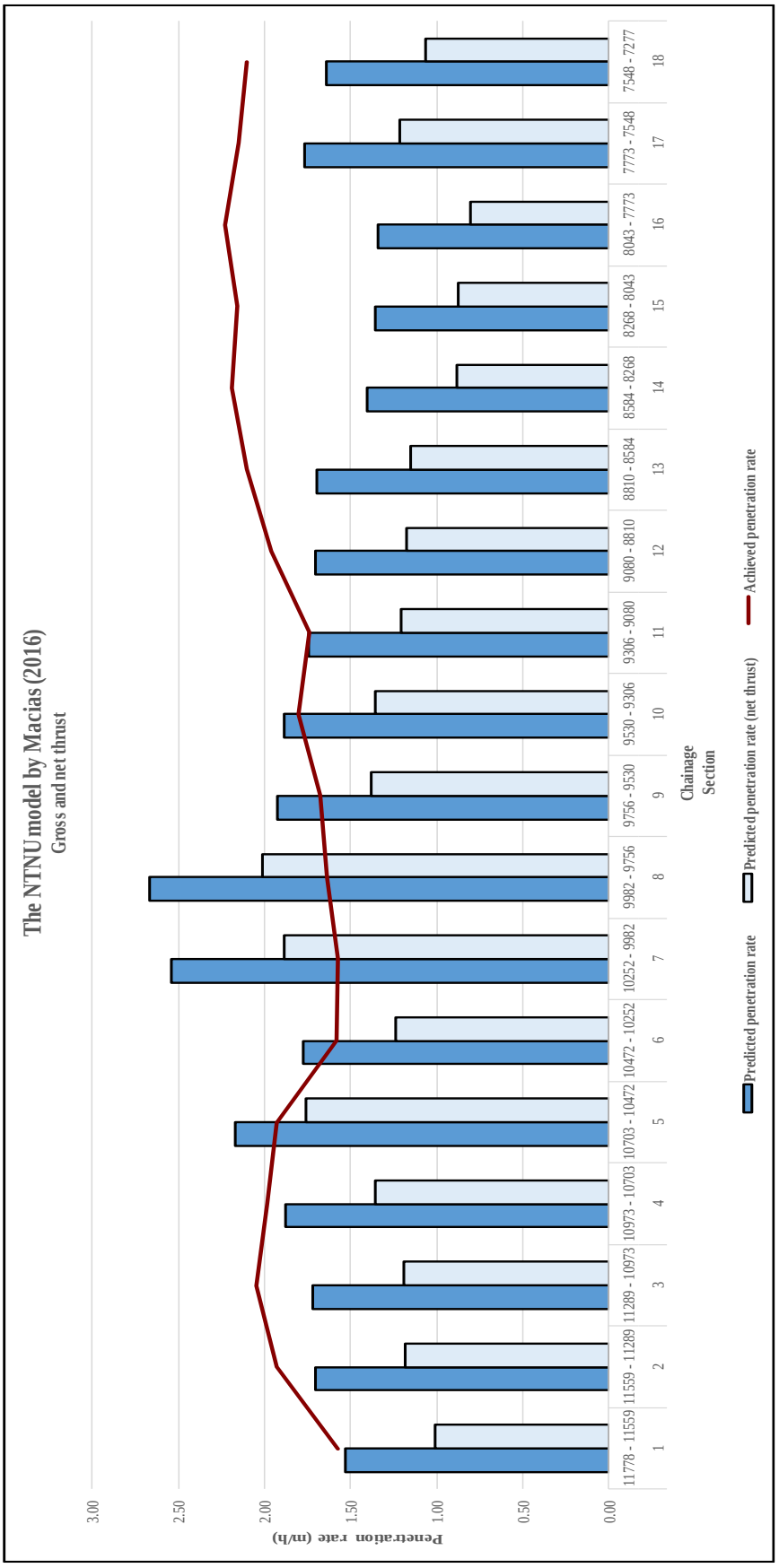

Figure 5.18 - *Average penetration rates for each section calculated with the NTNU model by Macias (2016). The results are compared to the achieved penetration rate (red line).*

5.2.2 The Colorado School of Mines (CSM) model

Results from the CSM model by Rostami (1997) will be presented first. Thereafter, the results from the MCSM model by Yagiz (2002) will be presented. Information about these models are presented in Chapter 3.2.

5.2.2.1 The CSM model by Rostami

The results calculated by this model are presented and compared to the achieved penetration rate in Figures 5.19 and 5.20.

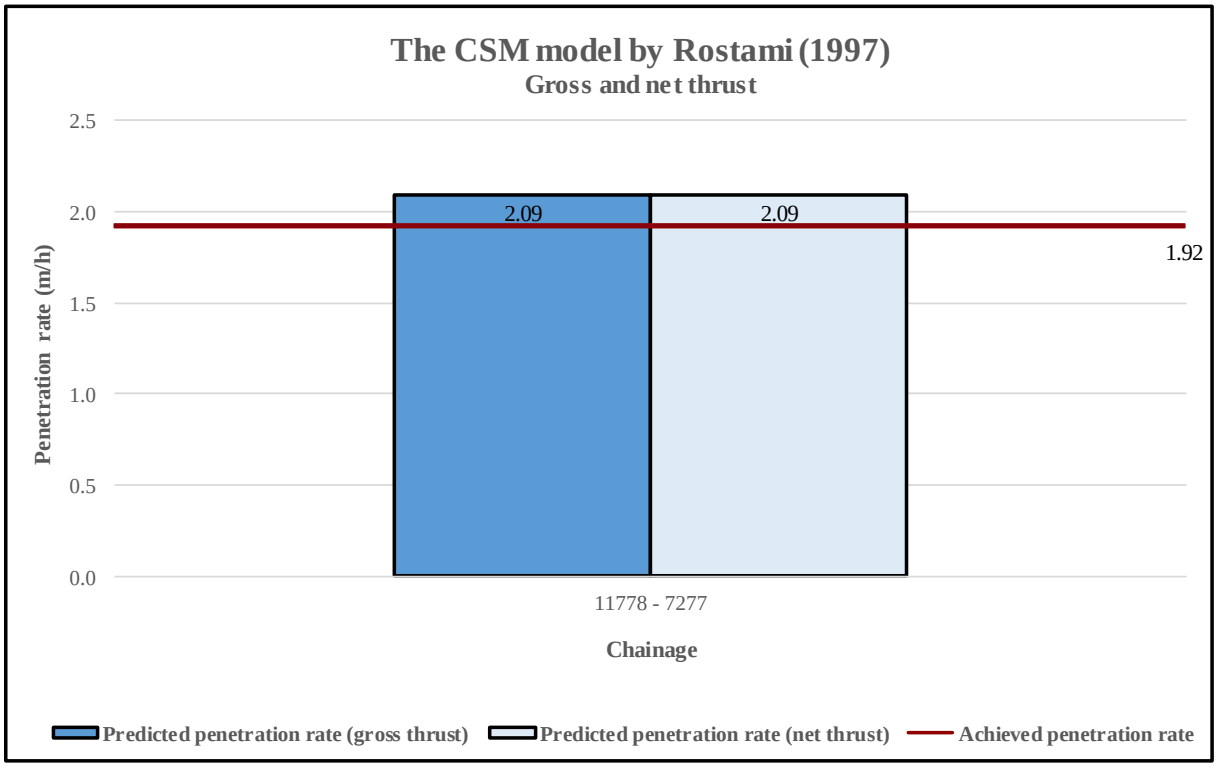

Figure 5.19 – *Weighted average penetration rate over the complete 4.5 km tunnel calculated with the CSM model by Rostami (1997). The results are compared to the achieved penetration rate (red line).*

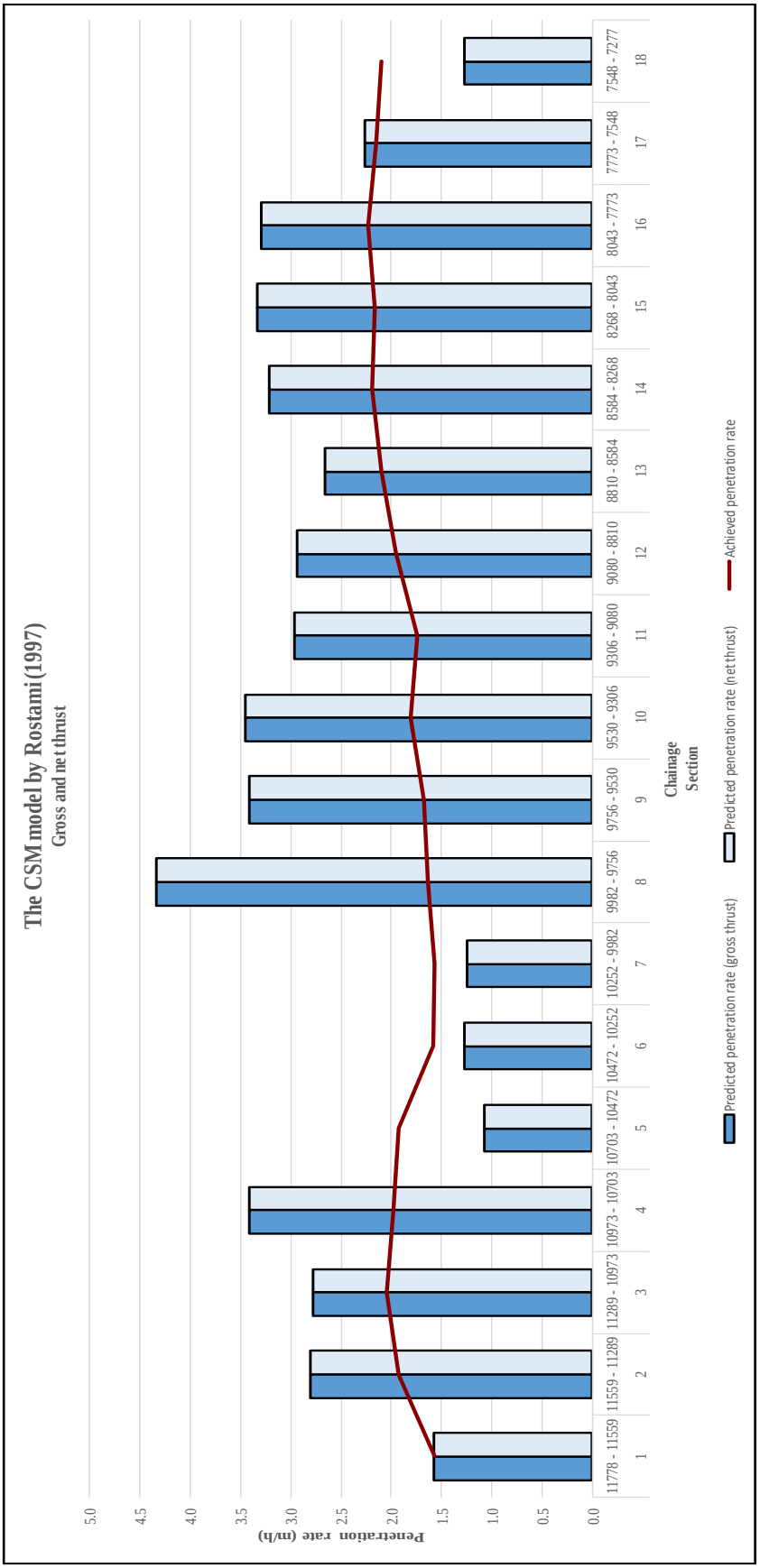

Figure 5.20 - *Average penetration rates for each section calculated with the CSM model by Rostami (1997). The results are compared to the achieved penetration rate (red line).*

5.2.2.2 The MCSM model by Yagiz

The results calculated by this model are presented and compared to the achieved penetration rate in Figures 5.21 and 5.22.

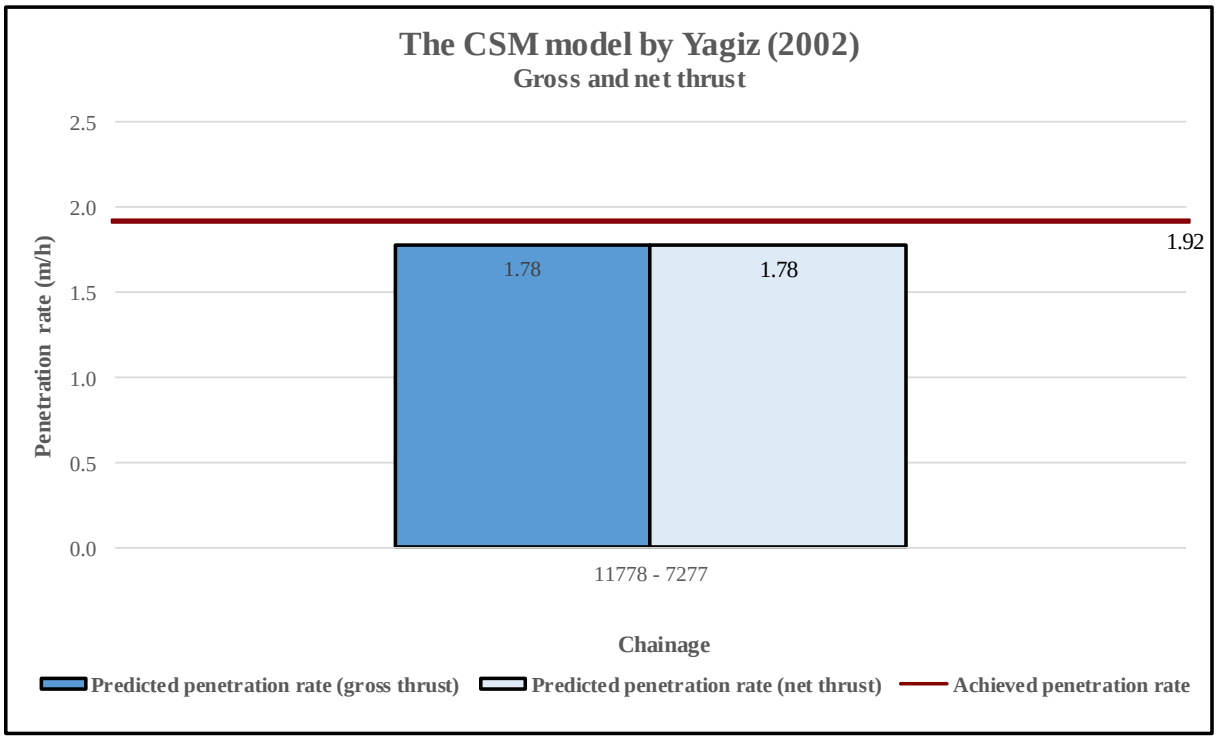

Figure 5.21 – *Weighted average penetration rate over the complete 4.5 km tunnel calculated with the MCSM model by Yagiz (2002). The results are compared to the achieved penetration rate (red line).*

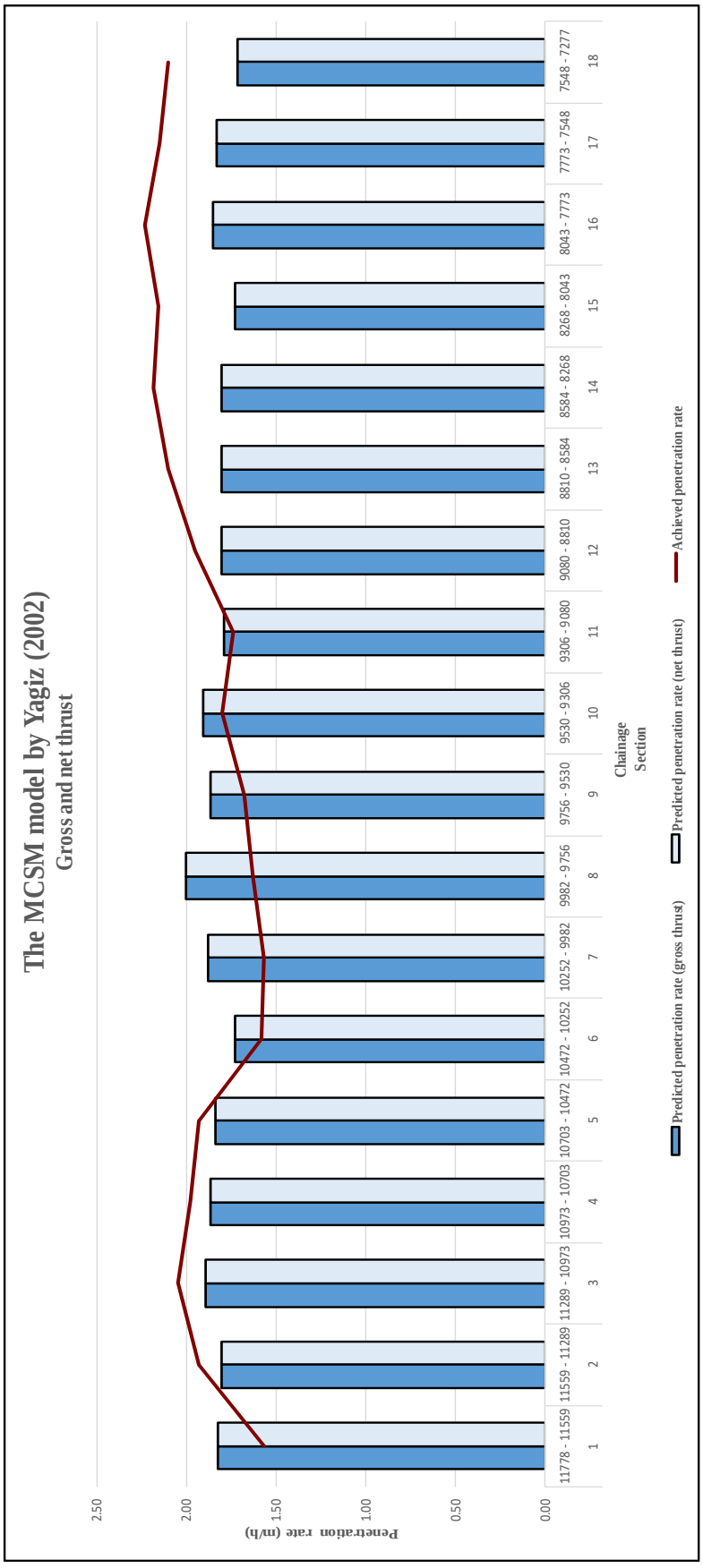

Figure 5.22 - *Average penetration rates for each section calculated with the MCSM model by Yagiz (2002). The results are compared to the achieved penetration rate (red line).*

5.2.3 The Gehring model

Results from the Gehring model by Gehring (1995) will be presented first. Thereafter, the results from the Alpine model by Wilfing (2016) will be presented. Information about these models are presented in Chapter 3.3.

5.2.3.1 The Gehring model by Gehring

The results calculated by this model are presented and compared to the achieved penetration rate in Figures 5.23 and 5.24.

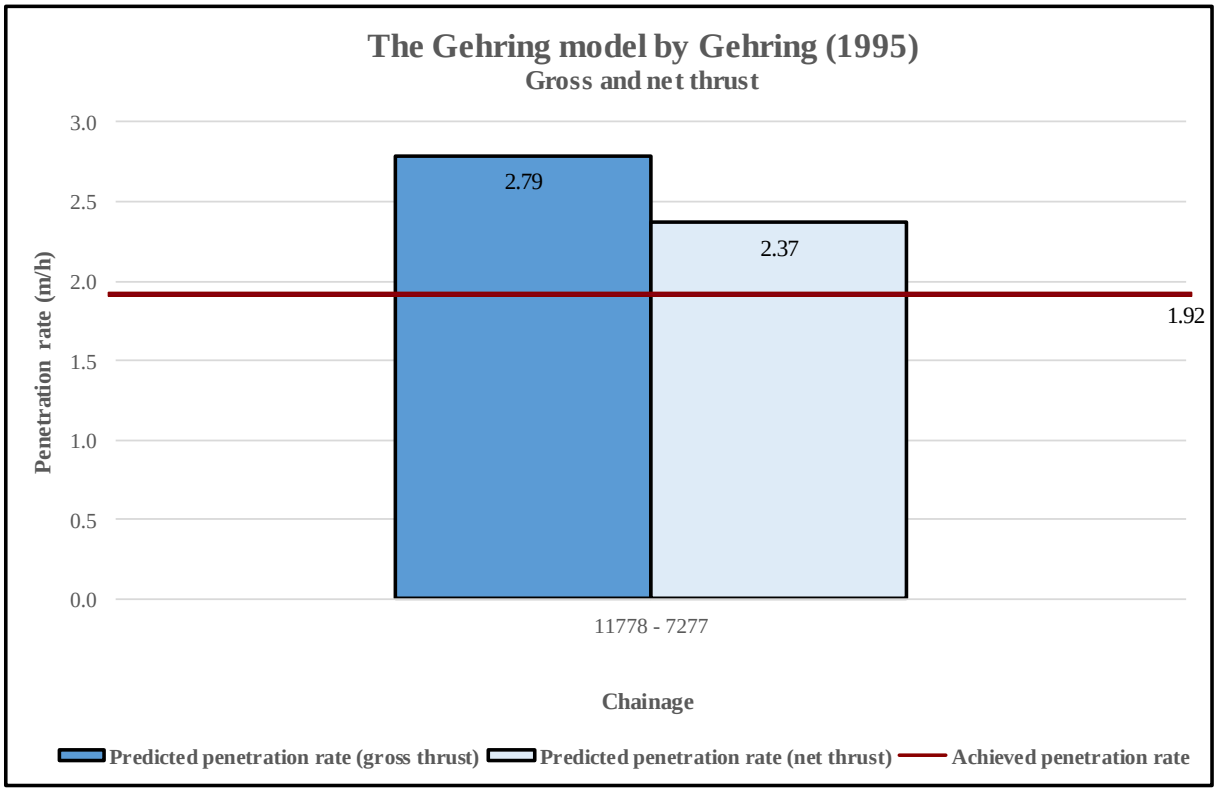

Figure 5.23 – *Weighted average penetration rate over the complete 4.5 km tunnel calculated with the Gehring model by Gehring (1995). The results are compared to the achieved penetration rate (red line).*

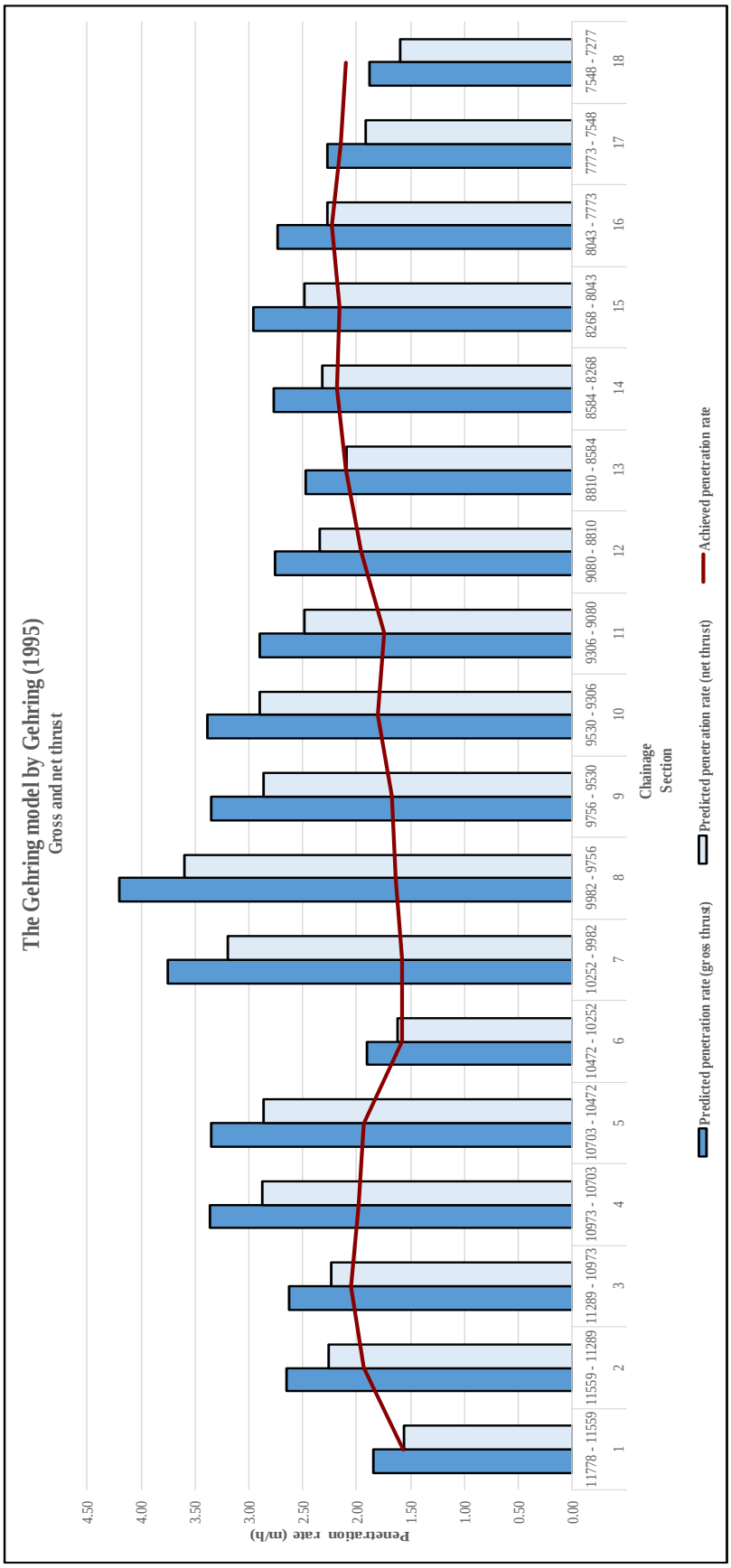

Figure 5.24 - *Average penetration rates for each section calculated with the Gehring model by Gehring (1995). The results are compared to the achieved penetration rate (red line).*

5.2.3.2 The Alpine model by Wilfing

The results calculated by this model are presented and compared to the achieved penetration rate in Figures 5.25 and 5.26.

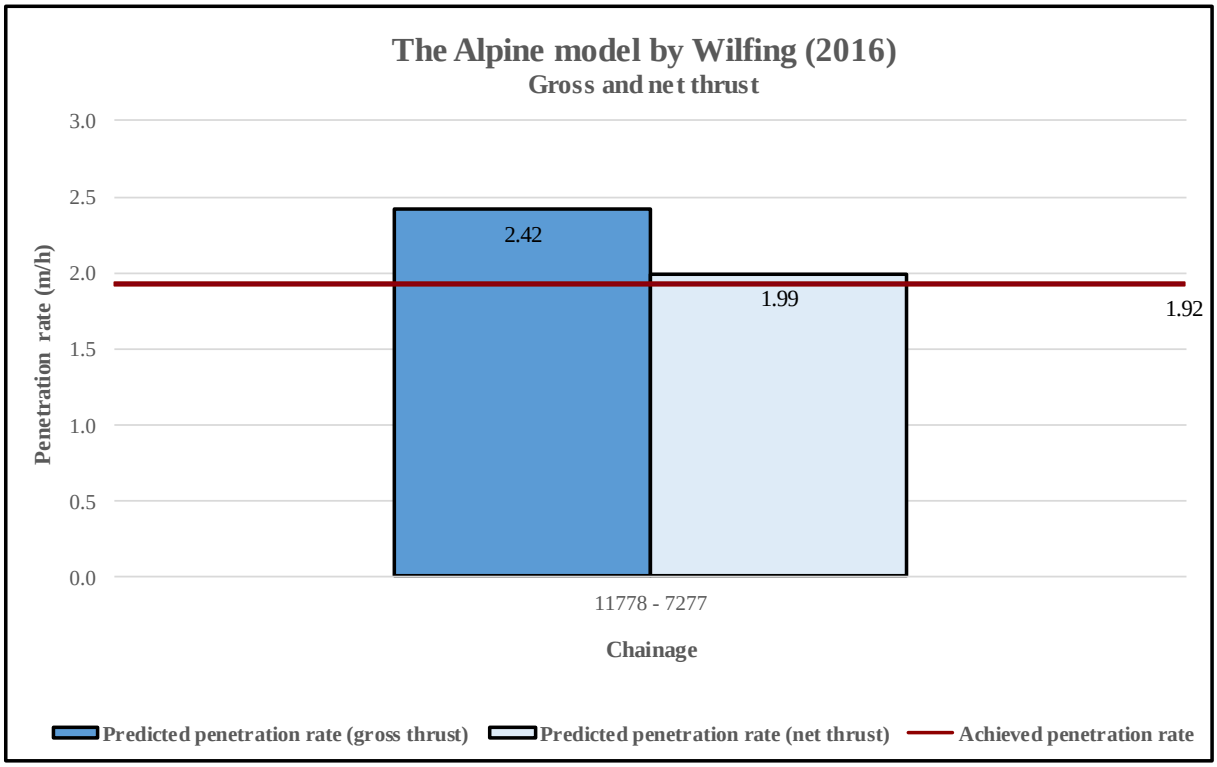

Figure 5.25 – *Weighted average penetration rate over the complete 4.5 km tunnel calculated with the Alpine model by Wilfing (2016). The results are compared to the achieved penetration rate (red line).*

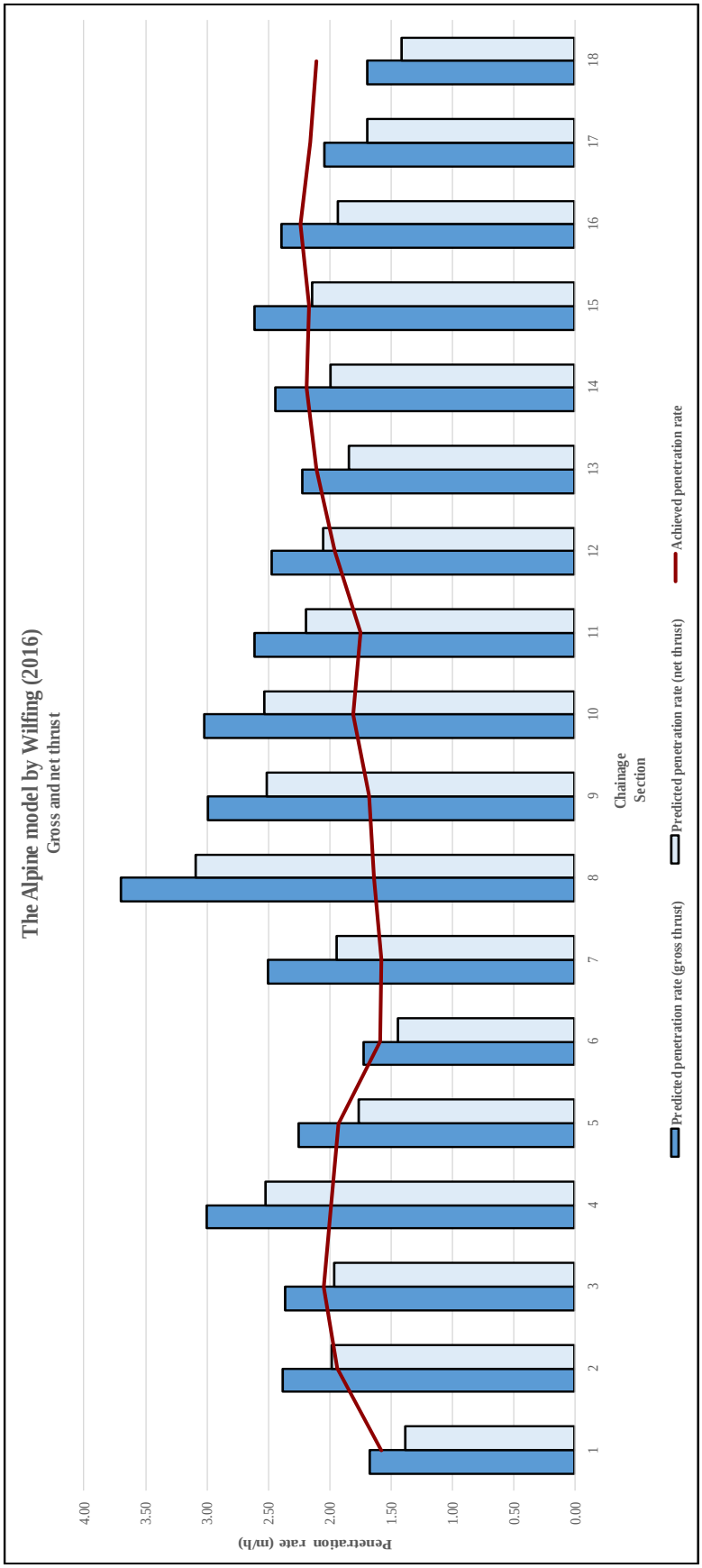

Figure 5.26 - *Average penetration rates for each section calculated with the Alpine model by Wilfing (2016). The results are compared to the achieved penetration rate (red line).*

5.2.4 The Q_{tbm} model by Nick Barton

Results from the Q_{tbm} model by Barton (2000) will be presented in the following. Information about this model is presented in Chapter 3.4.

The results calculated by this model are presented and compared to the achieved penetration rate in Figures 5.27 and 5.28.

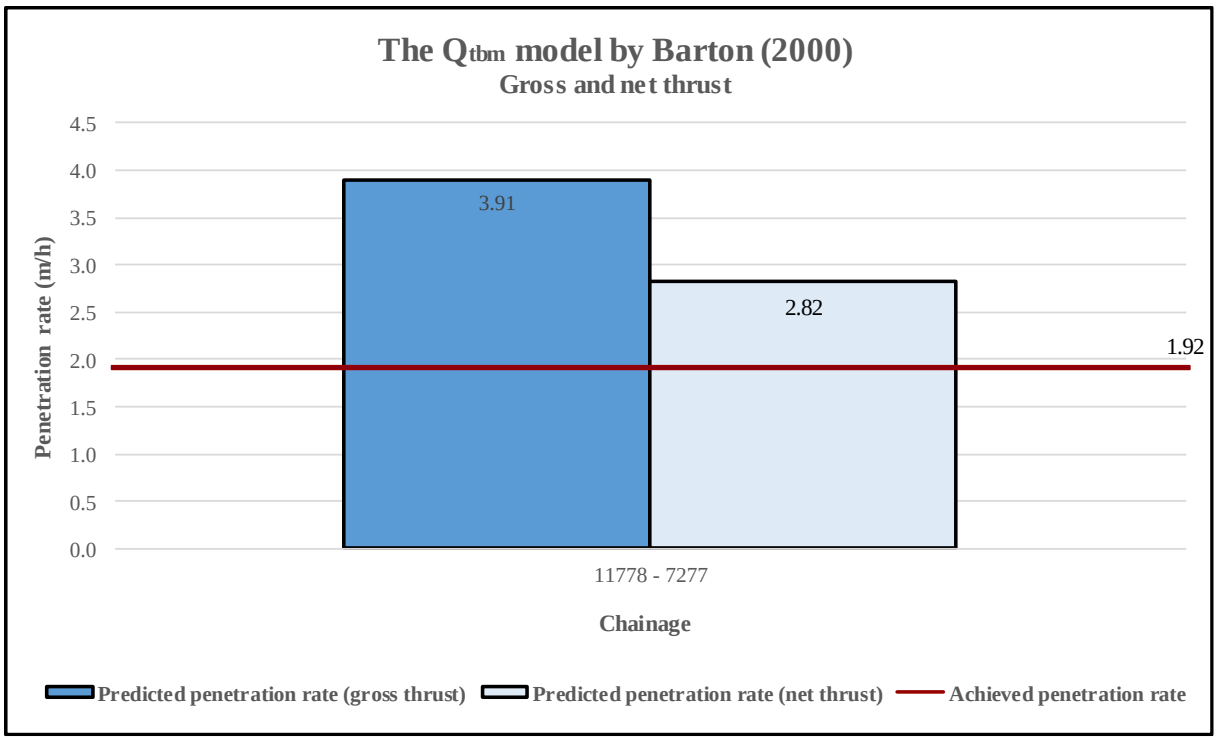

Figure 5.27 – *Weighted average penetration rate over the complete 4.5 km tunnel calculated with the Q_{tbm} model by Barton (2000). The results are compared to the achieved penetration rate (red line).*

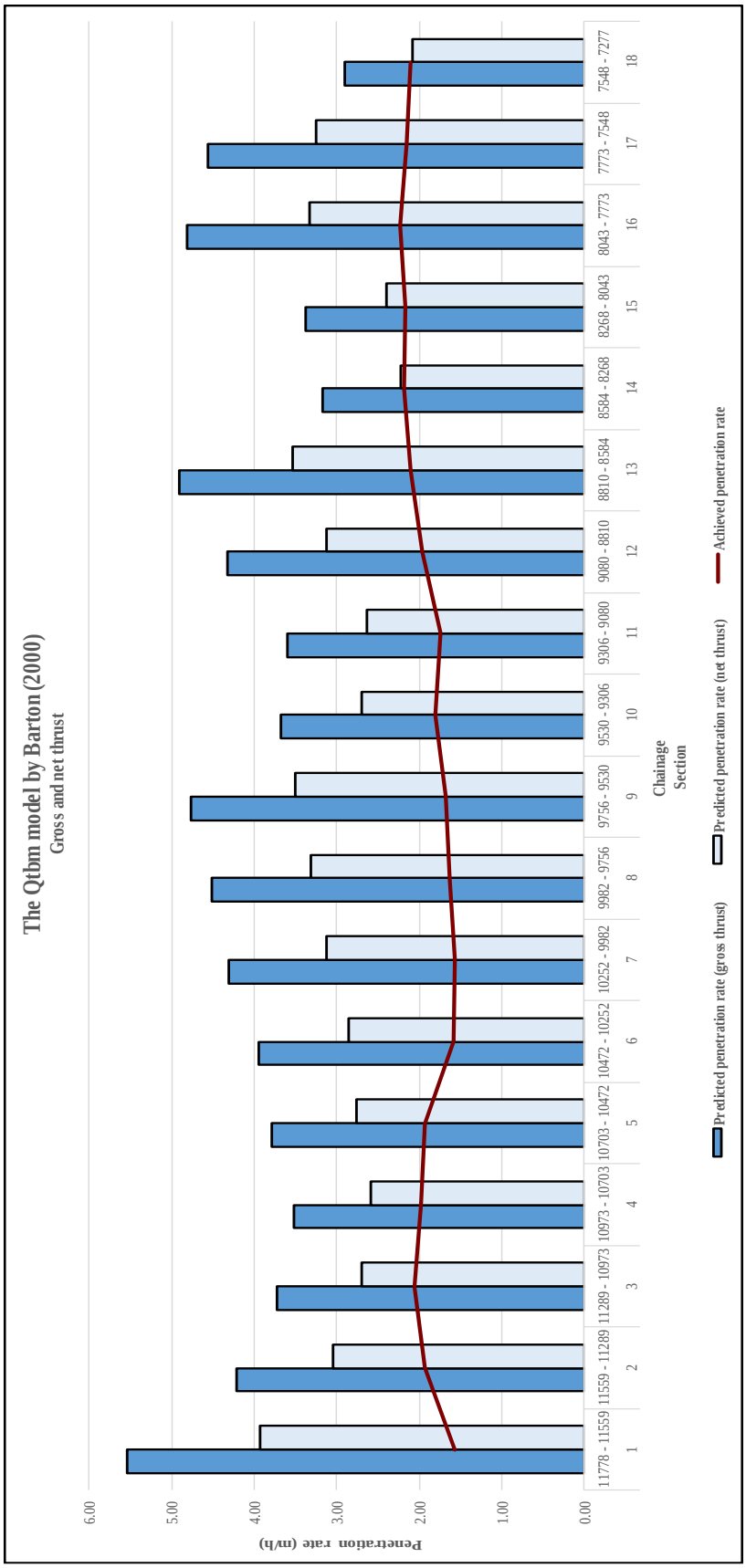

Figure 5.28 - *Average penetration rates for each section calculated with the Q_{tbm} model by Barton (2000). The results are compared to the achieved penetration rate (red line).*

5.2.5 The prediction model by Yagiz

Results from model by Yagiz (2008) will be presented in the following. Information about this model is presented in Chapter 3.5.

The results calculated by this model are presented and compared to the achieved penetration rate in Figures 5.29 and 5.30.

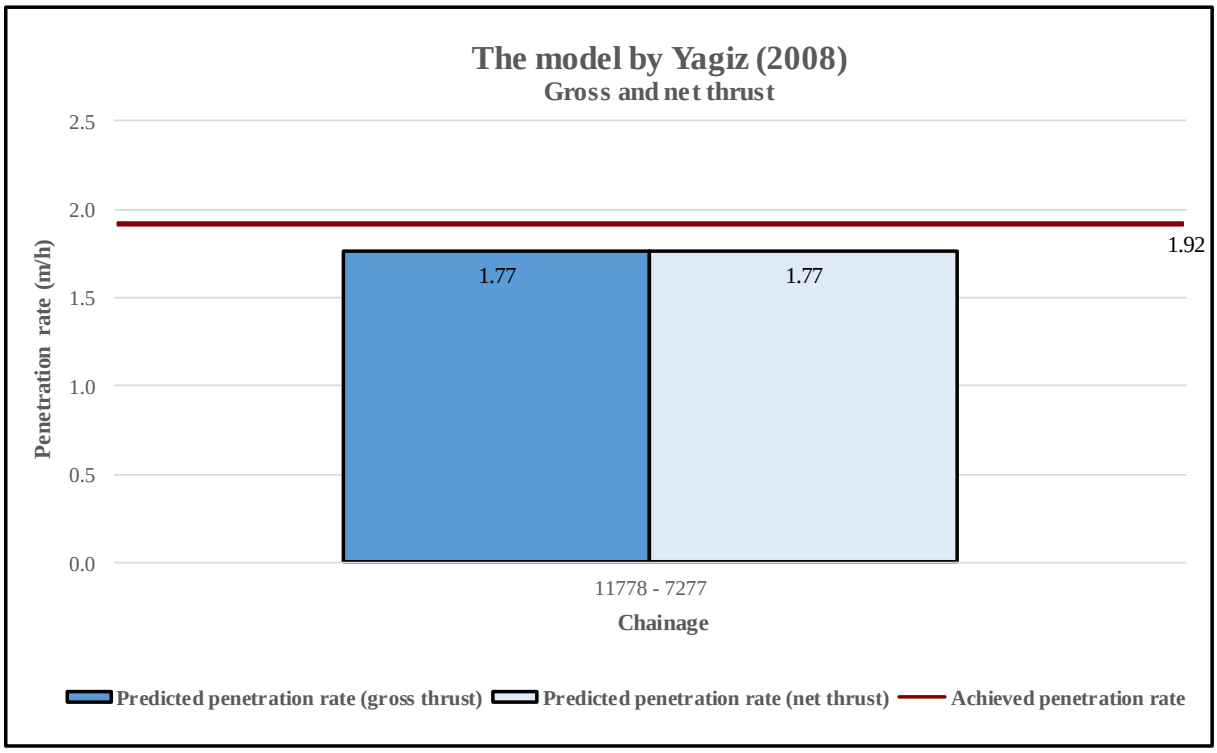

Figure 5.29 – *Weighted average penetration rate over the complete 4.5 km tunnel calculated with the model by Yagiz (2008). The results are compared to the achieved penetration rate (red line).*

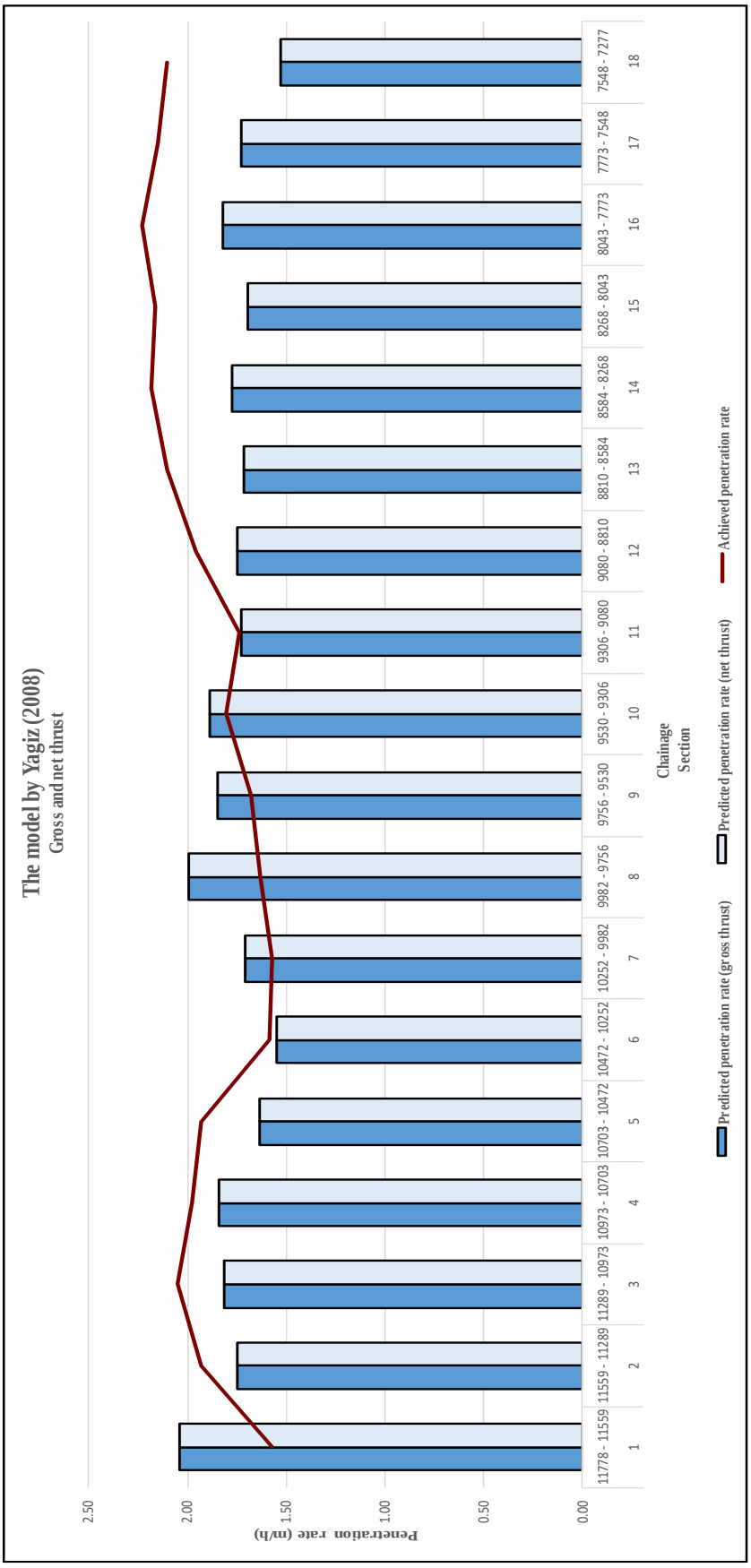

Figure 5.30 - *Average penetration rates for each section calculated with the model by Yagiz (2008). The results are compared to the achieved penetration rate (red line).*

5.2.6 The model by Hassanpour et al.

Results from the prediction model by Hassanpour et al. (2011) will be presented in the following. Information about this model is presented in Chapter 3.6.

The results calculated by this model are presented and compared to the achieved penetration rate in Figures 5.31 and 5.32.

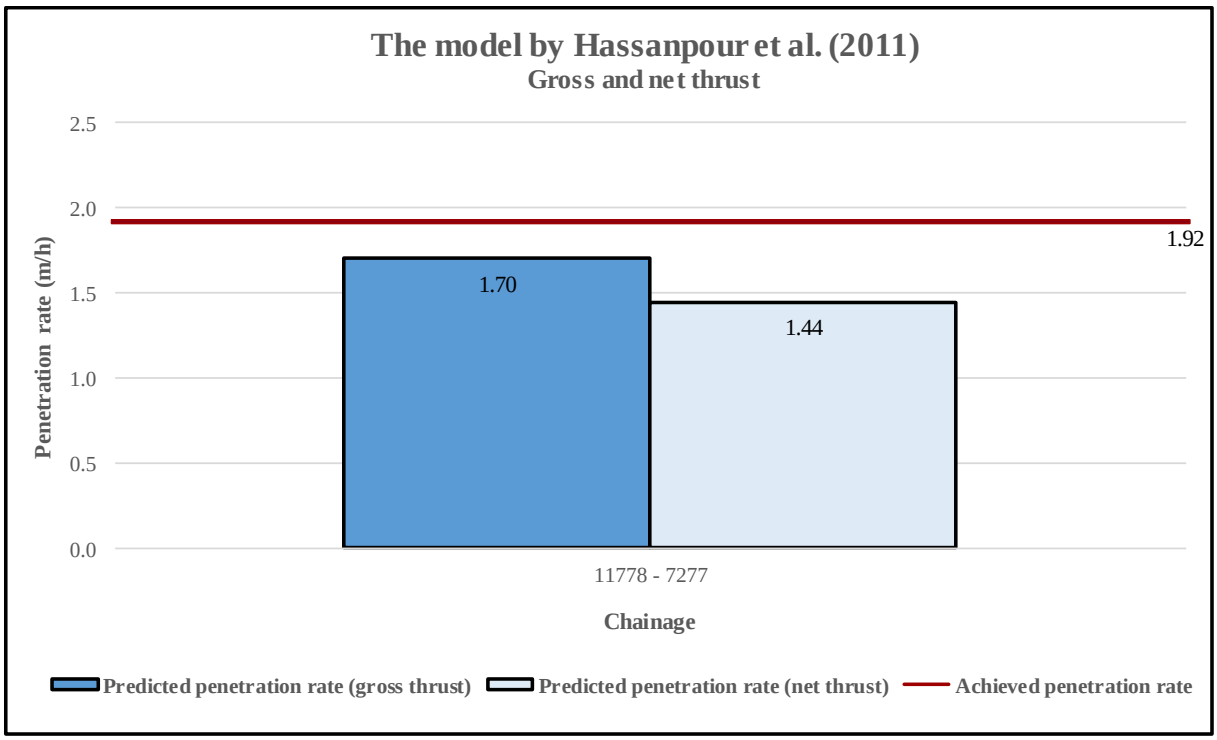

Figure 5.31 – *Weighted average penetration rate over the complete 4.5 km tunnel calculated with the prediction model by Hassanpour et al. (2011). The results are compared to the achieved penetration rate (red line).*

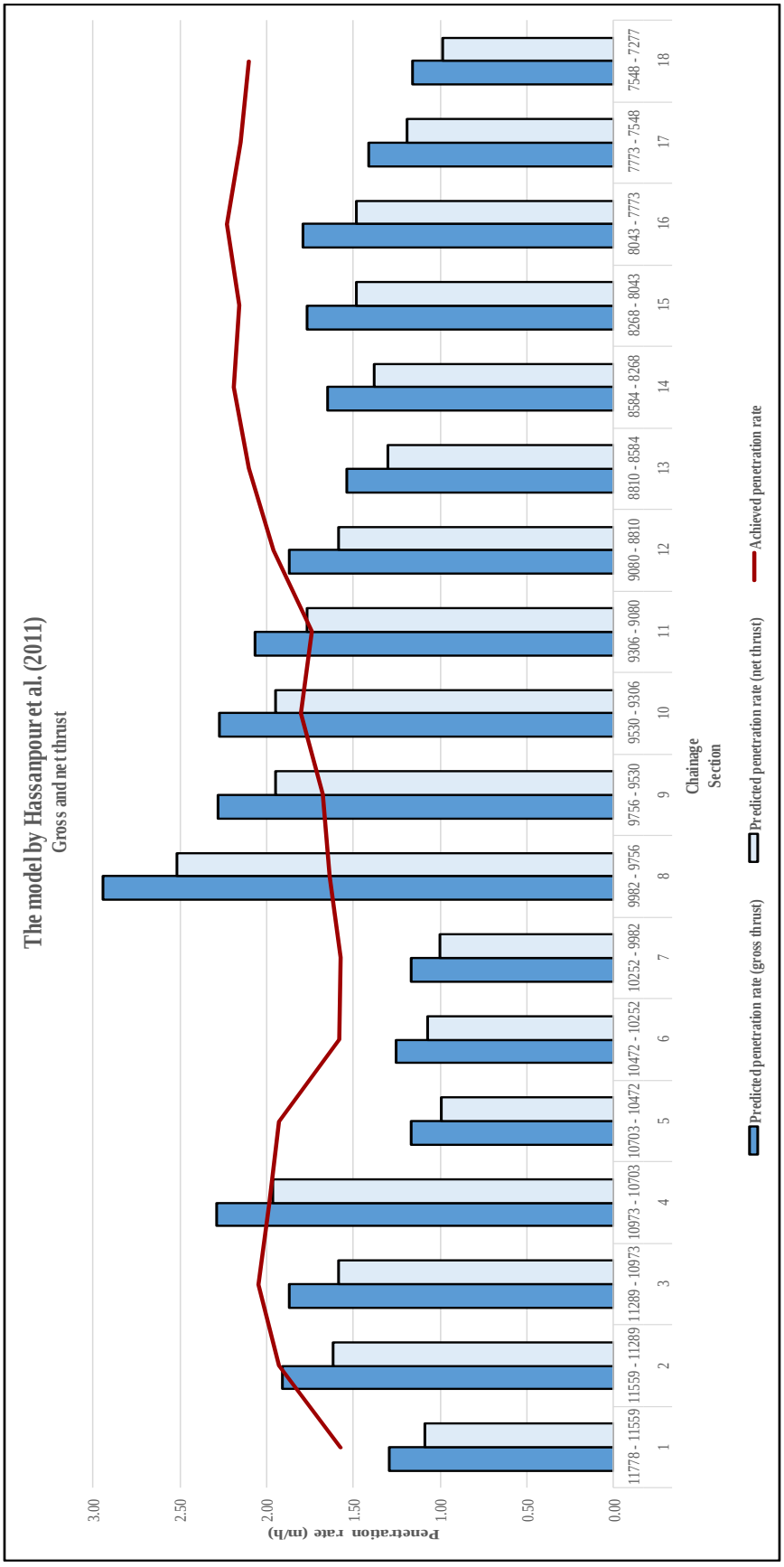

Figure 5.32 - *Average penetration rates for each section calculated with the model by Hassanpour et al. (2011). The results are compared to the achieved penetration rate (red line).*

5.2.7 The model by Farrokh et al.

Results from the prediction model by Farrokh t al. (2012) will be presented in the following. Information about this model is presented in Chapter 3.7.

The results calculated by this model are presented and compared to the achieved penetration rate in Figures 5.33 and 5.34.

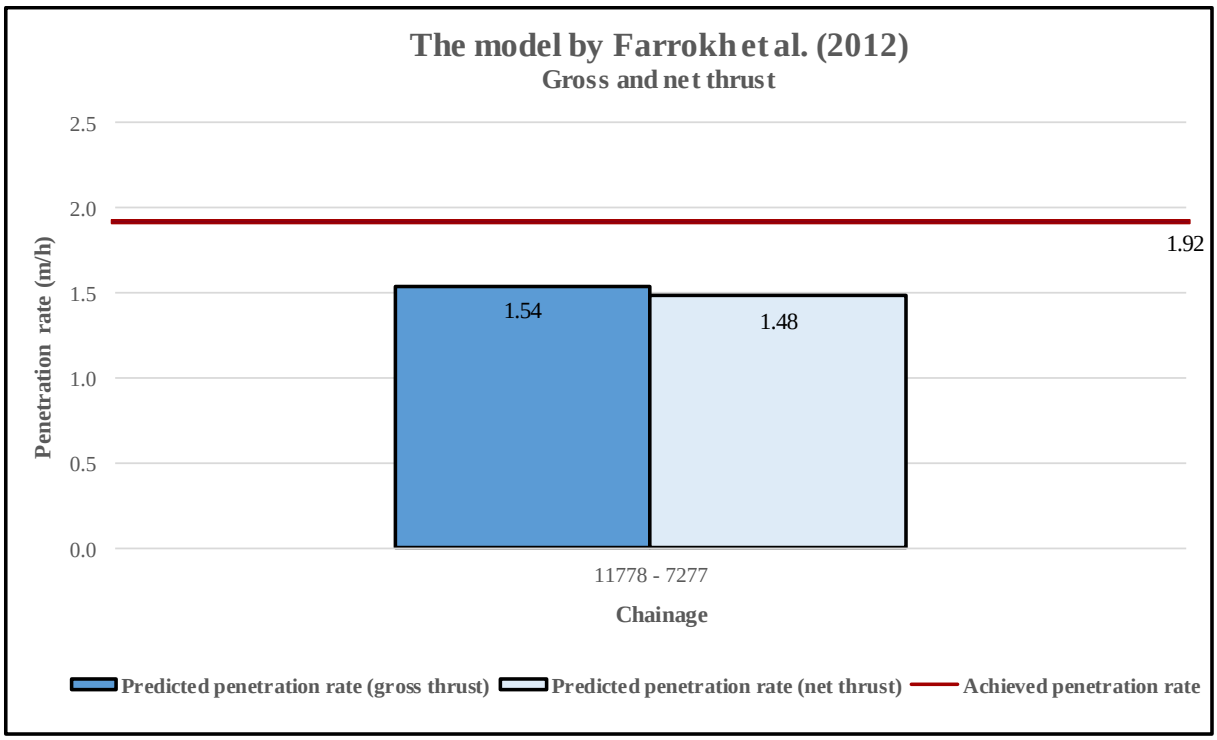

Figure 5.33 – *Weighted average penetration rate over the complete 4.5 km tunnel calculated with the prediction model by Farrokh et al. (2012). The results are compared to the achieved penetration rate (red line).*

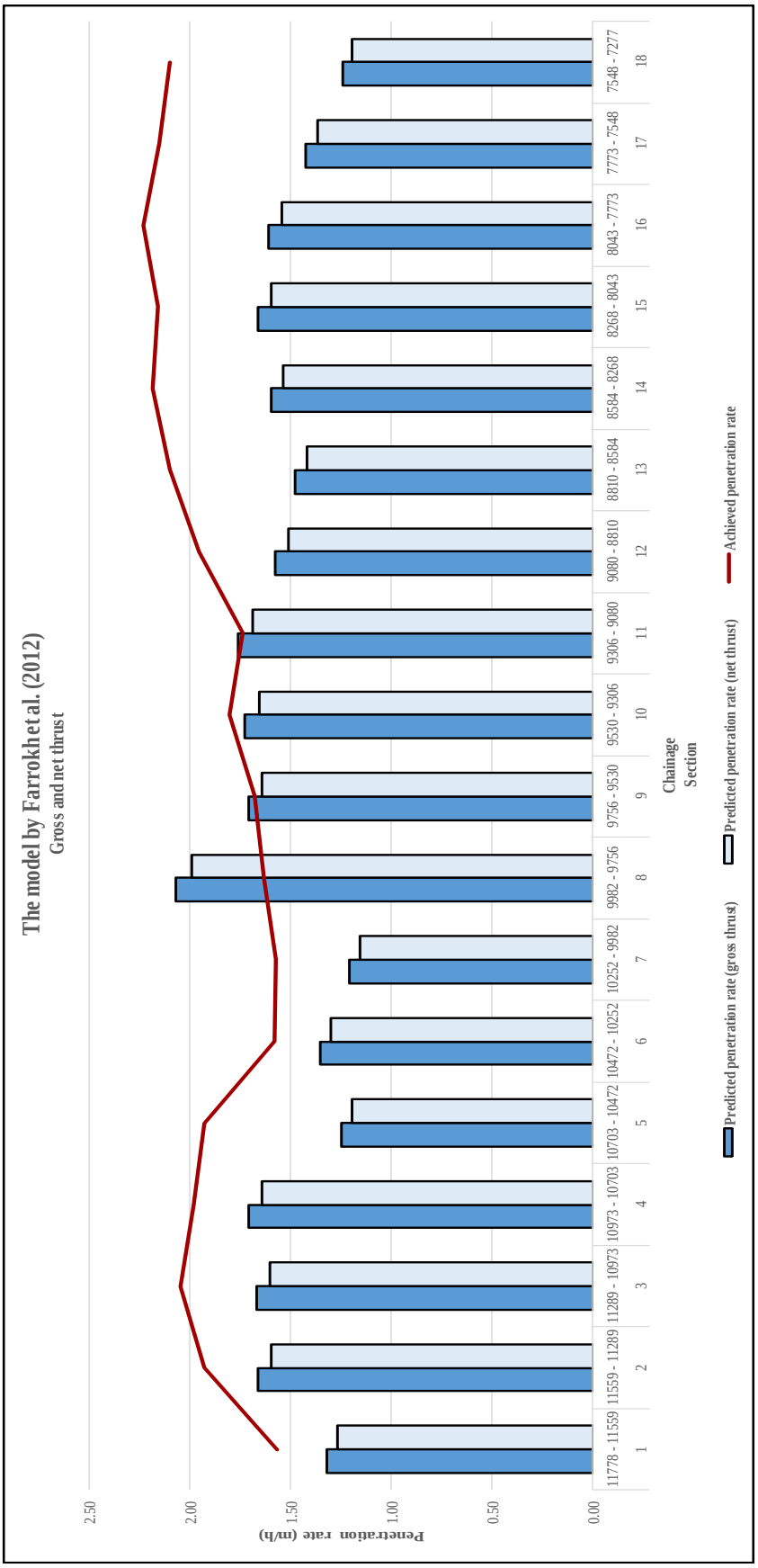

Figure 5.34 - *Average penetration rates for each section calculated with the model by Farrokh et al. (2012). The results are compared to the achieved penetration rate (red line).*

5.3 Influential parameters

By comparing different input parameters with the penetration rate, one can get an insight of how influential these parameters are. Such comparison can be done in two ways: One can either compare the parameter's influence on the achieved NPR, or one can compare the parameter's influence with the predicted NPR. Both comparisons have been performed in order to fully understand how the parameters behave at the Follo Line Project.

Chapter 5.3.1 presents relationships between parameters and the achieved NPR, and include both machine- and geological related parameters. If graphs are proportional or inverse proportional, it may represent a relationship. A coefficient of correlation (r^2) for the whole tunnel length is included. The method is explained in detail in Chapter 4.5.6.

Chapter 5.3.2 presents the most influencing parameters to the predicted NPR in each of the models. The sensitivity of each parameter is presented as a percentage change of the parameter in order to predict the same NPR as the achieved. The method is explained in detail in Chapter 4.5.6.

The most influential parameters on the achieved and the predicted NPR are discussed in Chapter 6.3. Calculations and illustrations are presented in Appendix H2.

5.3.1 Parameters influencing the achieved NPR

Applied cutter thrust

Figure 5.35 presents the relationship between the applied cutter thrust and the achieved NPR. Notice the correlation coefficient of 0.2471.

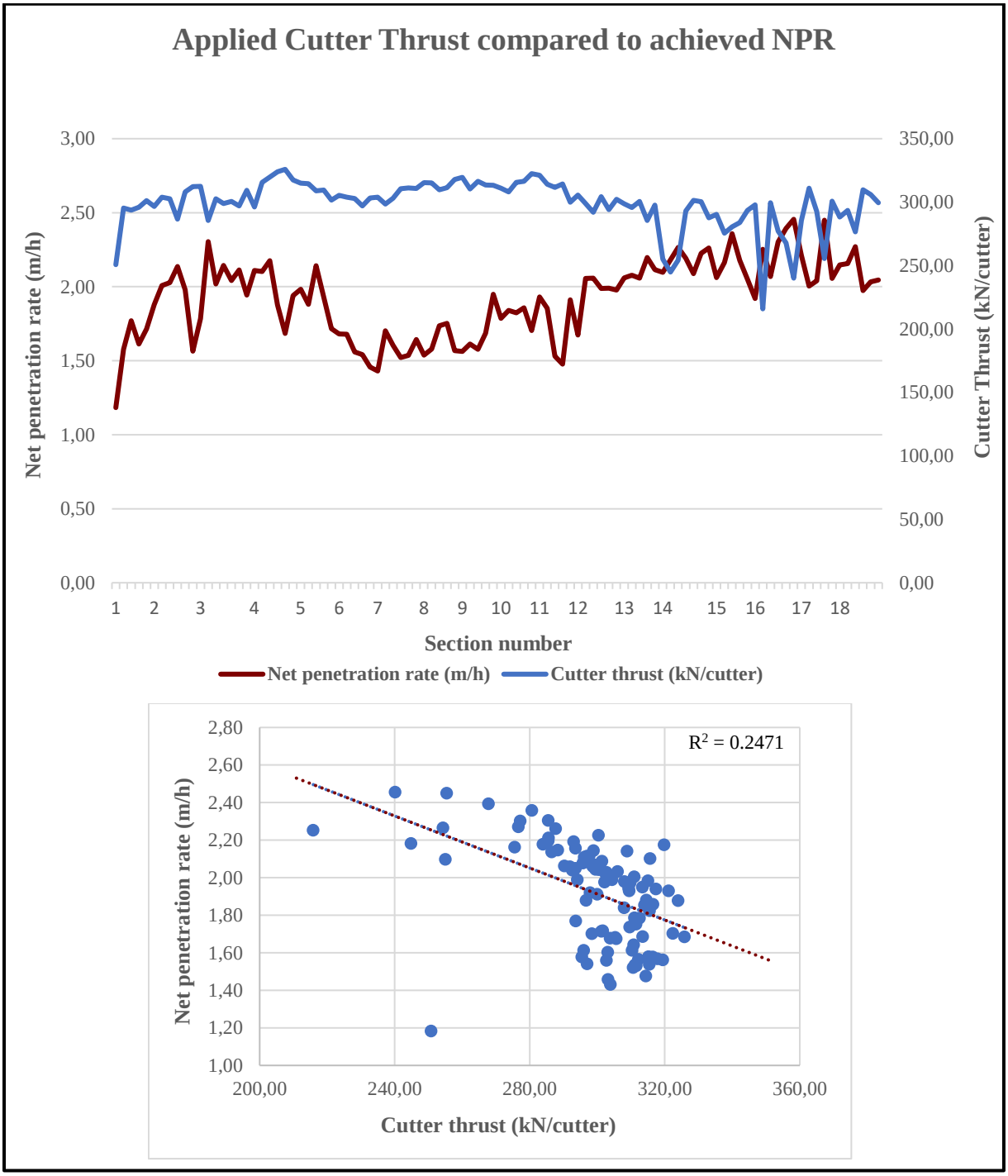

Figure 5.35 – *Relationship between applied cutter thrust and achieved net penetration rate.*

Cutterhead velocity

Figure 5.36 shows the relationship between the applied RPM and achieved penetration rate. Notice the correlation coefficient of 0.0246.

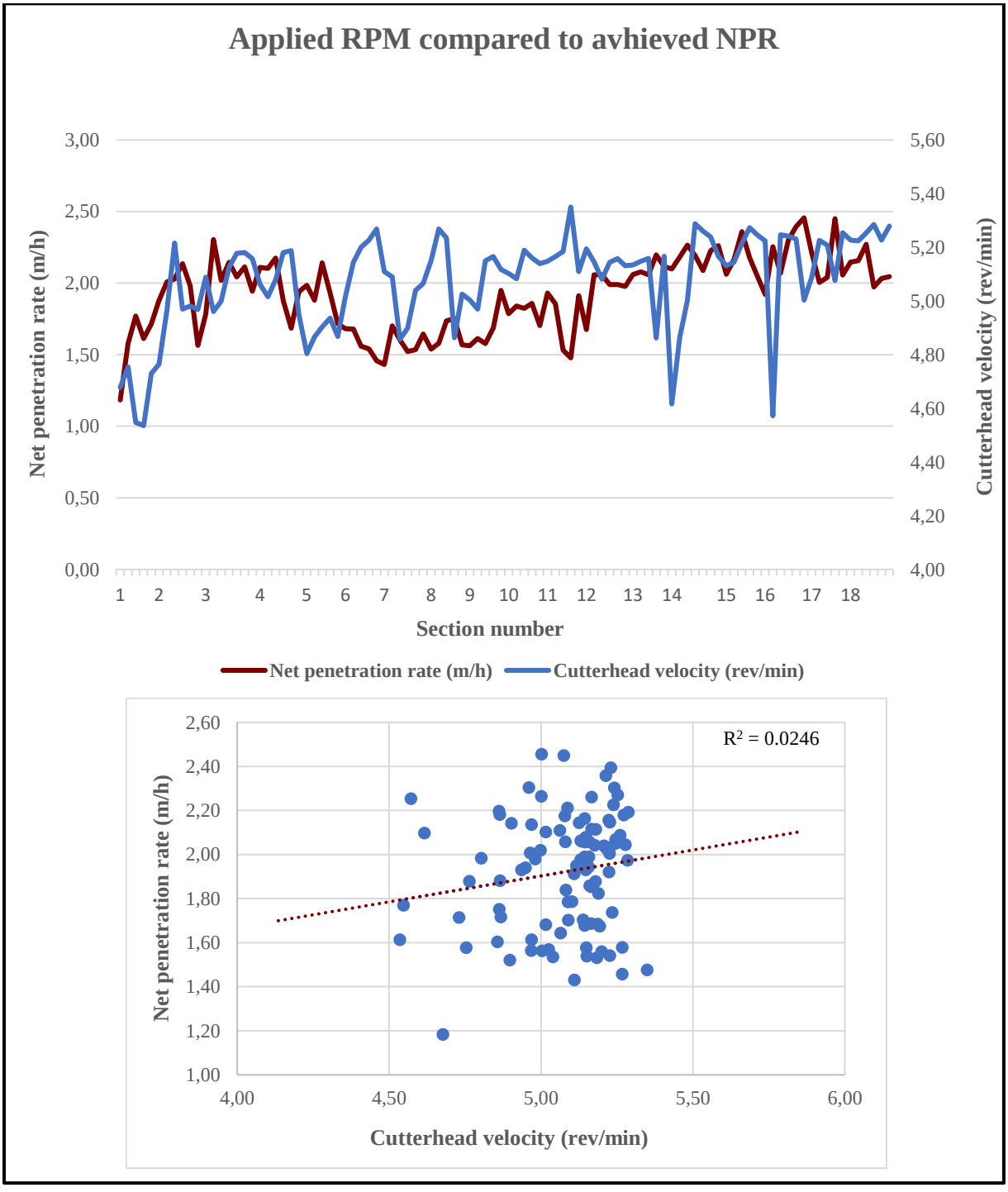

Figure 5.36 – *Relationship between applied RPM and achieved net penetration rate.*

Rock mass fracturing Factor

In the NTNU model, the total rock mass fracturing factor ($k_{s\text{-}tot}$) is an important parameter describing how the rock mass is fractured. This fracture information is important in several other prediction models as well, often only referred to as *orientation of fractures* and *spacing between fractures*. Figure 5.37 shows the relationship between the rock mass fracturing factor and the achieved penetration rate. Notice the correlation coefficient of 0.3938.

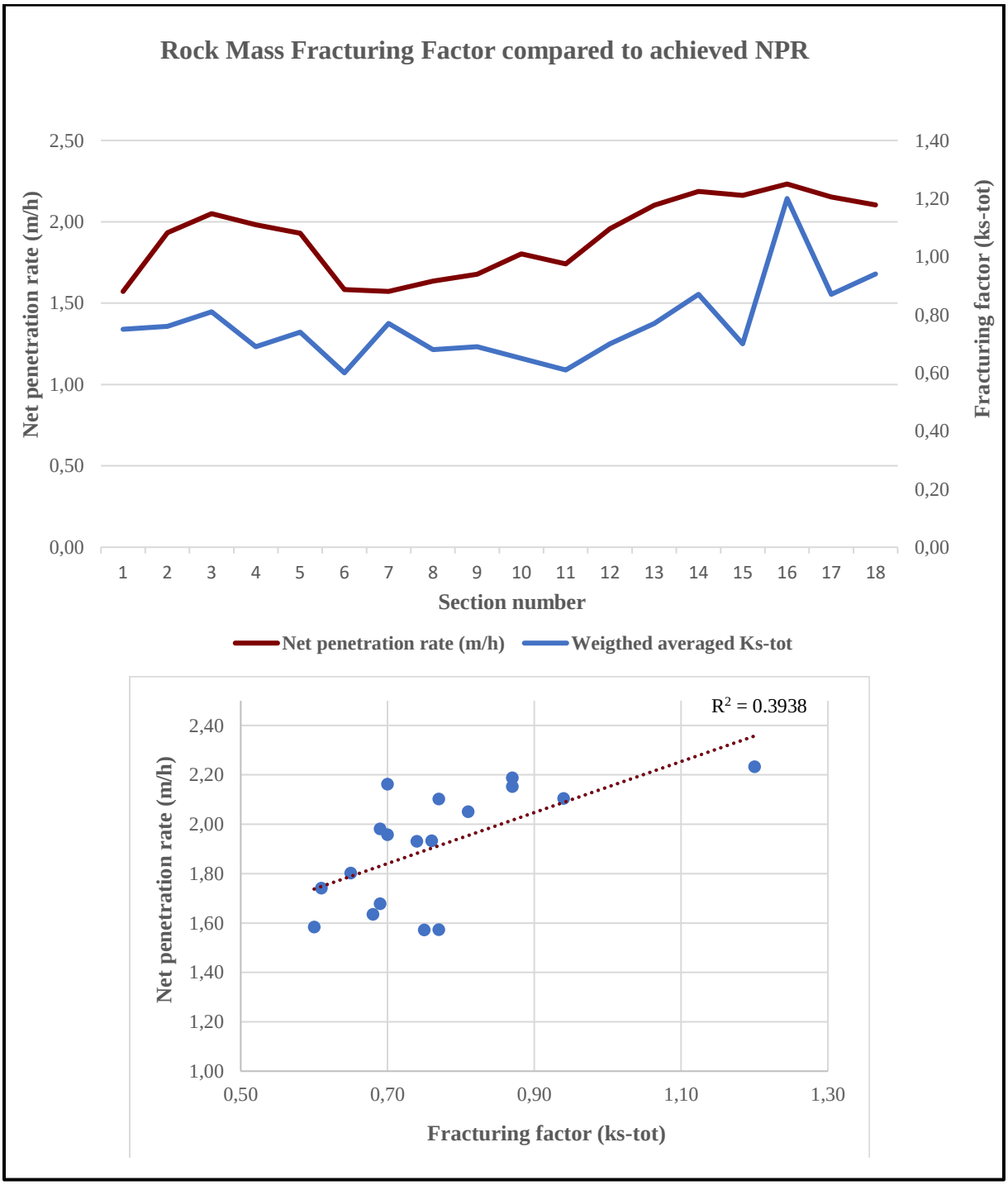

Figure 5.37 - *Relationship between total fracturing factor and achieved net penetration rate.*

Drilling rate index

Figure 5.38 shows the relationship between the DRI values and the achieved penetration rate. Notice the correlation coefficient of 0.024.

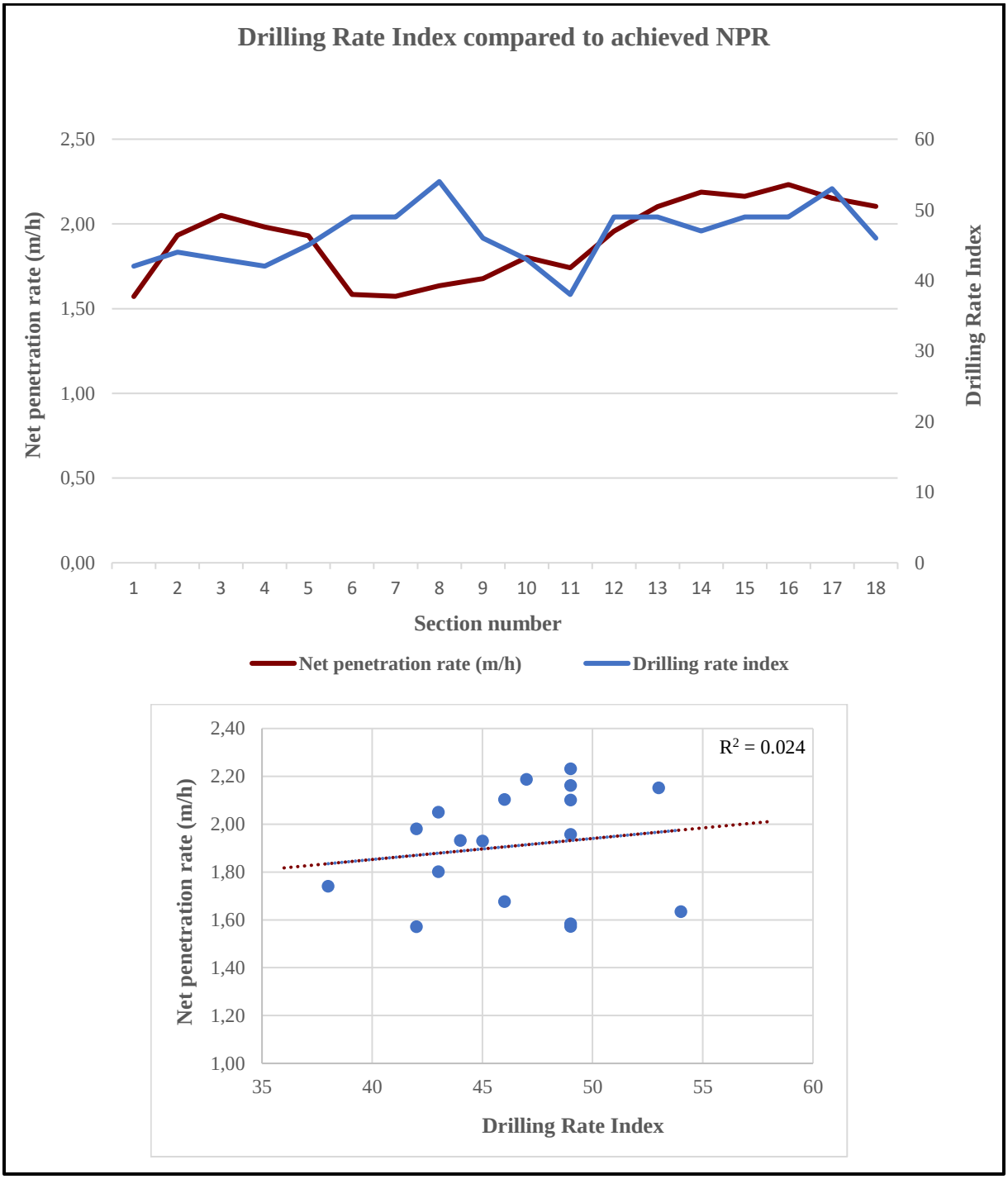

Figure 5.38 - *Relationship between DRI and achieved net penetration rate.*

Cutter life index

Figure 5.39 shows the relationship between the CLI values and the achieved penetration rate. Notice the correlation coefficient of 0.0641.

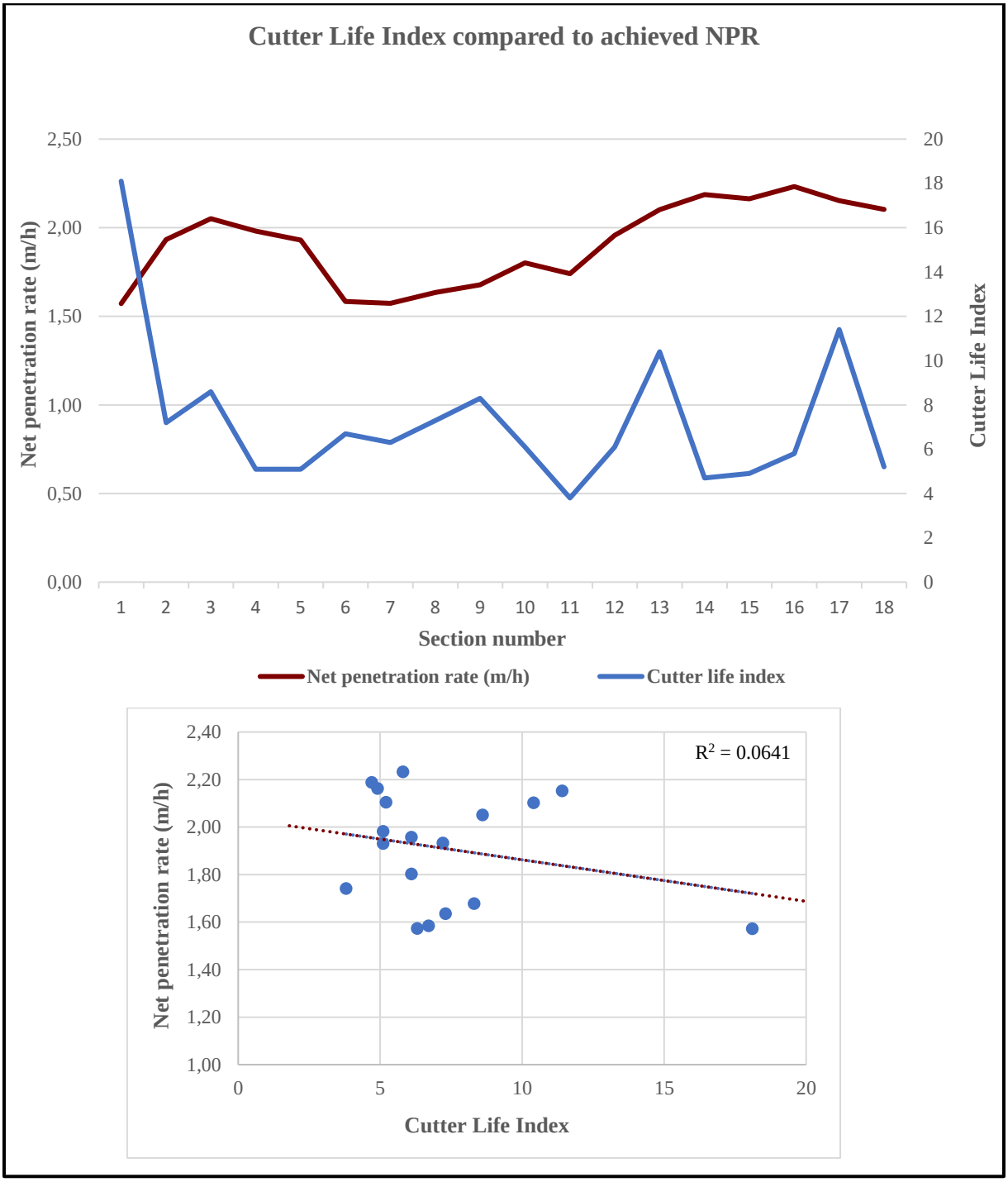

Figure 5.39 - *Relationship between CLI and achieved net penetration rate.*

Quartz content

Figure 5.40 shows the relationship between quartz content and the achieved penetration rate. Notice the correlation coefficient of 0.0197.

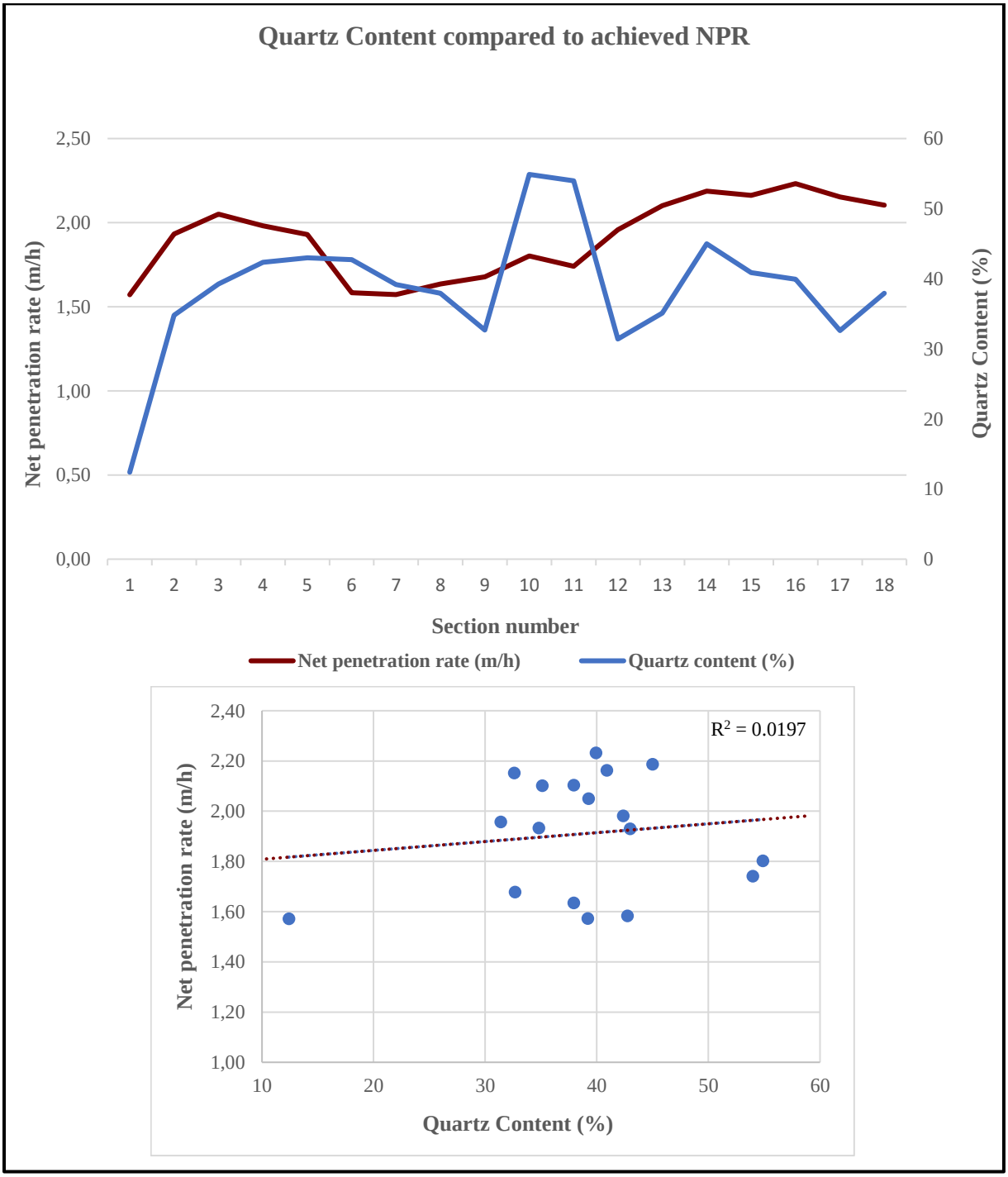

Figure 5.40 - *Relationship between quartz content and achieved net penetration rate.*

Uniaxial compressive strength

Figure 5.41 shows the relationship between the UCS-values and the achieved penetration rate. Notice the correlation coefficient of 0.2471.

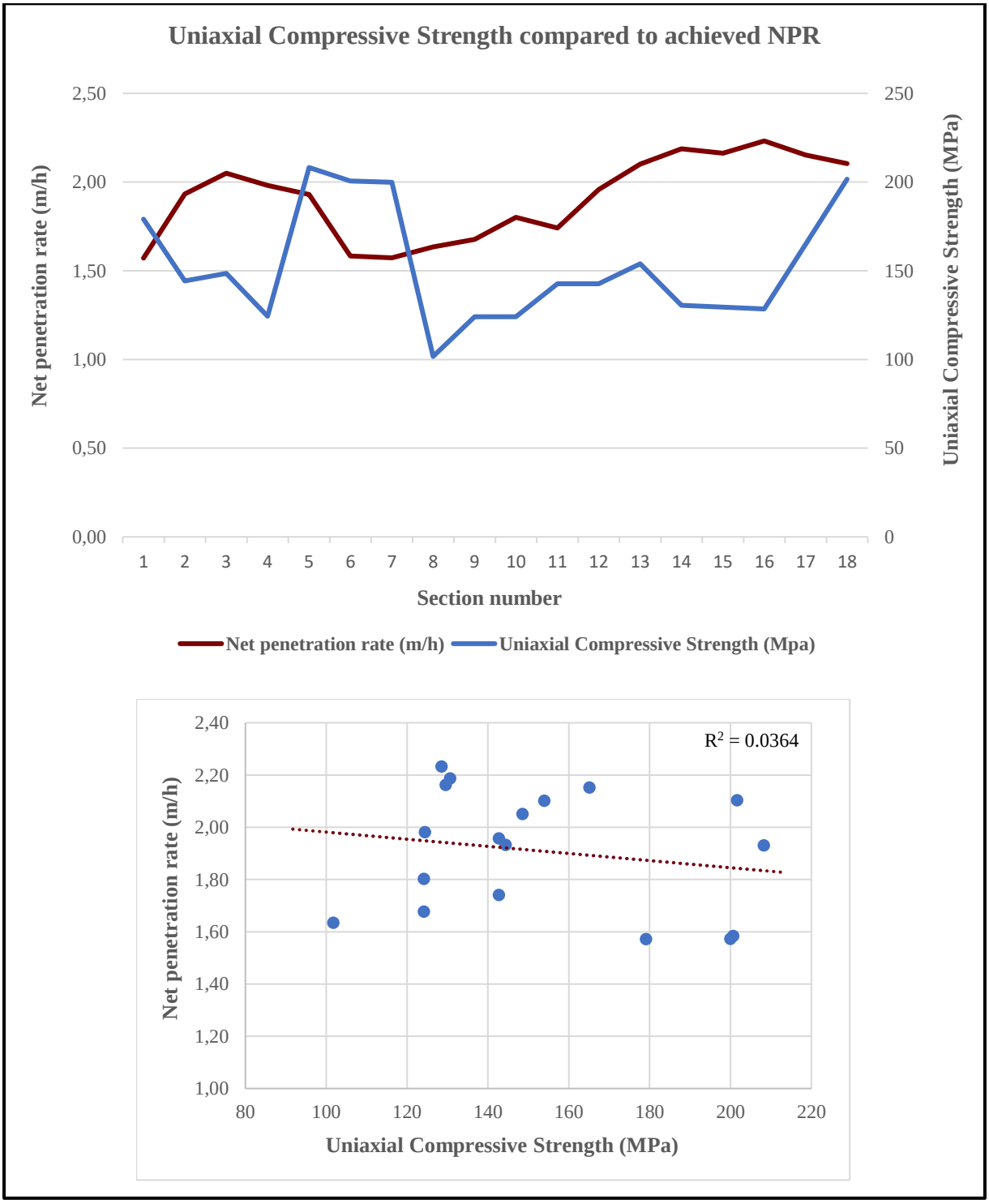

Figure 5.41 - *Relationship between UCS-values and achieved net penetration rate.*

5.3.2 Parameters influencing the predicted NPR

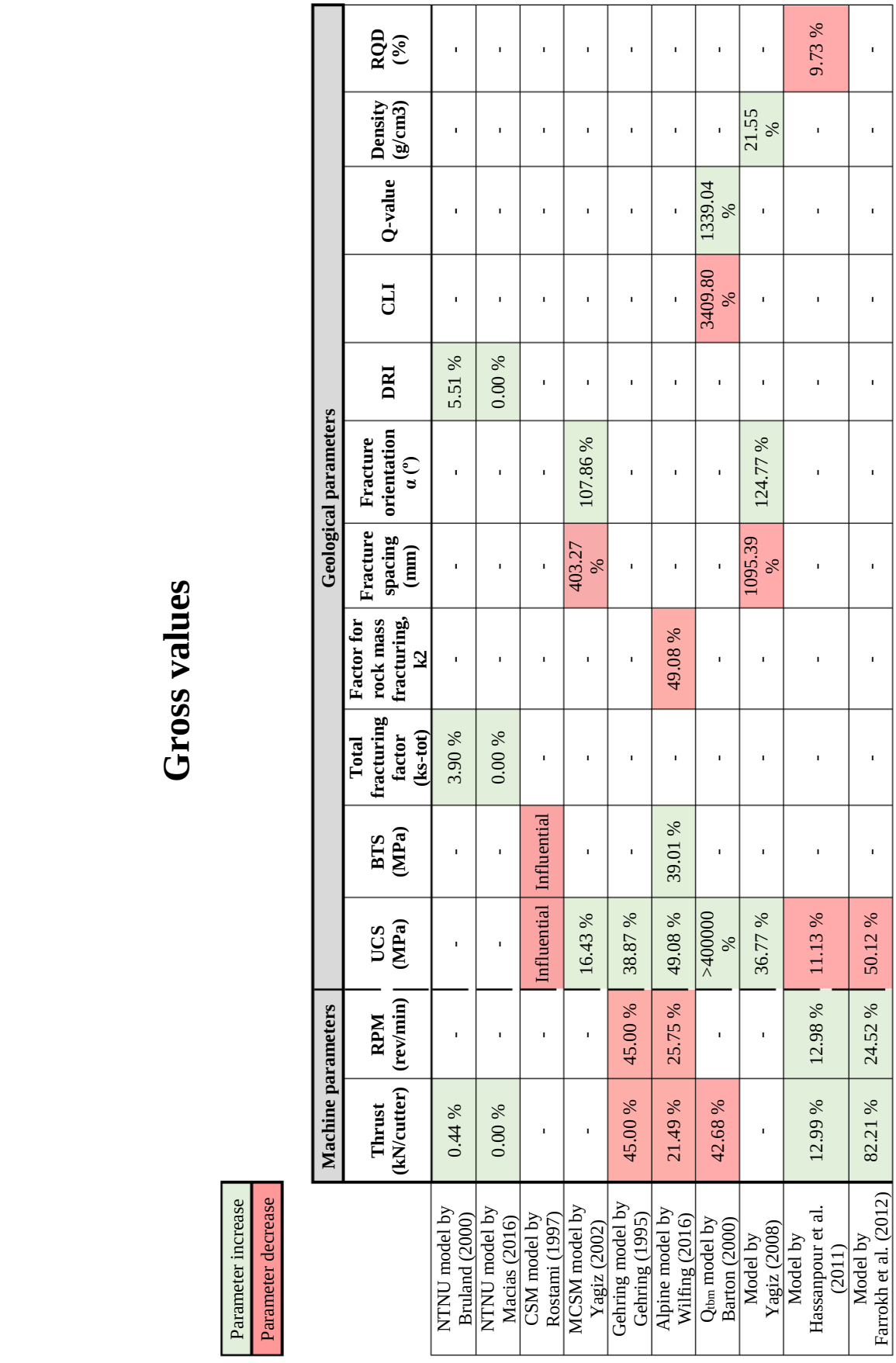

Figure 5.42 – *Parameter influence in each of the models using gross thrust. The values represent the percentage change of the parameter that is needed to make the predicted and achieved NPR the same.*

Net values

Parameter increase

Parameter decrease

	Machine parameters				Geological parameters								
	Thrust (kN/cutter)	RPM (rev/min)	UCS (MPa)	BTS (MPa)	Total fracturing factor (ks-tot)	Factor for rock mass fracturing, k2	Fracture spacing (mm)	Fracture orientation α (°)	DRI	CLI	Q-value	Density (g/cm3)	RQD (%)
NTNU model by Bruland (2000)	18.27 %	-	-	-	59.74 %	-	-	-	59.74 %	-	-	-	-
NTNU model by Macias (2016)	17.93 %	-	-	-	63.01 %	-	-	-	115.33 %	-	-	-	-
CSM model by Rostami (1997)	-	-	Influential	Influential	-	-	-	-	-	-	-	-	-
MCSM model by Yagiz (2002)	-	-	16.43 %	-	-	-	403.27 %	107.86 %	-	-	-	-	-
Gehring model by Gehring (1995)	23.13 %	23.13 %	20.19 %	-	-	-	-	-	-	-	-	-	-
Alpine model by Wilfing (2016)	3.17 %	3.80 %	7.23 %	6.65 %	-	7.29 %	-	-	-	-	-	-	-
Q_{tbm} model by Barton (2000)	21.17 %	-	>4000000 %	-	-	-	-	-	-	582.55 %	322.02 %	-	-
Model by Yagiz (2008)	-	-	36.77 %	-	-	-	1095.39 %	124.77 %	-	-	-	21.55 %	-
Model by Hassanpour et al. (2011)	33.06 %	33.04 %	30.58 %	-	-	-	-	-	-	-	-	-	26.17 %
Model by Farrokh et al. (2012)	114.57 %	29.64 %	65.33 %	-	-	-	-	-	-	-	-	-	-

Figure 5.43 – *Parameter influence in each of the models using net thrust. The values represent the percentage change of the parameter that is needed to make the predicted and achieved NPR the same.*

6 Comparison and discussion

This chapter discusses the results presented in Chapter 5. The first subchapter discusses the presentation methods and variation of the compiled data. Thereafter, a comparison between the predicted and the achieved NPR is performed with the aim of finding the superior model. Lastly, the various input parameters have been discussed in order to reveal the most influential parameters, both with respect to the achieved and the predicted NPR.

6.1 Compilation of data

One of the secondary scopes was to compile and present machine- and geology related data. The data have been compiled for 4.5 km of the outbound tunnel north (TBM 1) at the Follo Line Project. Geological data have been collected from Bane NOR`s geologists, as well as from field work during August 2017 to March 2018.

The geological data have mainly been presented as bar charts with a cumulated average. This is done to illustrate the averaged development of the parameters throughout the tunnel alignment. The fracturing parameters are presented as averaged values for each section. The laboratory tests have been executed every 250th meter, which means that there are laboratory parameters from one test connected to each section.

Regarding the machine data, each section consists of an averaged value from recordings every 10th second. This data has been presented in box plots, due to the high amount of data (Fig. 5.12 to 5.14). The upper and lower extremes are presented with a thin line. The middle line of the box represents the median value and the upper and lower lines of the box represent the first and the third quartile. Box plots are a good method to present the variation in the data set and the purpose is to show the variation within the sections. The standard deviations presented in Table 5.2 show relatively small deviations in the machine data (< 14%).

As Figure 5.12 to 5.14 illustrate, the highest variations in the machine data seem to be present in section 1, 8, 11 and 16. This variation is most likely a result of the geological conditions encountered in these sections. Section 1 is represented by high CLI values, and very low quartz content. There are low RQD- and UCS values in section 8. Section 11 has low DRI values. Section 16 has low RQD values and very low Q-values. These geological deviations might be the reason why the TBM is driven with various applied cutter thrusts and cutterhead velocities.

6.2 Comparison between predicted and achieved NPR

The main objective of the thesis is to determine the accuracy of the performance prediction models in order to find the most suitable prediction model at the Follo Line Project. To meet this objective, the predicted NPR for each model has been compared to the achieved NPR for the complete 4.5 km of tunnel.

Some models are either unclear or differ as to whether they use gross or net thrust values. To ensure an optimal comparison, all the calculations have been performed using both gross thrust and net thrust as input parameters (Chapter 5.2). The net thrust is defined as where the frictional forces are subtracted from the gross thrust. In the end, the final comparison using their related thrust have been performed.

A weighted average of both the achieved and predicted NPR has been calculated for the complete 4.5 km long tunnel. The achieved NPR is calculated to 1.92 m/h, and the predicted NPRs are compared and discussed in the following:

Gross thrust

Calculations using gross thrust as input parameter are presented in Figure 6.1. The models predicting higher than the achieved NPR are the CSM-, the Gehring- the Alpine- and the Q_{tbm} model. The Q_{tbm} model stands out with a predicted NPR of 46.88% above the achieved NPR. The models by Hassanpour et al. and by Farrokh et al. predict lower NPRs than achieved, with 33.33% and 29.73% respectively. The remaining models predict values close to the achieved NPR (within 10%).

Net thrust

Calculations using net thrust as input parameter are presented in Figure 6.2. The same models as described above predict higher penetration rates than the achieved. The Q_{tbm} model is still predicting very high NPR. The MCSM- and the Alpine model predict a NPR close to the achieved, with respectively 7.87% lower and 3.65% higher than the achieved. The NTNU models predict very close to the achieved NPR, whilst the model by Hassanpour et al. and the model by Farrokh et al. predict too low NPRs. The CSM-, MCSM model and the model by Yagiz (2008) predict the same NPR with gross and net thrust, because they do not include thrust as an input parameter in the calculations.

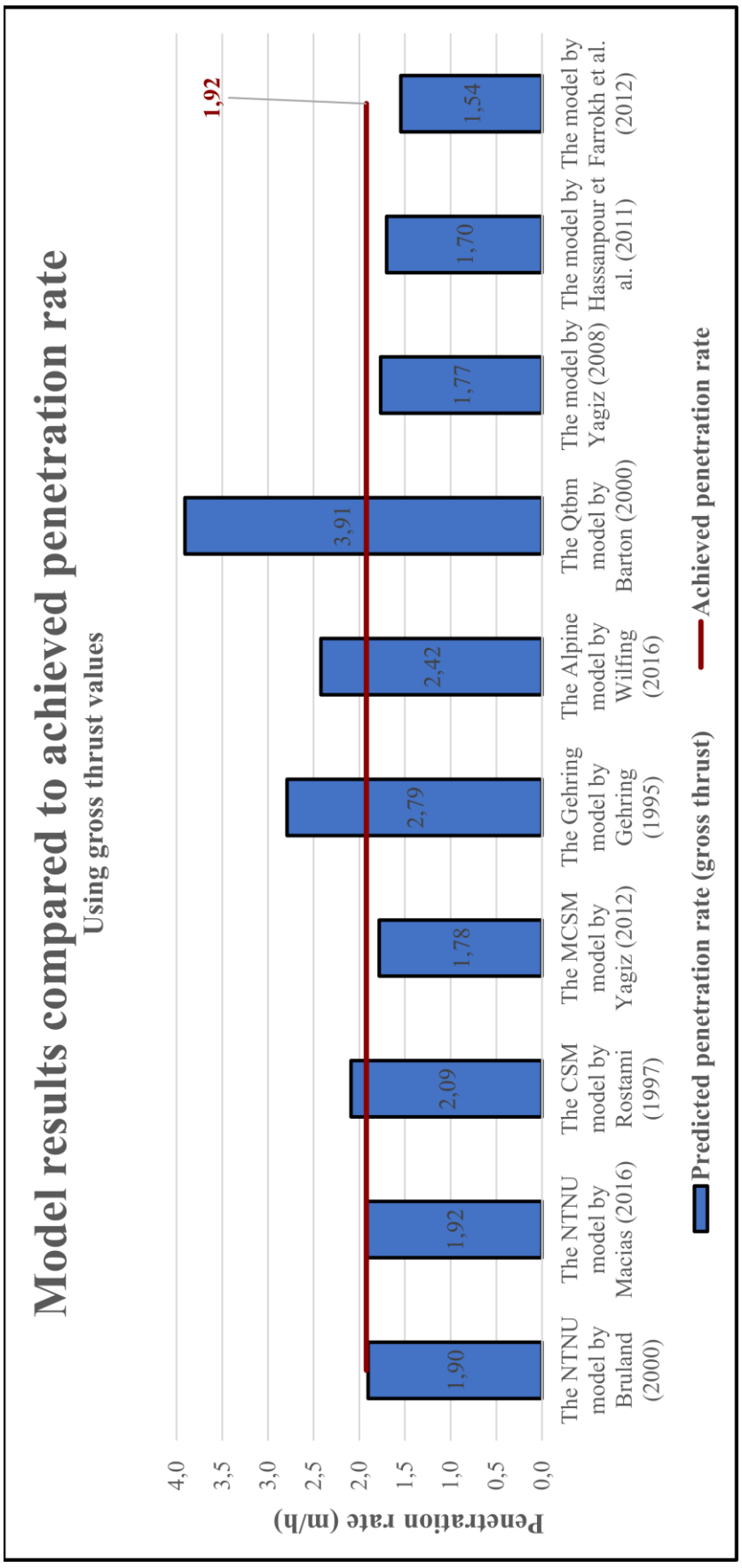

Figure 6.1 – *Comparison between predicted penetration rates (using gross thrust) and achieved penetration rate.*

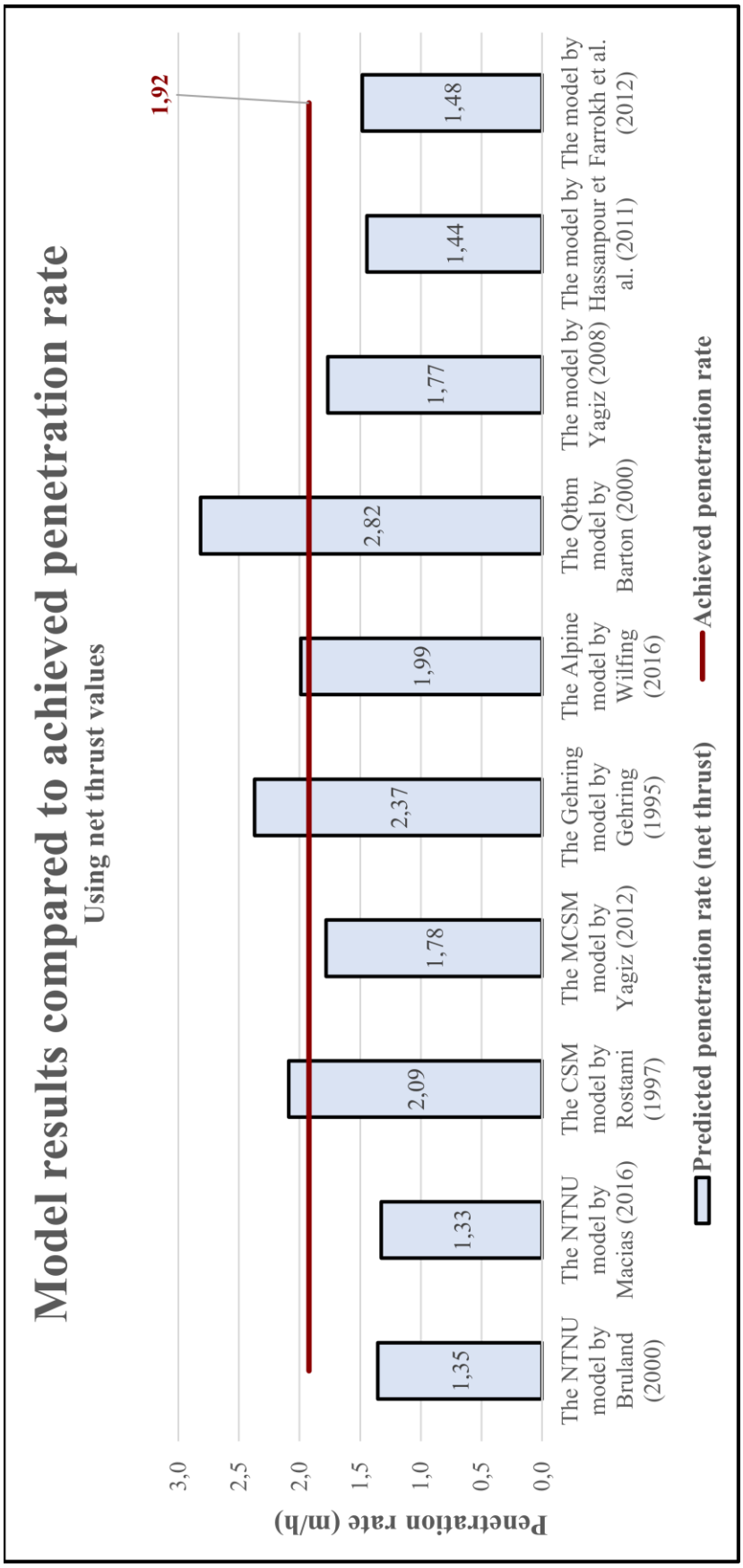

Figure 6.2 – *Comparison between predicted penetration rates (using net thrust) and achieved penetration rate.*

As described in Chapter 3, some of the prediction models use gross thrust while other use net thrust. Two of the models, the Q_{tbm} model and the model by Farrokh et al., have not stated whether they use gross or net thrust. For these two models, the net thrust values have been used, because net is the theoretical most correct approach. All deviations between predicted and achieved penetration rates by using the model's related thrust input are presented in Table 6.1.

Table 6.1 – *Deviations between predicted and achieved penetration rates. The red numbers represent values below achieved NPR, and the green values represent values above the achieved NPR.*

Performance prediction model	Applied cutter thrust value input	Deviation from achieved NPR
NTNU model	Gross	1.05 % ↓
Modified NTNU model	Gross	0.00 % -
CSM model	Not included	8.85% ↑
MCSM model	Not included	7.87% ↓
Gehring model	Net	23.44 % ↑
Alpine model	Net	3.65 % ↑
Q_{tbm} model	Not stated (net)	46.88 % ↑
Model by Yagiz	Not included	8.48 % ↓
Model by Hassanpour et al.	Net	33.33 % ↓
Model by Farrokh et al.	Not stated (net)	29.73 % ↓

The models that predict the closest NPR compared to the achieved NPR are both the original and the modified version of the NTNU model, as well as the Alpine model. In theory, the NTNU model calculates conservative results (~10% below the achieved NPR). Thus, the NTNU model predict too high penetration rates, and the Alpine model is the most accurate.

The MCSM-model and the model by Yagiz show promising results if conservative results are sought for.

Due to the results presented in Chapter 5.3.1, it is expected that the models including cutter thrust, fracture information and rock mass strength as input parameters give the most accurate results. Both the NTNU model, the Alpine model, the CSM model and the MCSM model do so.

6.3 Influential parameters and model behavior

6.3.1 Parameters influencing the achieved NPR

Several parameters have been presented together with achieved NPR (Chapter 5.3.1). To easily show how the parameters influence the actual achieved penetration rate. The parameter influence, both machine- and geology related, is discussed one by one in this subchapter. It is important to keep in mind that the achieved NPR is not only affected by the parameter focused on, meaning that each parameter might have an influence even if the correlation is bad. However, good correlation reflects a higher parameter influence on the achieved NPR.

The visual relationship between the plotted graphs in Chapter 5.3.1 illustrates local variations. In addition, a coefficient of correlation (r^2) over the whole tunnel length is added to the comparison. From the visual perspective, the applied cutter thrust, the rock mass fracturing and the UCS seems to have the best correlations with the achieved NPR, where peaks and troughs follow each other. From the correlation coefficients, the rock mass fracturing factor and the applied cutter thrust are by far the most influential parameters.

Applied cutter thrust

The applied cutter thrust is an input parameter in all the prediction models except the model by Yagiz. Because of the high number of models using cutter thrust, it believed to have a crucial impact on the penetration rate. Figure 5.35 presents the relationship between applied cutter thrust and the achieved NPR. It is observed a good correlation between the peaks and troughs, especially in the first 8 sections. The correlation of 0.2471 substantiate this.

In theory, the achieved NPR will increase with increased cutter thrust in homogenous, no-changing rock mass. In reality, the rock mass is changing with respect to the geological parameters, and thus in heterogeneous rock mass, the NPR is inverse proportional to the applied cutter thrust. Highly fractured rock conditions will for instance require lower cutter thrusts to achieve high penetration rates. If the NPR is lowered, the applied thrust will be adjusted up to maintain a continuous NPR. Both the geological- and the human factors are therefore decisive for the cutter thrust influence.

To illustrate this, the correlation between the applied cutter thrust and the rock mass fracturing factor have been presented (Fig. 6.3). The correlation is good enough to prove that the parameters are inverse proportional, which means that the applied cutter thrust will be increased when the fracturing factor, and thus the NPR, is lowered.

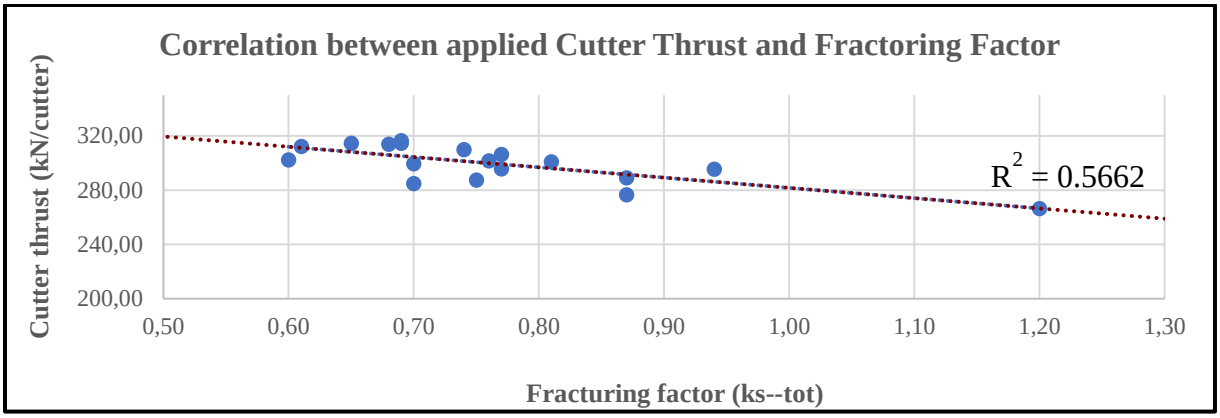

Figure 6.3 – *Correlation between applied cutter thrust and fracturing factor.*

Applied RPM

Figure 5.36 presents the relationship between applied RPM and the achieved NPR. The correlation between the peaks and troughs is hard to observe, but in some sections, the achieved NPR is lowered when the RPM increases. According to Bruland (2000a), this is not to be expected. The cutterhead velocity (as well as the net penetration rate) is inverse proportional to the TBM diameter, which means that the graphs for achieved NPR and the RPM should follow each other. This correlation should ideally be more visible in the figure. The bad correlation is confirmed by the correlation coefficient of 0.0246.

Rock mass fracturing factor

The rock mass fracturing factor ($k_{s\text{-}tot}$) is based on the spacing between the fractures and orientation between the fractures and the tunnel axis. The correlation to the achieved NPR is good in most of the sections, but relatively bad in section 15-18 (Fig. 5.37). As expected, the achieved NPR increases when the $k_{s\text{-}tot}$ value increases. According to Bruland (2000a), the rock mass fracturing is found to be the geological factor with the largest influence on the net penetration rate. This is confirmed by the high correlation of 0.3938.

Drilling rate index

The relationship between DRI and the achieved NPR is presented in Figure 5.38. Visually, the correlation does not look good. The achieved NPR is expected to increase with decreased DRI (Macias, 2016). This trend can be observed in the first 8 sections, but is missing in the remaining sections. A better correlation is expected. The DRI should according to Bruland (2000a) be well suited for the purpose since it is composed by the rock surface hardness. The coefficient of 0.024 represents a bad correlation.

Cutter life index and quartz content

Figure 5.39 shows that the CLI values are inverse proportional with the achieved NPR. A low CLI occurs in hard rock conditions or with high penetration rates, which may explain why the CLI is low when the achieved NPR is high. Hard rock conditions mean that there may be a high amount of quartz present. Therefore, low CLI values is expected in areas with high quartz contents. Figure 5.40 shows that an increase in quartz content will increase the achieved NPR, which is the opposite of what to expect. However, increased quartz content will increase the probability of inducing brittle fracturing, which will increase the NPR. These relationships are complex. Respectively, the correlation coefficients are 0.064 and 0.0197.

Uniaxial compressive strength

In theory, higher rock mass strength will decrease the achieved NPR. In reality, this theory is illustrated in some sections (Figure 5.41). The correlation coefficient of 0.036 is lower than what to expect from the visual relationship.

6.3.2 Parameters influencing the predicted NPR

A sensitivity analysis has been performed for all the prediction models in order to detect which parameters that are influencing the predicted NPR the most. Back calculations give a percentage of how much the parameters need to be changed in order to get a correlation where the predicted and the achieved NPR coincides. The detailed method behind this analysis is described in Chapter 4.5.6.

The parameters may behave differently in the model calculations than in reality, and it is important to detect the influence of the parameters in the models. Based on the discussions in subchapter 6.3.1, it is expected that the applied cutter thrust, the rock mass fracturing and the UCS will be most sensitive to changes in the sensitivity analysis. The parameter's sensitivity is illustrated in Appendix H2 and will be discussed by using their related thrust value.

The overall model behavior will be discussed in this subchapter, in addition to the discussion related to the parameter sensitivity. The sectionwise predictions presented in Chapter 5.3.2 is of importance to observe trends and to evaluate reasons behind the model's behavior. The model's behavior will be discussed by using their related thrust value as input parameter.

In addition, the main sources of error connected to each model will be discussed. These are only the sources that directly influence the prediction of NPR, and not general weaknesses of the model. General weaknesses (and strengths) are presented in Chapter 3.

6.3.2.1 NTNU model by Bruland

The NTNU model by Bruland (2000) is a conservative model, and calculates in theory 10% below the achieved NPR. The NTNU model uses gross thrust to calculate the NPR.

By using gross thrust, the model calculated a total NPR of 1.90 m/h, which is 1.05% below the achieved NPR (Fig. 5.15). This result is less conservative than originally sought for using the NTNU model and is very close to the achieved NPR of 1.92 m/h. To predict the same NPR as the achieved, the following changes are needed (Fig. 5.42):

- The gross thrust per cutter must be increased with 0.44% to 300.16 kN/cutter.
- The total rock mass fracturing factor ($k_{s\text{-}tot}$) must be increased with 3.90% to 0.8.
- The DRI must be increased with 5.51% to 49.00.

The sensitivity analysis shows that the applied thrust is the most sensitive parameter in this model. Only small changes are needed to reach the achieved NPR. Both the $k_{s\text{-}tot}$-value of 0.8 and a DRI value of 49 are realistic values, and show sensitive properties. These parameters are according to the graphs presented in Appendix H2 more sensitive with lower values, which may indicate that the rock mass in reality is more fractured than captured by the OTV-analyses. Zoorabadi et al. (2012) states that the joint spacing has significantly more influence than the orientation.

General model behavior

Looking at the calculations for each section (Figure 5.16), the predicted and the achieved values have a good correlation, especially in the first four sections and in section 11. For the other sections, the predicted NPR is either too high or too low compared to the achieved NPR. The fracturing factor and DRI values do not show any deviating trends in these sections, and according to the sensitivity analysis, there is reasonable to believe that the high and low values are a result of the application of wrong cutter thrust values.

Sources of error

The model is associated with some disadvantages described in Chapter 3.1.3. The main source of error that directly influences on the prediction of NPR is the possibility of inaccurate readings of multiple graphs presented in the model, which may lead to wrong results in the end. Regression formulas would have improved the accuracy of the results significantly**.** Errors linked to the gathering of rock mass fracturing factor and the DRI value are presented in Chapter 6.4.

6.3.2.2 NTNU model by Macias

The NTNU model by Macias (2000) is very similar to the already described NTNU-model by Bruland (2000). It is conservative and complex, and uses gross thrust to calculate the NPR.

When using gross thrust as input parameter in this model, the calculated total NPR was 1.92 m/h, which is exactly the same as the achieved NPR (Fig. 5.17). This result is 10% less conservative than originally sought for using the NTNU model. Since the predicted NPR is the same as the achieved NPR, no changes in the parameters are needed.

From the graphs presented in Appendix H2, the same observations as described in the NTNU model by Bruland are valid for this model.

General model behavior

The complexity in this model is of the same character as the model by Bruland (2000). The calculations for each section are also quite similar to the calculations performed with the "Bruland-model" (Fig. 5.18). The calculations are good, except for too high values in section 7 and 8, and too low values in section 14-16. This is most likely caused by the application of the wrong cutter thrust. However, Figure 5.7 shows high DRI values in the last sections, which might lower the predicted NPR, due to the great influence of DRI in this model.

Sources of error

General weaknesses of this model are described in Chapter 3.1.3. As pointed out, the model is based on empirical data from projects using open TBMs and having smaller cross-sections. This empirical approach can influence on the results.

The model is associated with the same main source of error as the model by Bruland (2000); inaccurate readings of graphs can influence the predicted NPR.

6.3.2.3 CSM model by Rostami

The applied thrust is not included in the CSM model, which makes it unnecessary to distinguish between applied gross or net thrust. Using the model, a total NPR of 2.09 m/h was calculated, which is 8.85% above the achieved NPR (Fig. 5.19). This is high compared to the predictions done with the other models.

The CSM model is earlier described in detailed in Chapter 3.2.1. To predict the same NPR as the achieved, the following changes are needed (Fig. 5.43):

- The UCS must be increased with 11.52% to 170.02 MPa.
- The BTS must be increased with 24.38% to 12.91 MPa.
- The RPM must be increased with 7.54% to 5.48.

The sensitivity analysis shows that the applied RPM is the most influential parameter. This parameter is most influential from 0.0 to 4.0 rev/min. After that point, the parameter is opposite proportional with the predicted NPR, and has a lower influence (Appendix H2). UCS and BTS show sensitive properties, with UCS as the most influential. Both parameters are most influential with low values (Appendix H2). The model could therefore have predicted better if the present strength parameters in the project area were lower.

General model behavior

Looking at the calculations for each section (Fig. 5.20), the predicted and the achieved values have a variated correlation. The predictions tend to be too high, except in sections 5 to 7. The low prediction in these sections may be a result of high UCS values (Fig. 5.10). On the other hand, very high prediction is present in section 8, which may be a result of low UCS values (Fig. 5.10). This behavior concludes that the theory from the trial and error method was correct.

Sources of error

The model is associated with some general weaknesses, described in Chapter 3.2.3. The main factors that might have a direct influence on the predicted NPR are connected to the execution of laboratory tests, which are further discussed in Chapter 6.4. The model is very complex with multiple calculations. Possible errors linked to the calculations are present.

6.3.2.4 MCSM model by Yagiz

The applied cutter thrust is not included in the MCSM model. Using the model, a total NPR of 1.78 m/h was calculated, which is 7.87% below the achieved NPR (Fig. 5.21). This is a good prediction, especially when conservative results are sought for.

To predict the same NPR as the achieved, the following changes are needed (Fig. 5.43):

- The UCS must be increased with 16.43% to 177.50 MPa.
- The predicted brittleness (BIp) must be increased with 18.10% to 33.51 kN/mm.
- The result from the CSM model must be increased with 68.46% to 3.52 m/h.
- The fracture orientation must be increased with 107.86% to 89.26°.
- The fracture spacing must be decreased with 403.27% to 15.30 cm.

The sensitivity analysis shows that UCS and the predicted brittleness are the most influential parameters. The result from the CSM model is based on multiple calculations and parameters. Therefore, it is hard to decide how much these parameters influence the NPR predicted from the MCSM model. The orientation and spacing of the fractures are not that influential.

General model behavior

Looking at the calculations for each section (Fig. 5.22), the predicted values are stable with small local variations. The correlation is good in the first sections. Towards the last sections, the predicted values are lower than expected, which might be due to lower predicted brittleness. Lower angles between the fractures and the TBM driven direction are present in the last sections as well (Fig. 5.5).

Sources of error

The general disadvantages of this model are presented in Chapter 3.2.3. The sources of error that directly influence the prediction of NPR are the same as for the CSM model. In addition, another source of error is connected to the formula used to predict the brittleness index (Eq. 3.16). According to Yagiz (2009), predicted results reveal a good fitting with a regression coefficient of 0.94. This is a suitable tool when punch penetration test is not available, and the risk of errors is small (Wilfing, 2016). Errors related to mapping of fractures are further discussed in Chapter 6.4.

6.3.2.5 Gehring model by Gehring

The Gehring model implements several correction factors to predict the NPR. One of the correction factors requires the thrust as an input parameter, and Gehring (1995) states that the net thrust values should be used.

By using net thrust in the model, a total NPR of 2.79 m/h was calculated, which is 23.44% above the achieved NPR (Fig. 5.23). This is the second highest predicted NPR of all the models. To predict the same NPR as the achieved, the following changes are needed (Fig. 5.43):

- The net thrust per cutter must be decreased with 23.13% to 206.11 kN/cutter.
- The UCS must be increased with 20.19% to 183.23 MPa.
- The RPM must be decreased with 23.13% to 4.12 rev/min.

The sensitivity analysis shows that the UCS is the most influential parameter, and requires the smallest changes in this model to reach the achieved NPR. Appendix H2 shows that the UCS is most influential with small values. The model could therefore have predicted better if the strength parameters present in the project area were lower. The applied net thrust and RPM are also very influential on the predicted NPR. The machine parameters are the only parameters that are adjustable in real life.

General model behavior

Visually speaking, the predicted and achieved values have a bad correlation for each section (Fig. 5.24). The predicted values are high, especially in section 8. The UCS value is very low in this section (Fig. 5.10), and with the sensitivity analysis in mind, this may be an explanation. The general high predicted NPR may be explained by overall low UCS values.

Sources of error

The model is associated with some disadvantages described in Chapter 3.3.3. The main source of error directly connected to the predicted NPR is in the correction factor for rock mass fabric (k_2), where spacing and orientation of the fractures are considered. Spacing above 50 cm will according to Gehring (1995) not influence the NPR. Compared to for instance the NTNU model, spacings up to 480 cm influence the NPR, which is considered a better approach (Macias, 2016). Errors linked to the execution of the UCS test are presented in Chapter 6.4.

6.3.2.6 Alpine model by Wilfing

The Alpine model implements several correction factors to predict the NPR, just like the Gehring model. Wilfing (2016) states that the net thrust is used in the calculations.

By using net thrust in the model, a total NPR of 1.99 m/h was calculated, which is 3.65% above the achieved NPR (Fig. 5.25). This is one of the predictions closest to the achieved NPR. To predict the same NPR as the achieved, the following changes are needed (Fig. 5.43):

- The net thrust per cutter must be decreased with 3.17% to 246 kN/cutter.
- The UCS must be increased with 7.23% to 163.47 MPa.
- The BTS must be increased with 6.65% to 11.06 MPa.
- The RPM must be decreased with 3.80% to 4.89 rev/min.
- The fracturing factor (k_2) must be decreased with 7.29% to 1.03.

The sensitivity analysis shows that all the parameters are of great influence. The machine parameters have a slightly bigger influence than the geological parameters, with the applied net cutter thrust as the most sensitive parameter.

General model behavior

The predicted and achieved values have a quite good correlation, especially in the first six and the last five sections (Fig. 5.26). The predicted values in the remaining sections are a bit high, especially in section 8. The UCS and the BTS values are low in these sections (Fig. 5.10 and 5.11), and with the sensitivity analysis in mind, this may be an explanation. It is reasonable to believe that the applied cutter thrust is the reason for the small deviations. The Alpine model has an overall better correlation for each section than the Gehring model.

Sources of error

General weaknesses of the model are described in Chapter 3.3.3. The sources of error discussed in the Gehring model have been corrected in this model. After the correction, a new source of error occurred: The newly incorporated y-intercept of BTS has a low regression coefficient, which might affect the result. In addition, the fracturing factor is according to Wilfing (2016) not fully developed and is connected to uncertain results. Errors linked to the execution of UCS and BTS values are presented in Chapter 6.4.

6.3.2.7 Q_{tbm} model by Barton

The Q_{tbm} model is one of the models that does not states whether it uses gross or net thrust as input value. As earlier described, net thrust values are chosen for these models.

By using net thrust in the model, a total NPR of 3.91 m/h was calculated, which is 46.88% above the achieved NPR (Fig. 5.27). This is the model predicting worst compared to the achieved NPR. To predict the same NPR as the achieved, the following changes are needed:

- The gross thrust per cutter must be decreased with 21.16% to 209.49 kN/cutter.
- The UCS must be increased with more than 32.700.000% to 5.000.000 MPa.
- The CLI must be decreased with 582.55% to 1.05.
- The Q-value must be increased with 322.02% to 89.30.
- The biaxial stress must be increased with 584.78% to 31.50 MPa.

The sensitivity analysis shows that the cutter thrust is by far the most influential parameter in this model, and it shows higher influence with increasing thrust (Appendix H2). The biaxial stress, CLI- and Q-values are not very sensitive, and the UCS has barely no influence at all, and show unrealistic values. Q-values, CLI-values, quartz content and induced biaxial stress are non-linear parameters, which reveals higher influence with lower values. If these values were lower, the Q-values would have been the most influential parameter (Appendix H2). Zoorobadi et al. (2012) confirms this. The model could therefore have predicted better if the present Q-values in the project area were lower.

General model behavior

The predicted and achieved values show a very bad correlation, where the predicted values are too high in all the sections (Fig. 5.28). The predicted values are the highest in section 1. This is likely due to low applied RPM values. Hassanpour et al (2016) addresses the same issue, there too high predictions seem to be common.

Sources of error

The model is associated with some general disadvantages described in Chapter 3.4.1. An example of an error that directly influence the predicted NPR is the calculation of the biaxial stress, which has not been tested along the tunnel, but calculated from the overburden. According to the sensitivity analysis, uncertainties related to the gathering of UCS- and biaxial stress values can be neglected in this model. Other errors linked to the execution of laboratory values and Q-values are presented in Chapter 6.4.

6.3.2.8 Model by Yagiz

The model by Yagiz (2008) is based on a practical predictive equation especially for fractured hard rock conditions. Applied thrust is not included in the model.

Using the model, a total NPR of 1.77 m/h was calculated, which is 8.48% below the achieved NPR (Fig. 5.29). To predict the same NPR as the achieved, the following changes are needed:

- The UCS must be increased with more than 36.77% to 208.50 MPa.
- The density must be increased with 21.55% to 3.33 g/cm^3.
- The fracture spacing must be decreased with 1095.39% to 0.06 mm.
- The fracture orientation must be increased with 124.77% to 96.52º.

The sensitivity analysis shows that the rock mass density is the most influential parameter in this model, followed by the UCS. The PSI parameter, which consists of both the density and the UCS, is therefore very sensitive. The fracture related parameters are not sensitive, especially not the fracture spacing. According to Yagiz (2008), the orientation of fractures should have been more influential. The explanation is illustrated in Appendix H2, where the fracture orientation is much more influential with low angles. The model could therefore have predicted better if the present angles between the fractures and the tunnel were lower.

General model behavior

The predicted and achieved values show good correlation, although the model does not reflect the local variations properly (Fig. 5.30). The predictions deviate most in section 1 and in the last five sections. This is related to high density- and UCS-values in section 1, and lower densities and compressive strengths in the last five sections. This is believed to be the reason because density and UCS are the two most influential parameters in this model.

Sources of error

The model is associated with some disadvantages described in Chapter 3.5.1. Machine parameters are excluded from the calculations, and seem to be the main source of error related to this model. Without adding any machine parameters, local variations are removed from the calculations, which are illustrated in Figure 5.30. Errors linked to the execution of laboratory values and fracture information are presented in Chapter 6.4.

6.3.2.9 Model by Hassanpour et al.

The model by Hassanpour et al. uses net thrust as input parameter.

By using net thrust in the model, a total NPR of 1.70 m/h was calculated, which is 12.94 % below the achieved NPR (Fig. 5.31). This is a good prediction if a conservative approach is sought for. To predict the same NPR as the achieved, the following changes are needed:

- The gross thrust per cutter must be increased with 12.99% to 337.69 kN/cutter.
- The UCS must be decreased with 11.13% to 137.18 MPa.
- The RPM must be increased with 12.98% to 5.74 rev/min.
- The RQD must be decreased with 9.73% to 83.64%.

The sensitivity analysis shows that the RQD is the most influential parameter, closely followed by the UCS. The machine parameters have the lowest influence on the predicted NPR, although all the parameters are influential.

General model behavior

For each section, the predicted and achieved NPR show varying correlations: In section 5 to 7 and the last six sections, the predicted NPRs are too low. Section 8 shows a too high predicted NPR. Figure 5.10 illustrates high UCS values in section 5 to 7 and is believed to be the reason for the low predictions. Low RQD- and UCS-values are present in section 8, and is believed to be the reason for the high prediction (Fig. 5.3 and 5.10). These assumptions are supported by the sensitivity analysis.

Sources of error

The model is associated with some general disadvantages described in Chapter 3.6.1. One of the main sources of error is that the fracture orientation is missing in the model. According to Macias (2016), Yagiz (2008) and Wilfing (2016), the orientation of the fractures influences the net penetration rate, and should therefore be included in the model. Errors linked to the gathering of UCS- and RQD values are presented in Chapter 6.4.

6.3.2.10 Model by Farrokh et al.

For the same reason as for the Q_{tbm} model, net thrust has been chosen as input parameter, in which Farrokh et al. (2012) do not state whether gross or net thrust should be applied.

By using net thrust, a total NPR of 1.54 m/h was calculated, which is 29.73 % below the achieved NPR (Fig. 5.33). To predict the same NPR as the achieved, parameter changes are needed:

- The gross thrust per cutter must be increased with 82.21% to 544.54 kN/cutter.
- The UCS must be decreased with 50.12% to 101.55 MPa.
- The RPM must be increased with 24.52% to 6.32 rev/min.

The sensitivity analysis shows that the RPM is the most influential parameter, almost twice as sensitive as the UCS. An applied cutter thrust of 544.54 kN/cutter equals a total applied force of more than 38 000 kN. That is far beyond the TBM's maximum thrust of 25 565 kN (Table 2.4) and can be disregarded.

General model behavior

The predicted and achieved values show medium correlation. The predictions are in general too low, and may according to the sensitivity analysis be a result of too low RPM values. Low NPRs are predicted in section 5 to 7 in several models, also in the model by Farrokh et al. High UCS values are believed to be the reason for this (Fig. 5.10). As for the model by Hassanpour et al., section 8 shows high predicted NPR, due to low UCS and high RPM (Fig. 5.13).

Sources of error

The model is associated with some disadvantages described in Chapter 3.7.1.

Just like the model by Hassanpour et al, the model by Farrokh et al. does not account for the rock mass fracturing orientation. The RQD is included as a numerical code, which does not reflect the variations of RQD within the rock mass properly. Errors linked to the execution of UCS tests and the gathering of RQD values are presented in Chapter 6.4.

6.4 Sources of error

The disadvantages related to the models are presented in Chapter 3 and uncertainties regarding the field work and laboratory tests are presented in Chapter 4.6. The errors presented in these chapters have a direct influence on the predicted NPR. Some errors are believed to have a higher influence on the results than others and require further discussion:

One of the main sources of error is related to the acquisition of UCS values, which are influential in several prediction models, especially in the CSM model (Fig. 5.42). As described in Chapter 4.3.2, the UCS values are based on both the results from pre-investigations and from rock samples tested along the tunnel alignment. As pointed out in the methodology, tests on samples taken along the tunnel resulted in low UCS values compared to the results from the pre-investigations. An overall agreement among the geologists concluded that the percentage variation in the results could be added to, or subtracted from, the results from the pre-investigations. By doing so, the local variations within each section would be taken into account. Figure 5.41 reveals a bad correlation between the UCS and achieved NPR, and the UCS might be affected by errors connected to this approach. Such errors increase the uncertainty in the results by the CSM and MCSM model. A more comprehensive basis of data would be appropriate to strengthen the statistical approach.

The BTS values are based on a correlation formula from the UCS values. The BTS values will therefore be exposed to the same errors as described above. Altindag and Gunay (2010) found a strong correlation between UCS and BTS of the different rock types, with a R^2 coefficient of 0.79. Although the correlation is strong, it brings an uncertainty into the calculations. It is believed that the results would be more accurate if BTS tests were executed along the tunnel.

As mentioned, samples to the laboratory tests are taken every 250th meter, which means there is a gap between the unique test results. The conducted values are therefore assumed applicable for at least a hundred meters on each side of the test area, referred to as *sections.* The sections are, as described in 4.5.1, divided into where these samples are taken, and one single test-value can represent a range of over 300 meters. These assumptions may give wrong results. To limit the possibility for errors by these assumptions, the sections have further been divided into where there is a clear change in geology, based on the variations of $k_{s\text{-}tot}$ values along the tunnel alignment (Appendix C)**.** Ideally, laboratory tests should be taken more frequently to improve the accuracy of the results. This suggestion is also applicable to the mappings related to the cross passages (Q-values, RQD etc.), which ideally should have been performed much more frequently. Regarding the determination of most influential

parameters affecting the achieved NPR, a bigger basis of data would be to prefer. 18 values are few and brings an uncertainty into the regression coefficients presented in Chapter 5.3.1.

It is important to avoid or minimize the errors connected to rock mass fracturing, as this is the most influential geological parameter (Chapter 5.3). To acquire information about the rock mass fracturing, it has been necessary to perform back-mapping with OTV-analyses. The degree of subjectivity when performing the OTV-analyses is most likely affecting the results. Working in WellCAD with OTV pictures is new for all the geologists at site, and it is especially challenging to define fractures in the same way for all analyses. Variations in picture quality makes the task more complicated. This can affect the fracture spacing, and thus, the results from the models that include the fracturing parameter. However, internal and external comparisons and cross-checking have shown that the lack of experience do not influence the determination of rock mass fracturing factor in a large extent.

RQD values have been gathered from OTV analyses in section 13, 15 and 17. These show high values compared to the other sections, and are most likely a result of the errors discussed above. The averaging of values over longer sections might remove the local variations.

Cutter thrust (kN/cutter) is an input parameter in almost all models, and is according to the sensitivity analyses the most influential parameter. All the machine data are logged every 10^{th} second. In order to compare the machine data with the geological data, weighted averaged values for each section have been calculated, which means that local variations have been flattened. Such flattening has been necessary, but it is not representing the actual conditions and performances adequately.

A constant frictional force of 3200 kN/cutter has been removed from the applied thrust values in order to calculate the net thrusts. In reality, the frictional drag forces are changing throughout the tunnel alignment. The execution of drag tests are expensive and time consuming, and have only been executed once. The frictional drag on a double shielded machine is bigger than for single shield TBMs. The NTNU model includes a frictional force corresponding to a single shield TBM in the calculations, which means that the predicted NPR with gross thrust should have been lower in this project (using a double shield TBM). This may explain why the predicted NPRs from the NTNU models are higher than the expected conservative predictions of 10% below the achieved. The differences in friction force between a single shield and a double shield TBM are hard to calculate it is still no agreement within the TBM tunnelling industry about the understanding of friction effect (Macias, 2016).

7 Conclusion

Conclusive remarks for the main- and secondary objectives will be presented in this chapter.

The overall purpose of this thesis was to find the superior performance prediction model based on data collected at the Follo Line Project. This has been done by comparing the predicted results with the actual achieved penetration rate from the first 4.5 km of the outbound north tunnel (TBM 1). In general, most of the performance prediction models show promising results compared to the achieved NPR. The NTNU models and the Alpine model turned out to be the most accurate ones. If conservative results are sought for, the MCSM-model and the model by Yagiz show promising results. The CSM-model and Q_{tbm} model predicts too high values.

In addition, three secondary objectives have been answered. Two of these was to collect and compile machine- and geological related data. In general, low DRI- and CLI-values, and very high UCS-values are present in the area. Local variations occur, and section 8 stands out with high predicted NPRs in every model. Low RQD- and UCS-values seem to be the explanation.

The third secondary objective was to determine the most influential parameters, both related to the actual achieved NPR and to the predicted NPR. In reality, the applied cutter thrust, the rock mass fracturing and the uniaxial compressive strength are the most influential parameters based on comparisons with the achieved NPR. Based on the sensitivity analyses of the models, the same parameters are the most influential.

Some parameters (e.g. Q- and UCS-values) show lower influence than expected. This is due to the parameter`s internal variation of influence, which shows higher influence with lower values. Therefore, the predictions with the Q_{tbm} model may have been more accurate for lower Q-values. All the models except the CSM-model use information about the fractures as input parameters. The great influence of these parameters is most likely the reason why the CSM-model predicts too high penetration rates.

Accurate predictions are important both before and during construction. To strengthen the accuracy and reliability of the predictions, it is recommended to use more than one prediction model in the calculations. Thus, errors connected to the models will be limited.

All the predictions and findings are project-specific in correlation with the Follo Line Project, and the final results may have been different in projects with other geological conditions.

References

Altindag, R. & Guney, A. (2010). *Predicting the relationships between brittleness and mechanical properties (UCS, TS and SH) of rocks*, in Scientific Research and Essays Vol. 5(16), 2107 – 2118.

Andreev, A. (2017). *Hard Rock TBM Tunnelling at the Follo Line Project.* Master's thesis. Norwegian University of Science and Technology, Trondheim, Norway. Unpublished.

Bane NOR. (2018a). Internal notes and reports.

Bane NOR. (2018b). Provided by personnel at site.

Barla, G. & Pelizza, S. (2000). *TBM tunnelling in difficult ground conditions*, in paper presented at the GeoEng2000 - An International Conference on Geotechnical and Geological Engineering, Melbourne, Australia.

Barton, N. (2000). *TBM tunnelling in jointed and faulted rock*, Rotterdam, A.A. Balkema.

Berg, S.B. (2015). *Tunnelboremaskinene er tilbake i Norge – vekker begeistring og fortvilelse.* Afternposten.no.
Available at: https://www.aftenposten.no/norge/Tunnelboremaskinene-er-tilbake-i-Norge--vekker-begeistring-og-fortvilelse-23993b.html (Accessed 15.01.18)

Brino, G., Peila, D., Steidl, A., & Fasching, F. (2015). *Prediction of performance and cutter wear in rock TBM: application to Koralm tunnel project*. Geam. Geoingegneria Ambientale E Mineraria

Bruland, A. (2000). *Hard rock tunnel boring.* PhD, Norwegian University of Science and Technology, Department of Building and Construction Engineering, Trondheim, Norway.

Bruland, A. (2000a). *Hard rock tunnel boring: Vol. 1: Background and discussion*, Norwegian University of Science and Technology, Department of Building and Construction Engineering, Trondheim, Norway.

Bruland, A. (2000b). *Hard rock tunnel boring: Vol. 3: Advance rate and cutter wear*, Norwegian University of Science and Technology, Department of Building and Construction Engineering, Trondheim, Norway.

Bruland, A. (2000c). *Hard rock tunnel boring: Vol. 6: Performance data and back-mapping*, Norwegian University of Science and Technology, Department of Building and Construction Engineering, Trondheim, Norway.

Bruland, A. (2000d). *Hard rock tunnel boring: Vol. 7: The boring process*, Norwegian University of Science and Technology, Department of Building and Construction Engineering, Trondheim, Norway.

Dahl, F. (2011) *DRI, BWI, CLI Standard.* SINTEF.

Dahl, F., Bruland, A., Jakobsen, P. D., Nilsen, B. & Grøv, E. (2012). *Classifications of properties influencing the drillability of rocks, based on the NTNU/SINTEF test method*. Tunnelling and Underground Space Technology, 28, 150-158.

Eide, L. (2015). *TBM tunnelling at the Stillwater Mine*. Master`s thesis. Norwegian University of Science and Technology, Trondheim, Norway.

Farrokh, E., Rostami, J. & Laughton, C. (2012). *Study of various models for estimation of penetration rate of hard rock TBMs,* in Tunnelling and Underground Space Technology incorporating Trenchless Technology Research, 30, 110-123.

Gehring, K. (1995). *Leistungs- und Verschleißprognose im maschinellen Tunnelbau*, in Felsbau Magazin, 13

Graversen, O. (1984). *Geology and Structural Evolution of the Precambrian Rocks of the Oslofjord-Øyeren Area, Southeast Norway,* in Norges Geologiske Undersøkelse **398**

Hansen, A.M. (1998). *The History of TBM Tunnelling in*, in Norwegian TBM Tunnelling: Publication 11. Norwegian Tunneling Society (NFF). 11-17. Available at: http://tunnel.no/publikasjoner/engelske-publikasjoner/ (Accessed 07.03.18)

Hansen, A.M., Bruland, A., Syversen, F. & Johannessen, S. (2017). *Tailor-made TBM design for boring in extreme hard rock conditions and examples from the Follo Line tunnel project.* Paper presented at World Tunneling Congress 2017 in Bergen.

Hassanpour, J., Ghaedi Vanani, A. A., Rostami, J. & Cheshomi, A. (2016). *Evaluation of common TBM performance prediction models based on field data from the second lot of Zagros water conveyance tunnel (ZWCT2)*, in Tunnelling and Underground Space Technology incorporating Trenchless Technology Research, 52**,** 147-156.

Hassanpour, J., Rostami, J. & Zhao, J. (2011). *A new hard rock TBM performance prediction model for project planning*, in Tunnelling and Underground Space Technology incorporating Trenchless Technology Research, 26, 595-603.

Herrenknecht. (2018a). Illustration. Available at: https://www.herrenknecht.com/en/products/coreproducts/tunnelling/gripper-tbm.html (Accessed: 08.03.18)

Herrenknecht. (2018b). Illustration. Available at: https://www.herrenknecht.com/en/products/core-products/tunnelling/single-shield-tbm.html (Accessed: 08.03.18)

Herrenknecht. (2018c). Illustration. Available at: https://www.herrenknecht.com/en/products/core-products/tunnelling/double-shield-tbm.html. (Accessed: 08.03.18)

Holtet, T. & Grue, Ø. (2013). *Gir tette tuneller.* Bane NOR, Jernbanemagasinet. Available at: http://www.banenor.no/Om-oss/Jernbanemagasinet/arkiv/Nyheter/2013/Gir-tette-tunneler (Accessed 28.11.17)

ISRM. (1978). *Suggested methods for the quantitative description of discontinuities in rock masses*, in International Journal of Rock Mechanics and Mining Sciences & Geomechanics Abstracts 15 (6), 319–368.

Kahraman, S., Fener, M., & Kozman, E. (2012). *Predicting the Compressive and Tensile Strength of Rocks from Indentation Hardness Index,* in Journal of the Southern African Institute of Mining and Metallurgy, 112(5), 331-339.

Macias, F. J. (2016). *Hard rock tunnel boring: performance predictions and cutter life assessment.* PhD, Norwegian University of Science and Technology, Faculty of Engineering Science and Technology, Department of Civil and Transport Engineering.

Macias, F. J. & Bruland, A. (2014). *D&B versus TBM: Review of the Parameters for a Right Choice of the Excavation method,* in Rock Engineering and Rock Mechanics: Structures in and on Rock Masses. CRC Press.

Maidl, B., Schmid, L., Ritz, W. & Herrenknecht, M. (2008*). Hard Rock Tunnel Boring Machines*. Ernst & Sohn Verlag, Berlin.

MTC (2018). Maidl Tunnelconsultants.
Available at: http://www.maidl-tc.de/en/Imprint.html (Accessed 26.01.2018)

Nazir, R., Momeni, E., Armaghani, D. J. & Amin, M. (2013). *Correlation between unconfined compressive strength and indirect tensile strength of limestone rock samples,* in Electr J Geotech Eng 18: 1737-1746.

NGI (2015). *Using the Q-system: Rock mass classification support design.* Handbook. Norges Geotekniske Institutt, Oslo.

Nilsen, B., Palmstrøm, A. & NFF. (2000). *Engineering geology and rock engineering*, Oslo, Norwegian Group for Rock Mechanics.

NTH (1976). *Hard Rock Tunnel Boring.* Trondheim, Norway: Norwegian Institute Technology, Div. of Construction Engineering and Geology

Ozdemir, L. (1977). *Development of theoretical equations for predicting tunnel borabillity*. PhD, Colorado School of Mines.

Yagiz, S. (2002). *Development of rock fracture and brittleness indices to quantify the effects of rock mass features and toughness in the CSM model basic penetration for hard rock tunneling machines.* Ph.D, Colorado school of Mines.

Yagiz, S. (2009). *Assessment of brittleness using rock strength and density with punch penetration test,* in Tunnelling and Underground Space Technology incorporating Trenchless Technology Research, 24, 66-74.

Yagiz, S., Rostami, J. & Ozdemir, L. (2012). *Colorado School of Mines Approaches For Predicting TBM Performance,* in International Society for Rock Mechanics.

Zoorobadi, M., Saydam, S. & Hebblewhite, B. (2012). *Parameter Study on Prediction Methods for TBM Penetration Rate,* in Geotech Geol Eng (2013) 31:783-791

Wilfing, L. (2016). *The Influence of Geotechnical Parameters on Penetration Prediction in TBM Tunneling in Hard Rock.* PhD, Technische Univerität München.

Williams, J. H. & Johnson, C. D. (2004). *Acoustic and optical borehole-wall imaging for fractured-rock aquifer studies,* in Journal of Applied Geophysics: Volume 55, issue 1.

Appendix A: Geological Profile

Appendix B: Tunnel Map Overview

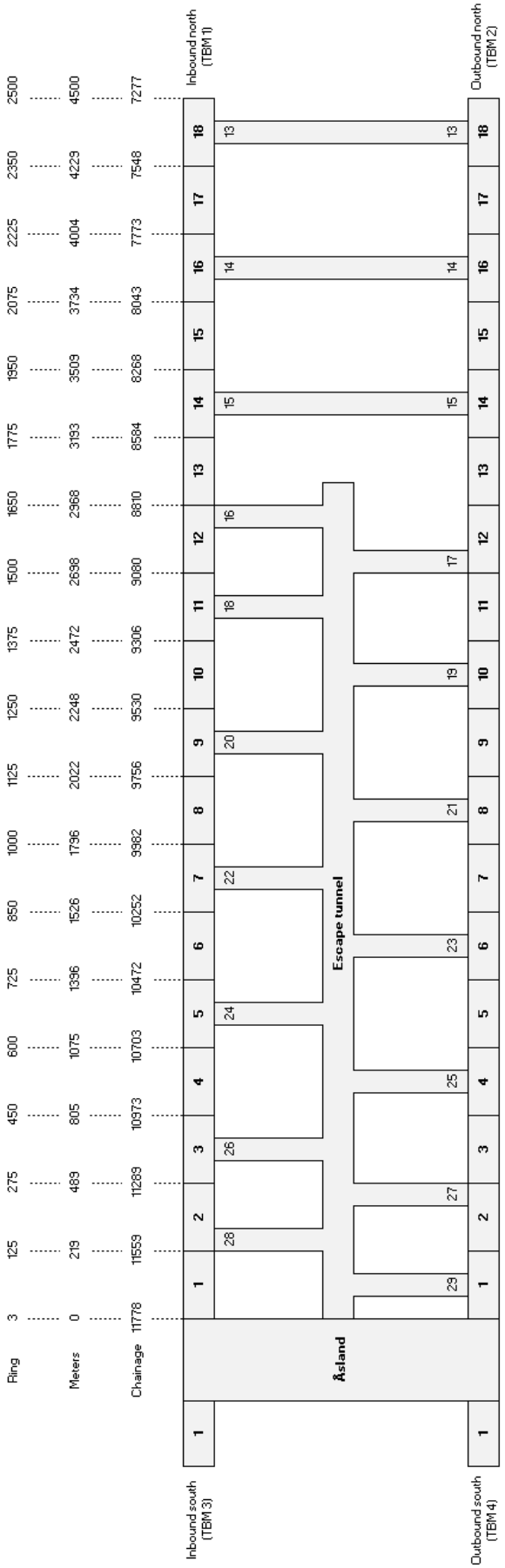

Appendix C: Fracture Information

(Digital appendix)

Appendix D: Laboratory Test Results

(Digital appendix)

Appendix E: Q-values

(Digital appendix)

Appendix F: Machine Data

(Digital appendix)

Appendix G: Model Calculations

(Digital appendix)

Appendix H: Parameter Influence

H1: Parameters influencing achieved NPR

(Digital appendix)

H2: Parameters influencing predicted NPR

(Digital appendix)

The calculations are presented in digital appendix H2. In addition, the variation of several parameter`s influence in each model is presented in the following:

The NTNU models

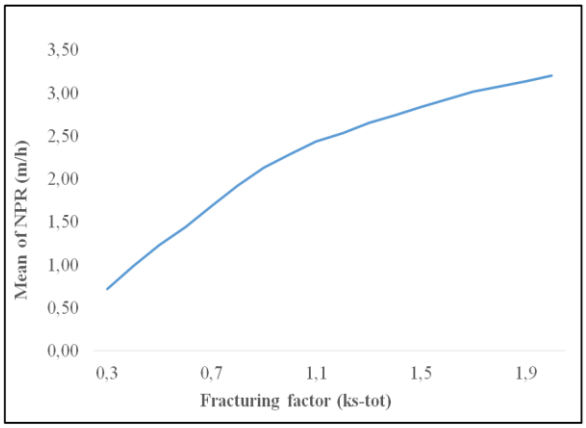

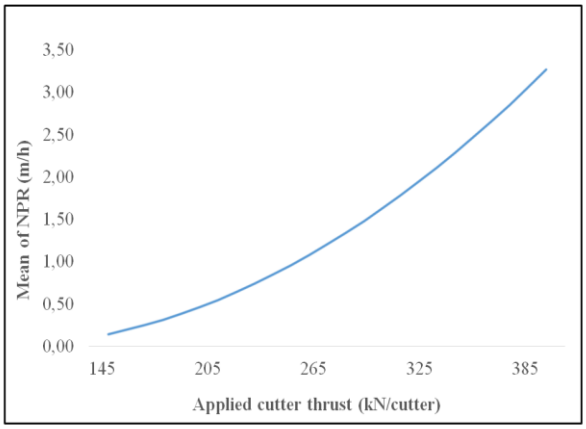

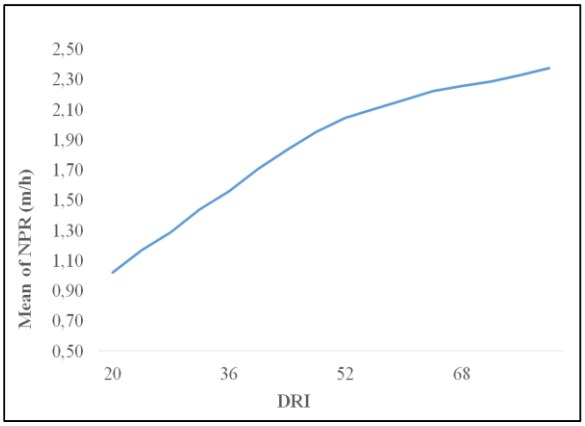

The CSM model

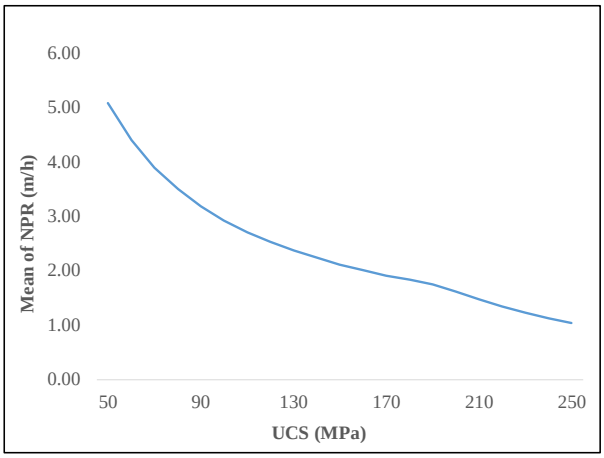

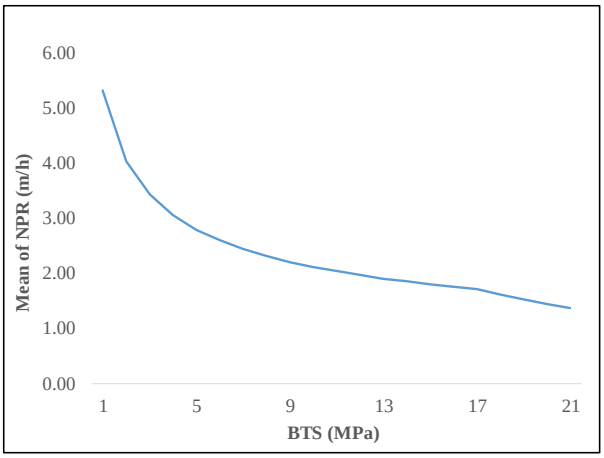

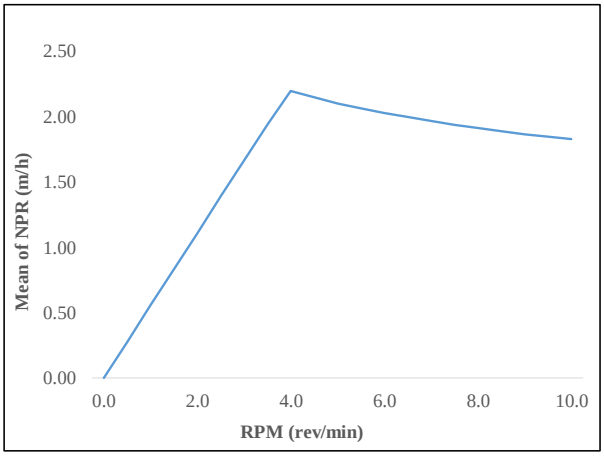

The MCSM model

The parameters included in this model are also implemented in the result from the CSM model. By that reason, the influence of the parameters in this model are impossible to determine.

The Gehring model

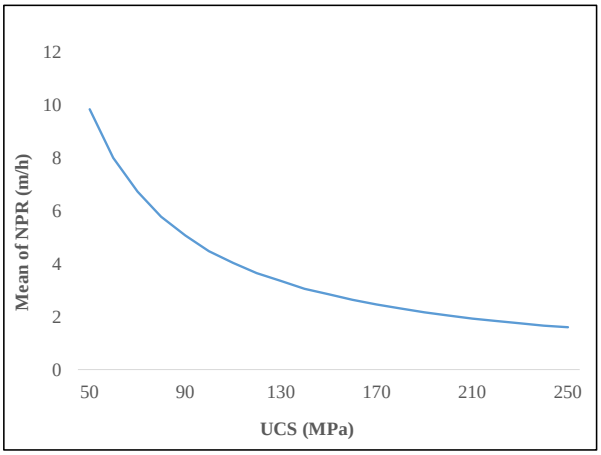

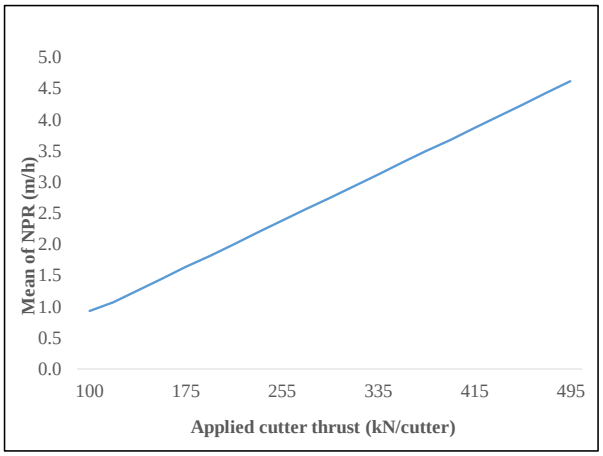

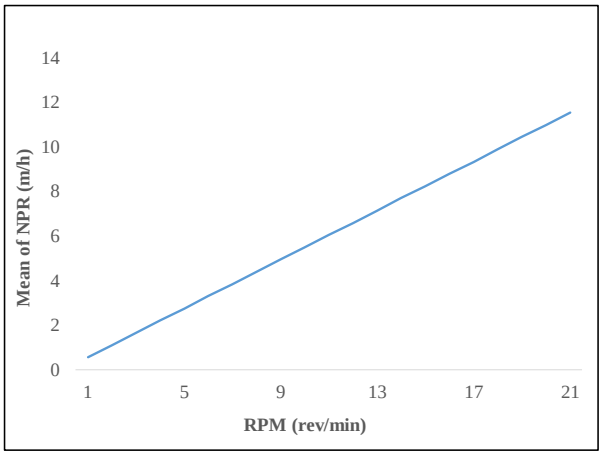

The Wilfing model

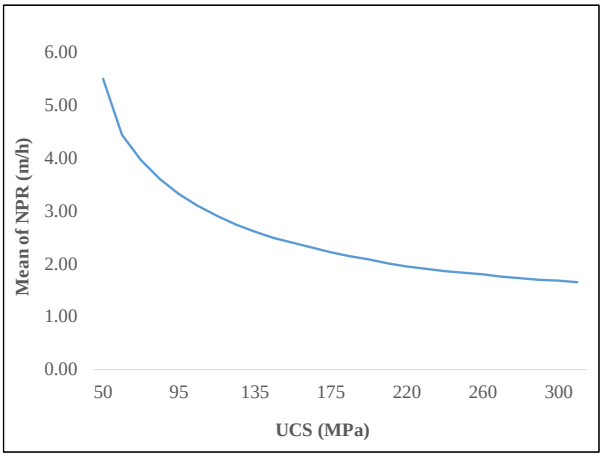

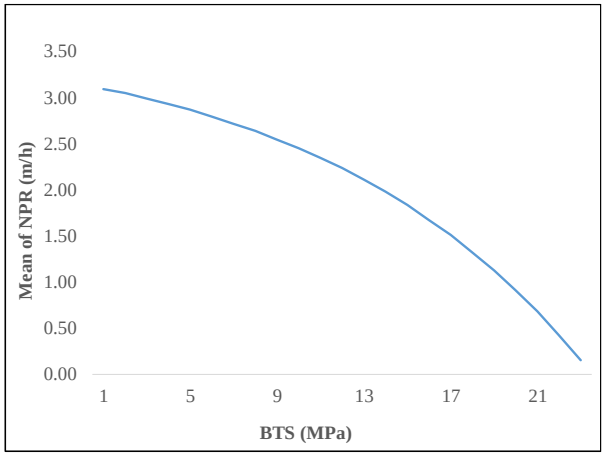

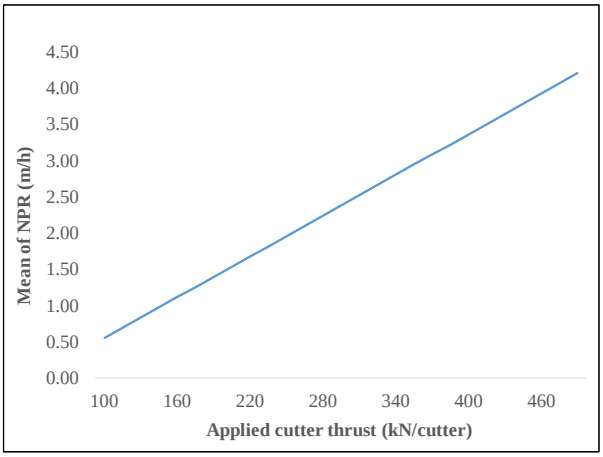

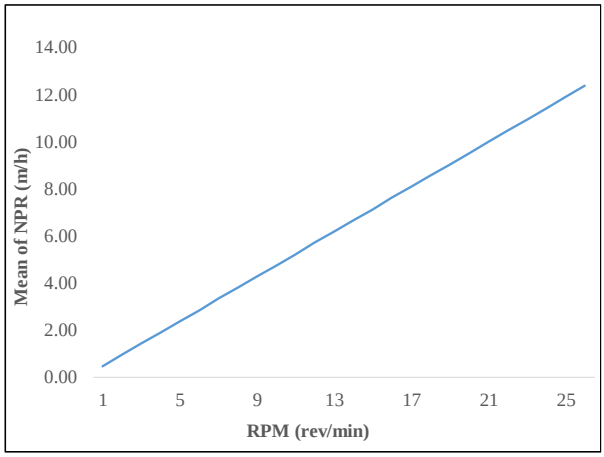

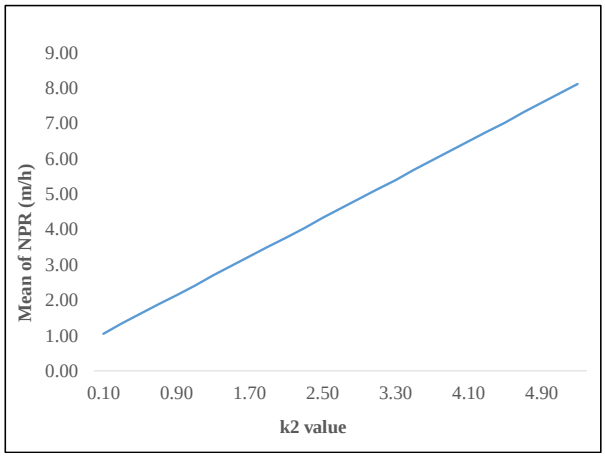

The Q_{tbm} model

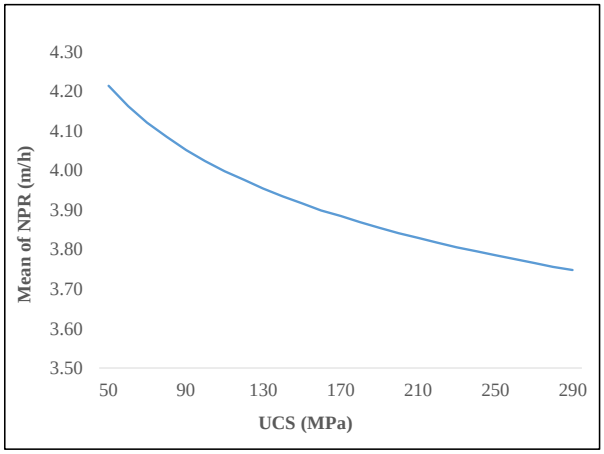

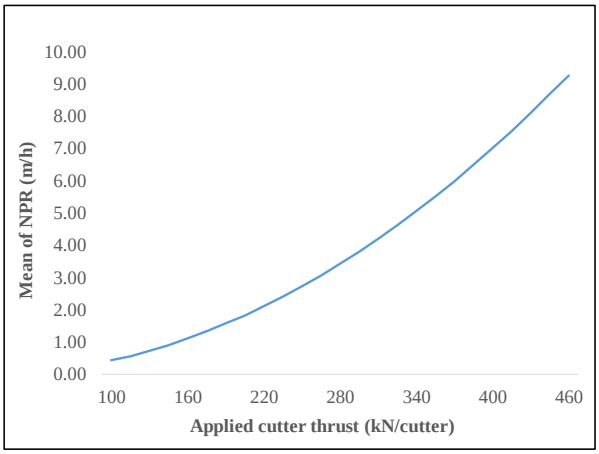

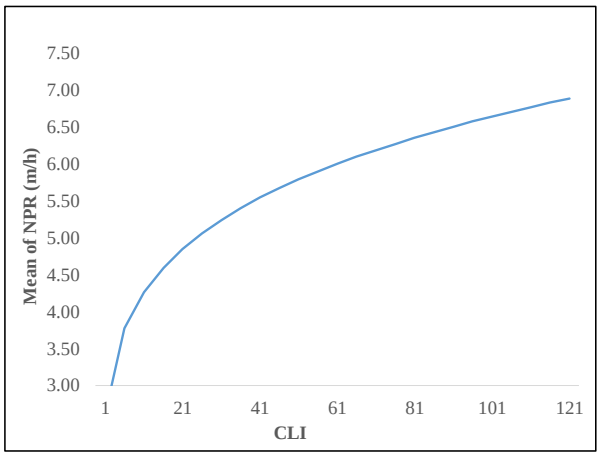

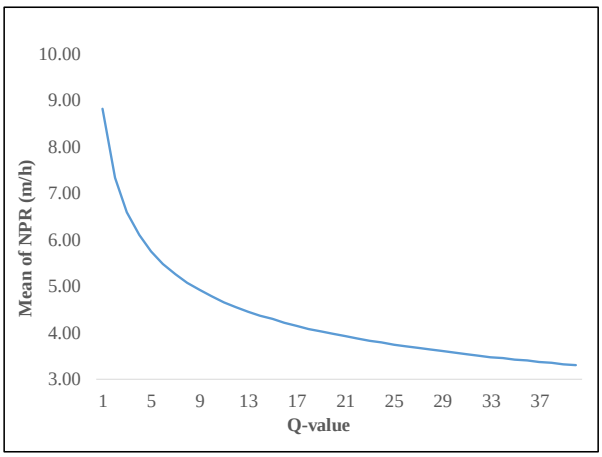

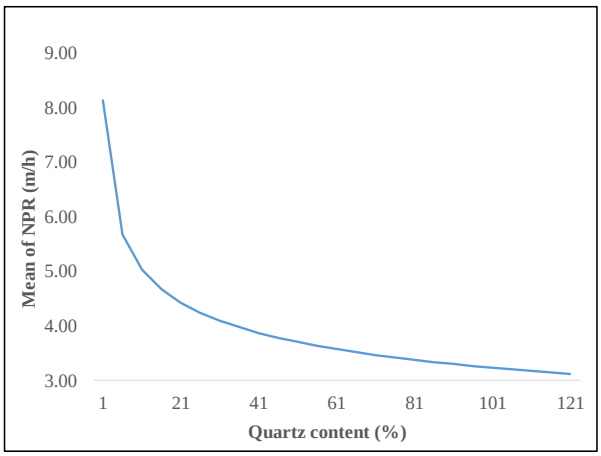

The model by Yagiz

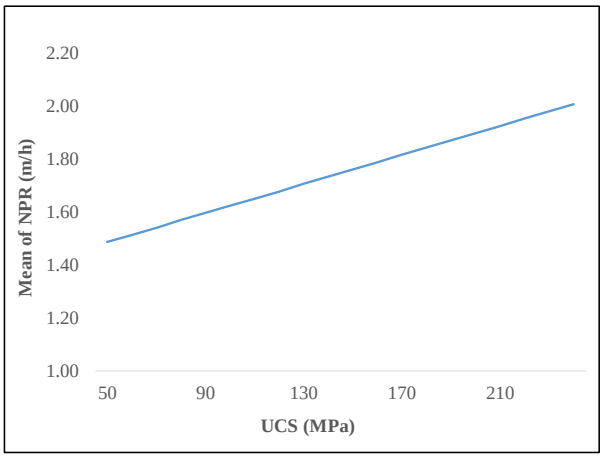

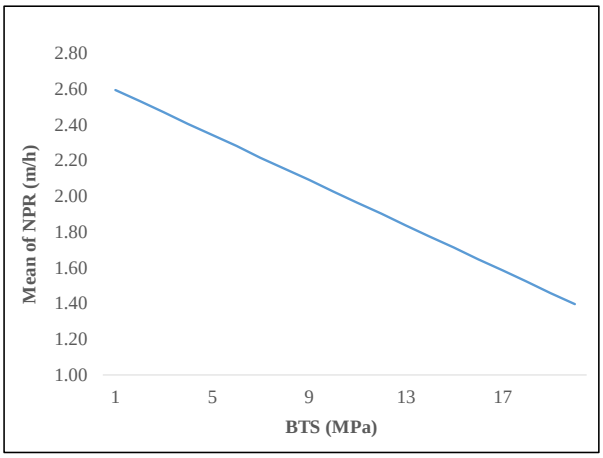

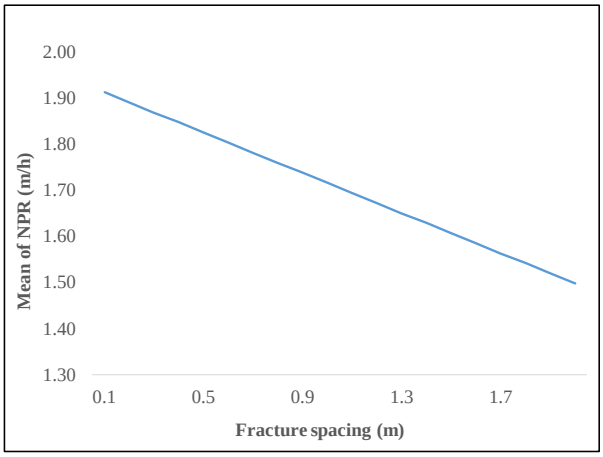

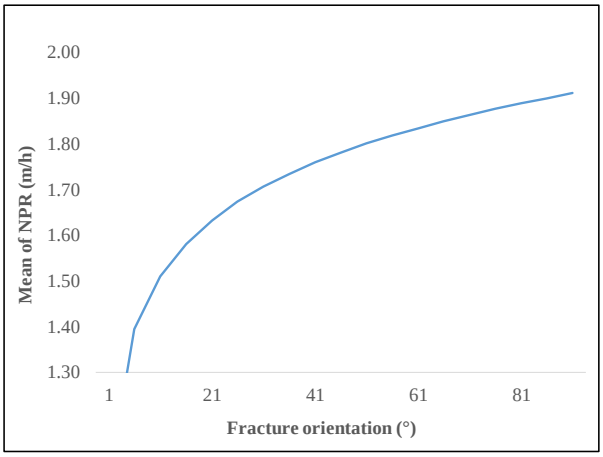

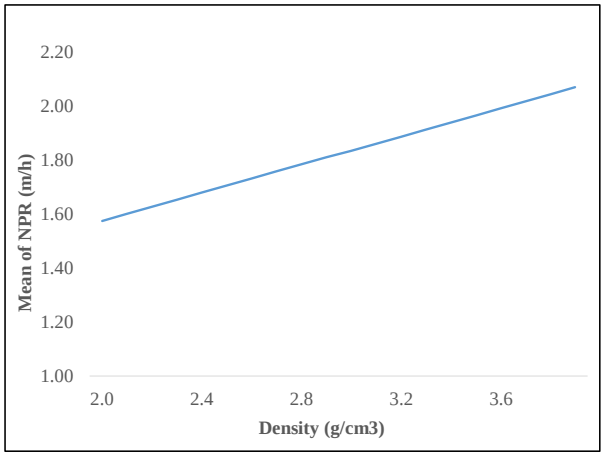

The model by Hassanpour et al.

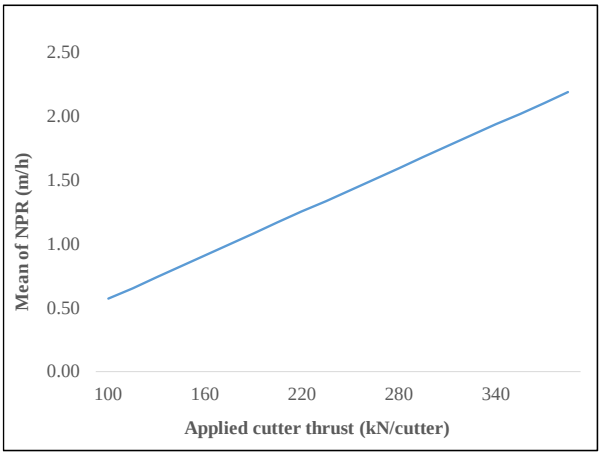

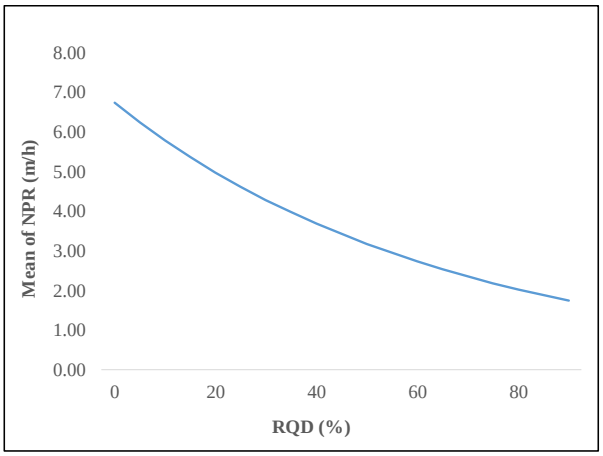

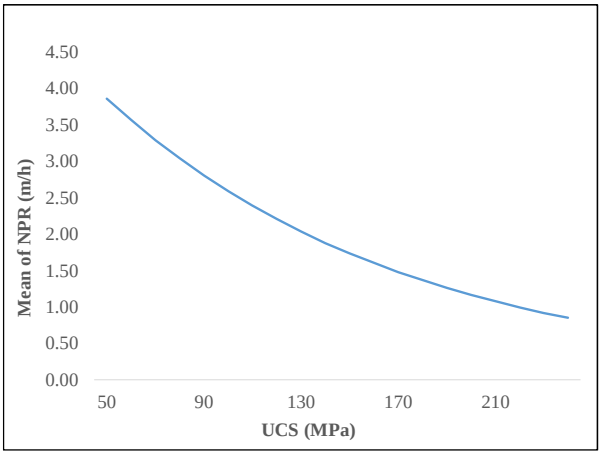

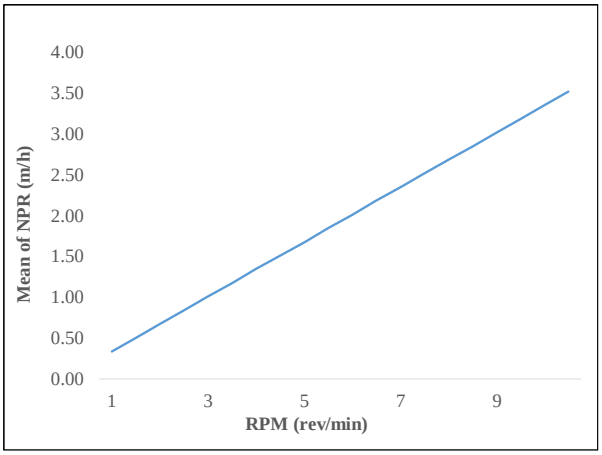

The model by Farrokh et al.

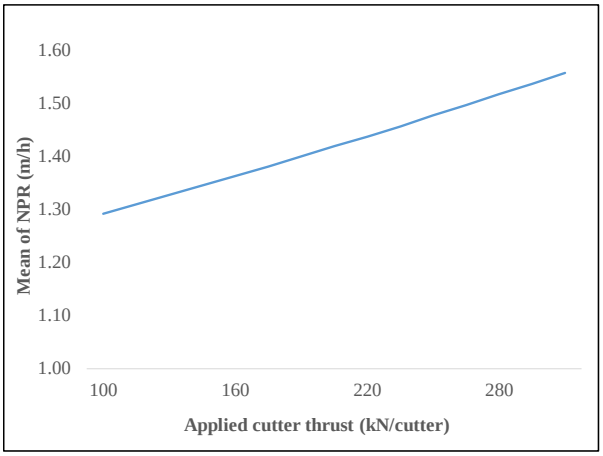

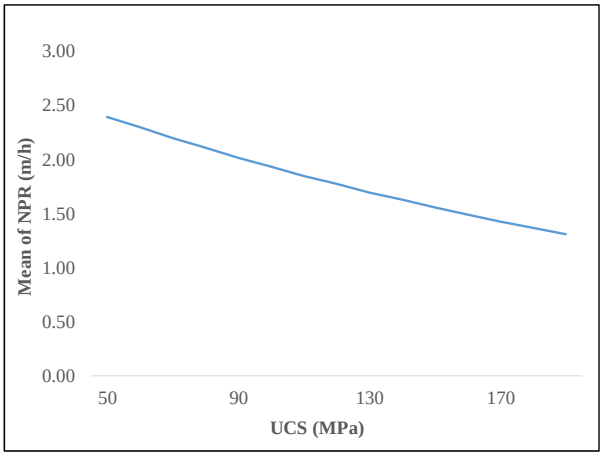

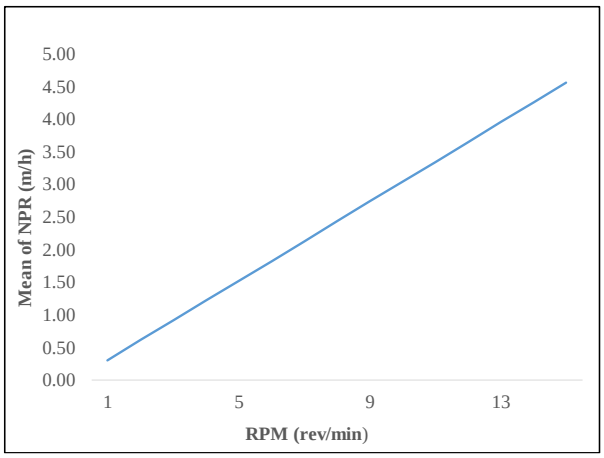

Appendix I: Summary and Compilation

(Digital appendix)